

IDENTIFICATION OF SELECTIVE INHIBITORS FOR METASTATIC
RECURRENCES OF CHILDHOOD MEDULLOBLASTOMA

M.Sc. Thesis – A. A. Adile; McMaster University – Biochemistry & Biomedical Sciences

THERAPEUTIC TARGETING OF METASTATIC RECURRENCES OF PEDIATRIC
MEDULLOBLASTOMA BY SELECTIVE KINASE AND HISTONE DEACETYLASE
INHIBITORS

By ASHLEY ANN ADILE, HON. B.SC.

A Thesis Submitted to the School of Graduate Studies in Partial Fulfilment of the
Requirements for the Degree Master of Science

McMaster University © Copyright by Ashley Ann Adile, May 2020

DESCRIPTIVE NOTE

MASTER OF SCIENCE (2020)

Biochemistry & Biomedical Sciences

McMaster University

Hamilton, Ontario

TITLE: Therapeutic targeting of metastatic recurrences of pediatric medulloblastoma by selective kinase and histone deacetylase inhibitors

AUTHOR: Ashley Ann Adile, Hon. B.Sc. (McMaster University)

SUPERVISOR: Dr. Sheila Kumari Singh

NUMBER OF PAGES: xiii, 111

LAY ABSTRACT

Medulloblastoma is an aggressive brain cancer in children. While current standard treatment improves patient survival, 30-40% of all medulloblastoma patients relapse at local (brain) or metastatic (spine) sites. Medulloblastoma metastatic recurrences remain poorly understood, yet they result in an alarmingly high mortality rate amongst patients due to inadequate treatment options currently available. Specific molecular targets are common in both medulloblastoma and metastatic cancer research. These targets are particularly important in governing cell signalling pathways that regulate tumour growth and migration. Therefore, treatment against these targets may be effective at preventing medulloblastoma metastatic recurrences.

As the collection of local and metastatic tumour samples at patient relapse are rare, the Singh lab developed an animal model that mimics human medulloblastoma recurrence. In this thesis, recurrent medulloblastoma metastases were isolated from our established animal model and tested against compounds that inhibit the specific molecular targets previously implicated in medulloblastoma and other metastatic tumours. We identified potent compounds that effectively target these metastatic cells. Next, we determined which compounds spared healthy cells and were able to penetrate the brain, given our future objective of targeting these MB cells from their source to ultimately prevent metastasis. The identified compounds substantially reduced the ability of these cells to divide. With further investigation, these compounds may pose as effective therapeutic agents to treat human medulloblastoma patients with metastatic recurrences.

ABSTRACT

Medulloblastoma (MB) is the most common malignant pediatric brain tumour. Of its four distinct molecular subgroups (WNT, SHH, Group 3, and Group 4), Group 3 MB patients hold the worst clinical prognosis due to their high incidence of tumour recurrence and metastasis to the spinal leptomeninges. Relapsed Group 3 MB patients, particularly those with *MYC* amplification (known as Group 3 γ), carry a mortality rate of nearly 100%, given the paucity of effective therapeutic options currently available. The most common cause of mortality amongst these patients is leptomeningeal metastasis, yet this metastatic disease is poorly characterized. Our understanding of MB tumour recurrence and leptomeningeal metastasis is further encumbered by the rare clinical opportunities at which specimens may be collected from relapsed patients. We were able to circumvent this obstacle by establishing a patient-derived xenograft mouse-adapted therapy model, which mimics the treatments administered in the clinic and in turn, recapitulates both local and metastatic human MB recurrence. This model system enabled the collection of valuable, patient-derived Group 3 γ MB tumour cells from the spinal leptomeninges at relapse. It provides an opportunity for chemical screening, with the aim of identifying small molecule inhibitors capable of eradicating these cells. Existing studies on MB leptomeningeal dissemination at diagnosis suggest that effective treatments may target signalling proteins, such as phosphatidylinositol 3-kinases and histone deacetylases (HDACs). Therefore, I hypothesized that selective kinase and HDAC inhibitors would pose as effective therapies against Group 3 γ MB metastatic recurrences.

In this thesis, I conducted a high-throughput screen of 640 kinase inhibitors and robust testing of novel HDAC6-selective inhibitors against these treatment-refractory, metastatic cells. Here, I showed that metastatic recurrences of Group 3 γ MB are therapeutically vulnerable to selective inhibitors of checkpoint kinase 1 (CHK1), platelet-derived growth factor receptor beta (PDGFR β), and HDAC6. Functional studies demonstrated that these inhibitors selectively target the aggressive, migratory Group 3 γ MB cells, while sparing healthy neural stem cells. They also showed effective blood-brain-barrier penetration *in silico* and *in vitro*, while significantly reducing MB tumour cell properties that are often associated with treatment failure. Taken together, my thesis highlights specific inhibitors of CHK1, PDGFR β , and HDAC6 that effectively target MB tumour cells that fuel treatment-refractory leptomeningeal metastases. With additional preclinical validation, these compounds may serve as potent therapeutic options to extend survival and improve the quality of life for patients that are ostensibly limited to palliation.

ACKNOWLEDGEMENTS

First and foremost, thank you, Lord for all of the blessings and opportunities that you have provided me. I am grateful for all the individuals that I had the pleasure of meeting, collaborating with, and working alongside throughout my time within the Singh lab.

I would like to sincerely thank Dr. Sheila Singh for seeing something in me during the early years of my undergraduate education. Thank you for the opportunity to study with you and your lab of innovative scientists; all of whom provided me with unwavering support and taught me lessons beyond any textbook. It has truly been such an honour to work alongside you, witnessing firsthand your intelligence, commitment, and professionalism, all the while being a clinician, active scientist, mentor and mother (to the lab and your own children). Thank you for all of the opportunities that you have provided me; I can genuinely say that acceptance into your research lab had an enormous impact on my life – one in which a thank you will never suffice.

Similarly, to Dr. Chitra Venugopal, a thank you cannot properly express how grateful I am to have met such a hard-working scientist. Your guidance throughout each stage of my time in the lab has been greatly appreciated. Since our initial meeting, you welcomed me so graciously and immediately became one of my biggest cheerleaders. Thank you for so enthusiastically celebrating my personal and academic successes. And thank you for providing a wise perspective on any obstacle I faced. Your advice, kind-hearted spirit, and constant support truly made the work environment fun – even on days with inconclusive results.

A huge thank you to my graduate mentor, Dr. David Bakhshinyan. Whether it was shadowing you in tissue culture to learn the lab's techniques during undergraduate training, staying late to finish mouse experiments or discussing scientific literature (to the point in which I would get a headache), you brought so much joy to this work. I am grateful to have been mentored by such an innovative scientist and critical thinker. Even more, I am grateful to have gained a great friend in the process. Thank you for your endless support. Also, a big thank you to Dr. Michelle Kameda-Smith for all of the guidance and support. Your work ethic (which is uncanny) and influence as a strong female role model are attributes that I aspire to be one day. To past and present Singh lab members, thank you for your care and guidance in both my project and personal development, along with your positive energy and the life-long friendships that I will continue to cherish!

To my committee members: Thank you both for your invaluable advice and continued support on my projects. Dr. John Hassell, thank you for asking the (many) difficult scientific questions. Your position on my committee has served to not only improve my research methodologies and project, but also my critical thinking skills. To Dr. Patrick Gunning, thank you for your enthusiasm and unique perspective on my projects (past and present). From screening your compounds as my initial undergraduate training to now

assessing them with more in-depth experiments, I have appreciated the collaboration with your lab.

A big thank you to my collaborators, especially David Uehling, Mehakpreet Saini, Ahmed Aman, and Jakob Magolan. I truly appreciate all of the time, effort, and great enthusiasm that you all had with my project. I know that this work would not have been possible without your help.

A special thank you to the Brain Tumour Foundation of Canada for their outstanding efforts to support those affected by brain cancer, as well as providing awareness and research funds for innovative projects. I want to sincerely thank Susan Ruypers for the continued support and unwavering positivity throughout my undergraduate and graduate projects.

To all of the patients and families that I have met along the way and have donated their tumour samples to this research, I cannot thank you enough! Your strength, compassion and generosity despite enduring such a difficult experience further my passion and commitment to the field of childhood brain cancer. My deepest thanks to the Garrett, Hill, Smith, and Rolke families; my happiest moments in the lab were rooted in meeting you. Xavier, Kelsey, Preston, and Addison will continue to hold a special place in my heart.

Thank you to all of the members of the Stem Cell and Cancer Research Institute; I have enjoyed your company over the past four years and am excited to see each of you flourish in the next stage of your lives.

Thank you, Kerri-Ann for all of your time, guidance, and encouragement.

Thank you to my family and close friends for not only listening to my many rambles of science jargon, but also for your constant support. Most importantly, thank you, mom and dad. Words will never be able to describe how eternally grateful I am to have you as my parents. Thank you for being my biggest supporters throughout this crazy journey. I dedicate this thesis to you both. You have pushed me to be a better version of myself each day, challenged me to stay optimistic and resilient even in times of troubleshooting and negative data, while being my #1 cheerleaders. You taught me to enjoy the journey and not focus on the destination. And while the journey has been bumpy along the way, I hope that throughout it all I have made you proud.

TABLE OF CONTENTS

DESCRIPTIVE NOTE	ii
LAY ABSTRACT	iii
ABSTRACT	iv
ACKNOWLEDGEMENTS	vi
LIST OF FIGURES & TABLES	x
LIST OF SYMBOLS AND ABBREVIATIONS	xi
DECLARATION OF ACADEMIC ACHIEVEMENT	xiii
CHAPTER 1: Introduction	15
1.1 Medulloblastoma.....	15
1.1.1 Epidemiology	15
1.1.2 Diagnosis, standard treatment regimens, and risk stratifications	16
1.2 Histopathological and molecular classification of medulloblastoma	19
1.2.1 Histopathology	19
1.2.2 Current molecular subgroups and clinical prognosis	20
1.2.2.1 Developmental origins of medulloblastoma subgroups.....	24
1.2.2.2 Stem cells vs. cancer stem cells	27
1.2.2.3 Identification of medulloblastoma stem cells	29
1.3 Medulloblastoma recurrence	30
1.3.1 Genetic divergence between primary and recurrent specimens	30
1.3.2 Local vs. metastatic tumour recurrence.....	31
1.3.3 Clinical outcome of medulloblastoma recurrences	33
1.3.4 Medulloblastoma leptomeningeal metastases	35
1.3.4.1 Current models of metastatic medulloblastoma	36
1.3.4.2 Singh lab model of Group 3 γ medulloblastoma recurrence	39
1.4 Summary of intent.....	40
CHAPTER 2: Materials & Methods	41
5.1 Cell cultures	41
5.2 Patient-derived xenograft mouse-adapted therapy model.....	43
5.3 Inhibitors	45
5.4 Fluorescence-activated cell sorting	45
5.5 Large scale high-throughput screening	46
5.5.1 Z prime (Z') assay and optimization	46
5.5.2 High-throughput screen.....	47
5.6 Madin-Darby canine kidney strain II (MDCKII) assay	48
5.6.1 MDCKII cell culture	48
5.6.2 MDCKII permeability assay	49
5.6.3 MDCKII assay data analysis	50
5.6.4 Liquid chromatography-mass spectrometry (LC/MS).....	51
5.7 Cell viability.....	52
5.8 Sphere formation assays.....	53

CHAPTER 3: Identification of kinase inhibitors that effectively target recurrent Group 3γ medulloblastoma leptomeningeal metastases.....	54
3.1 Role of kinases in normal vs. cancer system.....	54
3.1.1 Implications of kinase inhibitors in medulloblastoma	54
3.2 Results.....	55
CHAPTER 4: Novel HDAC6 inhibitors target metastatic, treatment-refractory Group 3γ medulloblastoma.....	71
4.1 Role of histone deacetylases in normal vs. cancer system.....	71
4.1.1 Implications of histone deacetylase inhibitors in medulloblastoma	71
4.1.2 Migratory role of histone deacetylase 6 in cancer	72
4.2 Results.....	73
DISCUSSION	80
5.1 Biological relevance of high-throughput kinase screen hits	81
5.2 HDAC6 inhibitor therapy for Group 3 γ medulloblastoma metastatic recurrences.....	84
5.3 Future directions	86
REFERENCES.....	89
APPENDIX: Academic Achievements	108

LIST OF FIGURES & TABLES

CHAPTER 3 FIGURES.....	61
Figure 1. High-throughput screen identified kinase inhibitors that target Group 3 γ MB metastatic recurrences	61
Figure 2. BI 2536, CHIR-124, Hesperadin, JNJ-10198409, and SB-218078 selectively targeted metastatic Group 3 γ MB cells at tumour recurrence and spared healthy neural cells	63
Figure 3. <i>In vitro</i> functional profile of CHK1 (CHIR-124) and PDGFR β (JNJ-10198409) inhibitors demonstrated reduced BBB permeability and stem cell properties	64
Supplementary Figure 1; Related to Figure 1. High-throughput screen optimization and filtering criteria	66
Supplementary Table 1; Related to Figure 1. Predicted Percepta blood-brain barrier permeation properties of screen hits	68
Supplementary Figure 2; Related to Figure 2. Validation of optimal cell density plating in additional cell lines	69
Supplementary Figure 3; Related to Figure 3. Dose response studies of CHIR-124 and JNJ-10198409 did not show selectivity to metastatic Group 3 γ MB cells at tumour recurrence	70
CHAPTER 4 FIGURES	76
Figure 4. Belinostat showed a substantial therapeutic window between Group 3 γ MB spinal leptomeningeal metastatic cells at relapse and hNSCs	76
Figure 5. Dose response studies of novel HDAC6-selective inhibitors demonstrated variable therapeutic windows between Group 3 γ MB metastatic recurrences and hNSCs ..	77
Figure 6. <i>In vitro</i> functional profile of top HDAC6-selective inhibitors revealed variable response in stem cell assays, compared to citarinostat	78
Supplementary Figure 4; Related to Figure 5. Additional dose response curves of selective HDAC6 compounds	79

LIST OF SYMBOLS AND ABBREVIATIONS

α	Alpha
β	Beta
γ	Gamma
μ	Micro
AB	Apical to basolateral chamber
AKT	Protein kinase B
AML	Acute myeloid leukemia
ARNT	Aryl hydrocarbon nuclear translocator/hypoxia-inducible factor 1 β
AURKB	Aurora kinase B
BA	Basolateral to apical chamber
BBB	Blood-brain barrier
BET	Bromodomain and extra-terminal motif
BTIC	Brain tumour initiating cell
c-Abl	Abelson murine leukemia viral oncogene homolog 1
CCL2	Cysteine-cysteine motif chemokine ligand
CCR2	Cysteine-cysteine motif chemokine receptor
CCRK	Cell cycle-related kinase
CD133	Cluster of differentiation 133
CDC2	Cyclin-dependent kinase 2, or cell division cycle protein 2
CDK	Cyclin-dependent kinase
CHK	Checkpoint kinase
cMDR1, cP-gp	Canine multidrug resistance protein 1 or p-glycoprotein
CNS	Central nervous system
CSC	Cancer stem cell
CSF	Cerebrospinal fluid
c-Src	Tyrosine-protein kinase Src
DMEM	Dulbecco's Modified Eagle Medium
DMSO	Dimethyl sulfoxide
EGFR	Epidermal growth factor receptor
EMT	Epithelial-mesenchymal transition
ER	Efflux ratio
ERAS	Embryonic stem cell-expressed Ras
ERK	Extracellular signal-regulated kinase
FBS	Fetal bovine serum
FLT	FMS-like tyrosine kinase
GBM	Glioblastoma
GCP	Granule cell precursor
GDI2	Rab GDP dissociation inhibitor
GFI1	Growth factor independent 1
GSK	Glycogen synthase kinase
Gy	Gray (unit of irradiation)
HBSS	Hank's balanced salt solution
HDAC	Histone deacetylase

hMDR1, hP-gp	Human multidrug resistance protein 1 or p-glycoprotein
hNSC	Human neural stem cell
IC ₅₀	Half maximal inhibitory concentration
IGF1R	Insulin-like growth factor 1 receptor
IKK	I kappa B kinase
JAK	Janus kinase
KI	Knock-in
KO	Knockout
KDR	Kinase insert domain receptor
LC/MS	Liquid chromatography-mass spectrometry
LHX1	LIM homeobox protein
LDA	Limiting dilution analysis
MAPK	Mitogen-activated protein kinase
MB	Medulloblastoma
MDCKII	Madin-Darby canine kidney strain II
MRI	Magnetic resonance imaging
mTOR	Mammalian target of rapamycin
MYC	V-myc avian myelocytomatosis viral oncogene homolog
NOD SCID	Nonobese diabetic-severe combined immune-deficiency
NCC	NeuroCult Complete media
OICR	Ontario Institute for Cancer Research
OTX	Orthodenticle homeobox 2
P _{app}	Permeability coefficient
PAR	Post-assay recovery
PBS	Phosphate buffered saline
PDGFR β	Platelet-derived growth factor receptor beta
PDX	Patient derived xenograft
PI3K	Phosphatidylinositol 3-kinase
PIM	Proviral integration site for Moloney murine leukemia virus
PKC	Protein kinase C
PLK	Polo-like kinase
PTEN	Phosphatase and tensin homolog
Rho	Ras-homologous
ROCK	Rho-associated coiled-coil kinase
scRNA-seq	Single-cell RNA sequencing
SHH	Sonic Hedgehog
TGF- β , TGF β R	Transforming growth factor beta, receptor
TPPP1	Tubulin polymerization promoting protein 1
TSP1	Thrombospondin-1
UBC	Unipolar brush cell
WHO	World Health Organization
WNT	Wingless
Z'	Z prime

DECLARATION OF ACADEMIC ACHIEVEMENT

During my graduate studies, I contributed to 10 research papers, 3 book chapters, as well as presented at local and international conferences. The work described in this thesis is a result of the combined effort of myself, Dr. David Bakhshinyan, Dr. Chitra Venugopal, and Dr. Sheila K. Singh. It was built from the innovative patient-derived xenograft model of medulloblastoma recurrence that Dr. David Bakhshinyan established in his doctoral studies in the Singh lab. In this thesis, I contributed to the experimental design, execution, interpretation of data, and writing of all sections. Dr. Sheila K. Singh supervised all research projects and aided in data interpretation, alongside Dr. Chitra Venugopal and Dr. David Bakhshinyan. Probing of *in silico* blood-brain barrier permeability software, Percepta and SwissADME, was completed by Dr. Jacob Magolan and Mehakpreet Saini, respectively. Mehakpreet Saini also conducted the *in vitro* (Madin-Darby canine kidney strain II) blood-brain barrier permeability assay and analysis to deduce the permeability for select compounds.

CHAPTER 1: Introduction

1.1 Medulloblastoma

1.1.1 Epidemiology

Central nervous system (CNS) tumours are the most common solid malignancies in children and are the leading cause of childhood cancer-related mortality (Northcott et al., 2012a; Pui, Gajjar, Kane, Qaddoumi, & Pappo, 2011). In Canada, such tumours account for 34% of cancer-related deaths among children (Siegel, Naishadham, & Jemal, 2012). These pediatric brain tumours are predominantly located in the posterior fossa, particularly the cerebellum. As the most common malignant brain cancer in children, medulloblastoma (MB) originates in the cerebellar region of the brain. MB was first described in 1925 by Bailey and Cushing (Bailey & Cushing, 1925). It constitutes approximately 20% of all childhood CNS neoplasms (Rossi, Caracciolo, Russo, Reiss, & Giordano, 2008). This embryonal disease represents over 64% of all CNS tumours in American children and adolescents age 0-14 years, with the median age of diagnosis at ~6 years old (Khanna et al., 2017; Ostrom et al., 2019). MB incidence rates decline with increasing age after 9 years old (Ostrom et al., 2019). Conversely, adult MB is a rare disease entity, accounting for only 1% of CNS tumours (Lassaletta & Ramaswamy, 2016). Hereafter, MB is defined as pediatric MB, unless otherwise stated.

With nearly uniform incidence rates across geographical regions and ethnicities, MB affects 14.6 per 1,000,000 children and adolescents age 0-14 years in the United States of America, annually (Ezzat et al., 2016; Ostrom et al., 2019). An earlier study indicated that

4.82 per 1,000,000 Canadian children and adolescents age 0-14 years are affected each year (Johnston et al., 2014). Additionally, MB is twice as common in males by comparison to females (Khanna et al., 2017).

1.1.2 Diagnosis, standard treatment regimens, and risk stratifications

The cerebellum is responsible for fine motor coordination, gait, balance control, vestibular ocular reflex, sensory-motor learning, spatial memory and speech (Hatten & Roussel, 2011). MB patients present with a combination of impairments in these functions and symptoms related to increased intracranial pressure due to the obstructive hydrocephalus occluding the flow of cerebrospinal fluid (CSF) between ventricles – primarily involving the fourth ventricle or its outlets (Schneider et al., 2015). Differential diagnosis from other childhood brain tumours relies on these clinical symptoms, neurological assessment, advanced neuraxis imaging, tissue biopsy from surgery, as well as subsequent molecular and histopathological analysis. When necessary, a lumbar puncture may be performed for CSF cytology analysis.

The current standard treatment protocol consists of maximal safe surgical resection for all MB patients. Adjuvant treatment of craniospinal irradiation and cytotoxic chemotherapy regimens depend on age and clinical paradigms (i.e., volume of residual tumour following surgery and extent of disease metastasis), which determine patient risk stratification (Ellison, 2010; Packer et al., 2006). Standard-risk patients are 3 years of age or older and, who present with less than 1.5cm² of post-operative tumour and negative metastatic results

(M0; defined below) by craniospinal magnetic resonance imaging (MRI) and CSF cytology (Fouladi et al., 1999; Polkinghorn & Tarbell, 2007). Typical protocol for standard-risk patients includes gross total resection, a combination of chemotherapy regimens, in addition to 23.4 Gy of upfront craniospinal irradiation and a localized boost of 54 Gy to the primary tumour (A. Gajjar et al., 2006; ISPN, 2020). In comparison, high-risk patients are 3 years of age or older with 1.5cm² or more residual tumour, with or without evidence of leptomeningeal metastasis (M1-M3, or M+; defined below). These patients receive near-total or gross total tumour resection, chemotherapy, and intensified radiotherapy, often involving “full-dose” craniospinal irradiation of 36.0 Gy, and conformal boost of 55.8 Gy to the posterior fossa and focal sites of metastases (A. Gajjar et al., 2006; ISPN, 2020; Polkinghorn & Tarbell, 2007; Ramaswamy et al., 2016). As intensive craniospinal irradiation causes deleterious damage to the developing CNS, MB patients younger than 3 years old at diagnosis are also considered high-risk and generally receive only intensive chemotherapy with or without autologous bone marrow or stem-cell transplant (Bouffet, 2010). Recent chemotherapy protocols for children with MB employ a combination of cisplatin, vincristine, cyclophosphamide, and lomustine (Martin, Raabe, Eberhart, & Cohen, 2014; Packer et al., 2006). While all warrant toxicity to both cancerous and healthy tissue, each differs in their mechanism of action in ablating fast-growing cells. For example, cisplatin is a platinum-based, antineoplastic agent that induces DNA damage by cross-linking with purine bases, which interferes with DNA repair mechanisms and subsequently activates apoptosis (Dasari & Tchounwou, 2014). Vincristine causes metaphase arrest through binding to tubulin in microtubules, which leads to the inhibition of microtubule

formation in mitotic spindles (Rowinsky & Donehower, 1991). Both cyclophosphamide and lomustine are alkylating agents; used interchangeably with cisplatin and vincristine treatment protocols (Martin et al., 2014; Packer et al., 2006). In addition, induction chemotherapy for infants with MB, whom do not receive any craniospinal irradiation, typically includes cisplatin, vincristine, cyclophosphamide, and etoposide; the latter of which forms a complex with DNA and topoisomerase II to induce double-stranded breaks in DNA and prevent DNA re-ligation (ISPN, 2020; Montecucco, Zanetta, & Biamonti, 2015).

To classify disease dissemination, the Chang staging system consists of five highly prognostic stages that define the degree of metastasis (Chang, Housepian, & Herbert, 1969; Polkinghorn & Tarbell, 2007).

- (1) M0: No evidence of metastatic disease by CSF cytology and craniospinal MRI;
- (2) M1: Positive CSF cytology without gross leptomeningeal tumour deposits visible on neuroaxis imaging (MRI);
- (3) M2: Presence of gross nodular seeding in cerebellum, third or lateral ventricles, or cerebral subarachnoid space;
- (4) M3: Presence of gross nodular seeding in spinal subarachnoid space;
- (5) M4: Metastatic disease outside of the CNS.

The greater propensity of MB to metastasize by comparison to other types of CNS tumours poses challenges for effective treatment development (R. E. Taylor et al., 2005). Analysis of 547 MB patients across multiple clinical trials demonstrated the direct correlation

between high M-stage and poor clinical outcome (Ellison et al., 2011; Kortmann et al., 2000; Zeltzer et al., 1999). Of note, extraneural metastases (Chang M4-stage) are rare, only occurring in 1-5% of MB patients and are often related to ventriculoperitoneal shunt complications (Muioio et al., 2011).

Advancements in diagnostic testing, imaging techniques, molecular and histopathological analysis, and treatment modalities substantially increased the overall survival of MB patients over the past 40 years. Five-year survivorship among standard- and high- risk patients now range from 70-86% and 59-70%, respectively (Gandola et al., 2009; Jakacki et al., 2012; Packer et al., 2006; Ramaswamy et al., 2016; R. E. Taylor et al., 2003). However, particularly troubling is the fact that MB survivors still experience severe neurocognitive, neuroendocrine, and developmental long-term sequelae, along with the uncertainty of secondary tumour formation, irrespective of the best current treatment protocols (Laughton et al., 2008; Mabbott, Penkman, Witol, Strother, & Bouffet, 2008; Mabbott et al., 2005; Palmer et al., 2013; Spiegler, Bouffet, Greenberg, Rutka, & Mabbott, 2004).

1.2 Histopathological and molecular classification of medulloblastoma

1.2.1 Histopathology

Additional complexity emerged from histological and cytogenic profiling of MB, which combined with clinical parameters, revealed that it is not a single disease entity. Based on such features, the 2007 World Health Organization (WHO) classification of CNS tumours

stratified MB into five subtypes – (i) classic, (ii) desmoplastic/nodular, (iii) MB with extensive nodularity, (iv) large cell, and (v) anaplastic MB (Louis et al., 2007; Ruser, Wu, Eberhart, Taylor, & Wechsler-Reya, 2014). This order also denotes the histological progression of each subtype, such that large cell and anaplastic MB are considered to be highly malignant. Given the substantial degree of cytological overlap between these subtypes, large cell and anaplastic MB are often grouped together as large cell/anaplastic histology and correlate with poor clinical outcome. However, as multiple histological subtypes were observed in a single tumour biopsy, this system provided limited prognostic value (Kool et al., 2012; Louis et al., 2007; M. D. Taylor et al., 2012).

1.2.2 Current molecular subgroups and clinical prognosis

Unsupervised hierarchical clustering of bulk primary MB tumours led to the stratification of four distinct molecular subgroups – Wingless (WNT), Sonic Hedgehog (SHH), Group 3 and Group 4 MB (Kool et al., 2008; Northcott et al., 2011; M. D. Taylor et al., 2012; Thompson et al., 2006). These subgroups account for 10%, 30%, 25% and 35% of all MB patients, respectively (J. Wang, Garancher, Ramaswamy, & Wechsler-Reya, 2018). Each are associated with a unique clinical, genomic, epigenomic, gene expression, and histological profile (e.g., age at diagnosis, somatic single-nucleotide variants (SNVs) and copy number alterations, cytogenetics, clinical outcome, pattern of patient relapse, incidence of metastasis). Constituent activation of WNT and SHH signaling pathways characterize WNT and SHH MB, respectively; however, Group 3 and 4 MB lack defined mechanisms of action for driving their initiation and progression (Kool et al., 2008;

Northcott et al., 2011; M. D. Taylor et al., 2012; Thompson et al., 2006). Such differences in tumour biology across each molecular subgroup relate to their varied responses to therapy. Integrative genomic analyses confirmed that these subgroups guide patient prognosis (Cho et al., 2011; J. Wang et al., 2018). Patients diagnosed with WNT MB have a favourable clinical outcome. Constitutive WNT activation in MB mediated by mutant *CTNNB1* expression and/or nuclear stabilization of β -catenin, leads to abnormal fenestration of the vascular endothelium, which comprises the blood-brain barrier (BBB) (Clifford et al., 2006; Phoenix et al., 2016). The resulting porosity and corresponding lack of a functional BBB in genetic mouse models of human WNT MB make these tumours vulnerable to systemic, cytotoxic chemotherapy regimens – even vincristine, which was previously shown to have limited BBB penetration (Boyle, Eller, & Grossman, 2004; Phoenix et al., 2016; Verstappen et al., 2005). Aberrant vasculature and paracrine signaling formed in WNT MB contribute to excellent patient survival, even upon rare, metastatic WNT MB tumours. This is in stark contrast to SHH MB, and particularly the aggressive non-WNT/SHH MB subgroups. Group 3 and 4 MBs are associated with a high incidence of tumour recurrence and metastasis – both of which are indicators of poor clinical outcome (M. D. Taylor et al., 2012). Overall, SHH and Group 4 MB have intermediate patient prognosis, while Group 3 MBs are associated with extremely poor outcomes (i.e., best to worst survival: Wnt > SHH > Group 4 > Group 3) (Fults, Taylor, & Garzia, 2019).

Development of integrative genomic algorithms enabled further division of these four molecular subgroups into twelve subtypes (i.e., two WNT, four SHH, three Group 3, and

three Group 4 MB subtypes), demonstrating intra-subgroup (termed intertumoral) heterogeneity based on somatic copy-number aberrations, differentially activated signalling pathways, and clinical prognosis (Cavalli et al., 2017). This robust intra-subgroup classification system expedited discussions of clinical trials focused on de-escalation of conventional chemoradiotherapy treatment for WNT MB and infant subgroups of SHH MB, as such patients have low risk of relapse and favourable prognosis (Cavalli et al., 2017; Kuzan-Fischer, Guerreiro Stucklin, & Taylor, 2017). This new stratification also underscores the presence of three distinct subtypes within Group 3 MB:

- (a) Group 3 α frequently metastasizes upon diagnosis in infants and young children, yet patients hold the best clinical outcome (66.2% 5-year survival) relative to other Group 3 subtypes;
- (b) Group 3 β is found in children and adolescents with high expression of growth factor independent 1 (GFI1) family transcription factor and amplification of orthodenticle homeobox 2 (*OTX2*), in which patients hold intermediate 5-year survival (55.8%) based on other subtypes in this subgroup;
- (c) Group 3 γ is present in infants and young children with v-myc avian myelocytomatosis viral oncogene homolog (*MYC*) amplification and high frequency of metastasis, which confers the worst patient prognosis (41.9% 5-year survival).

Even upon re-classification of MB, Group 3 α , β , and γ MB collectively hold the worst 5-year overall survival among all subtypes in each of the four molecular subgroups (Cavalli et al., 2017). Additionally, MB patient outcomes are increasingly hindered by the disease's

paucity of somatic SNVs, extensive intertumoral heterogeneity, low tumour incidence relative to its adult brain tumour counterpart (i.e., incidence rate of glioblastoma (GBM) is more than double the rate of MB, at 40.6 per 1,000,000 people annually), and prominent research focus on the primary, rather than the recurrent disease (Walker, Davis, & Affiliates, 2019).

Overall, an integrated approach to MB diagnosis has redefined previous predictors of prognosis. Both histological and molecular variants should be taken into account when determining risk stratification and thereby treatment protocols. As outlined by the WHO, Group 3 MB patients with classic histology are considered to have a standard-risk tumour, while large cell/anaplastic histology clinically correlates with high-risk prognosis (Louis et al., 2016). Hill *et al.* (2015) also noted that large cell/anaplastic histology defines high-risk strata, as does *MYC* amplification, *TP53* mutation, chromosome 17 defects, and disease dissemination. Similarly, Ramaswamy *et al.* (2016) emphasized that Group 3 MB patients with metastases have very high-risk tumours. MBs harbouring somatic *TP53* mutations were initially thought to be an independent predictor of poor clinical outcome (Tabori et al., 2010). However, this was later shown to be subgroup dependent, as WNT MB patients with *TP53* mutations have excellent prognosis (Lindsey et al., 2011; Ramaswamy, Nor, & Taylor, 2015; Zhukova et al., 2013). In Group 3 MB, these mutations are not commonly observed; rather, they are prevalent at relapse, often associated with *MYC* amplification (Hill et al., 2015). In addition, the most common cytogenetic feature of Group 3 MB is isochromosome 17q, which constitutes a coordinate loss of chromosome 17p and gain of

chromosome 17q. This occurs in 40% of Group 3 MB patients and correlates with poor survival (Shih et al., 2014).

1.2.2.1 Developmental origins of medulloblastoma subgroups

To develop improved therapeutic strategies, it is necessary to have a comprehensive understanding of the biology and specifically, the cell of origin for MB. However, patient-to-patient variability and intertumoral heterogeneity convolute this investigation, which ultimately confounds the development of effective, curative therapies (Pugh et al., 2012).

WNT MB is thought to originate from cells in the extracerebellar lower rhombic lip of the developing brain stem (Gibson et al., 2010). SHH, Group 3, and Group 4 MB were previously described to arise in the cerebellum (Kawauchi et al., 2012; P. Li et al., 2013; Pei et al., 2012; Wallace, 1999; Wechsler-Reya & Scott, 1999). Previous data suggested that SHH and Group 3 MB arise from granule cell precursors (GCPs) and Nestin-expressing cells, respectively, while Group 4 MBs are part of the glutamatergic cell lineage (Northcott et al., 2012b; Schuller et al., 2008; Z. J. Yang et al., 2008). Until recently, no definitive evidence has validated this speculation.

While transcriptomic sequencing of bulk MB tumours provided these molecular insights, such techniques cannot render a more detailed picture of the dynamics of MB tumorigenesis. Researchers must instead look at individual cellular subpopulations. Recent advancements in sequencing technology now offer a unique opportunity to analyze single

cells within bulk tumours to deconstruct the heterogeneous cell populations that drive tumour initiation and progression (Suva & Tirosh, 2019). For the first time, Vladoiu *et al.* (2019) exploited in-depth single-cell RNA sequencing (scRNA-seq) to elucidate the cells of origin for cerebellar MB subgroups (SHH, Group 3, and Group 4 MB). Unbiased scRNA-seq of normal murine cerebella was performed at several embryonic and post-natal timepoints, which aimed to discern the underlying transcriptomics of the developing cerebellum, and by extension how this development goes awry in MB. This enabled the identification of 30 cell clusters (or cell types), which when coupled with pseudo-time trajectory analysis, allowed the authors to pinpoint when specific cell lineages arose in normal development. Expression of stem cell marker, Nestin, (Nestin+) was prevalent in early cerebellar development, after which neuronal cells related to various neurotransmitters (glutamatergic and GABAergic) primarily appeared. Glial cells were seen at a relatively later timepoint in normal development. To validate this model, the group referenced mouse/human orthologues when conducting bulk RNA sequencing of 145 MB (60 SHH, 40 Group 3, and 45 Group 4 MB) patient-derived tumour samples. Comparison of specimen cell types to normal murine cerebellar cell clusters confirmed previous literature and speculation of the cell of origin or lineage for each subgroup. Cells identified from SHH MB were most similar to GCPs as previously suggested; however, they demonstrated a substantial degree of intertumoral heterogeneity, which further validates the recent sub-stratification of SHH MB into four subtypes (Cavalli *et al.*, 2017; Vladoiu *et al.*, 2019). Group 3 MB cell clusters best matched to Nestin+ and GABAergic cell clusters, while also showing resemblance to GCP and unipolar brush cells (UBCs) (Vladoiu *et al.*,

2019). Building on previous reports, this study demonstrated that Group 4 MB samples best matched with UBCs, which descend from the glutamatergic cell lineage, suggestive that glutamatergic neurons and UBCs are the putative cells of origin for this subgroup (Hovestadt et al., 2019; Vladoiu et al., 2019).

As results from bulk RNA sequencing of these cerebellar MB tumours were consistent with scRNA-seq of normal murine cerebellar cells, the next logical comparison involved scRNA-seq of human MB tumours. As such, scRNA-seq analysis of 8 MB patient samples (2 SHH, 2 Group 3, and 4 Group 4 MB) yielded results consistent with their initial findings from bulk RNA sequencing (Vladoiu et al., 2019). While scRNA-seq of normal human cerebellar cells would be the ideal comparator to transcriptomic data of human MB, clinical opportunities to collect such samples are rare. Even with this limitation, findings from scRNA-seq suggest that Group 3 MBs demonstrate multi-lineage differentiation, such that this subgroup may be derived from an uncommitted cerebellar stem cell (Vladoiu et al., 2019). Consistent with this hypothesis is scRNA-seq analysis of 25 patient and patient-derived xenograft (PDX) MB samples that identified the molecular programs within each subgroup (Hovestadt et al., 2019). Here, the authors reported on the differentiation gradient between Group 3 and Group 4 MB; dominated by undifferentiated progenitor-like cells and differentiated neuronal-like cells, respectively (Hovestadt et al., 2019). This data aligns with previous findings, which emphasized the overlap in transcriptional and epigenetic signatures of non-WNT/SHH MB (Cho et al., 2011; Northcott et al., 2017). Furthermore,

alterations in stem cell maintenance and differentiation in Group 3 MB further support the notion of an early cerebellar stem cell origin.

1.2.2.2 Stem cells vs. cancer stem cells

Canadian scientists, Ernest McCulloch and James Till first identified the presence of adult stem cells in the 1960s, upon transplantation of bone marrow cells into irradiated mice. Through *in vivo* assays, they observed hematopoietic stem cell colonies formed in the spleen (Becker, McCulloch, & Till, 1963; Siminovitch, McCulloch, & Till, 1963). Equally important was the understanding that stem cells required functional characterization. This involves the use of specific markers and assays to determine whether a single cell has the capacity to give rise to macroscopic colonies (Siminovitch et al., 1963).

Self-renewal defines the unique quality of stem cells. As a determinant of stemness, self-renewal describes the ability of a parental cell to symmetrically or asymmetrically divide, generating either two identical daughter cells, or a combination of an identical and differentiated progeny, respectively (Yoo & Kwon, 2015). This property can be tested using a surrogate *in vitro* assay, whereby a single cell is plated in chemically defined media and visually observed for the presence or absence of a clonal, spherical colony of cells (Reynolds & Weiss, 1992, 1996). Consequently, this single-cell derived sphere formation assay is considered to be a surrogate assay for stem cell activity. Modification to this experiment to conduct a limiting dilution analysis (LDA), wherein various cell densities

are plated (e.g., 1 to 1,000 cells), can measure the frequency of these colonies, and in turn the frequency of prospective stem cells (Seyfrid et al., 2019).

A similar sub-population of stem cells were described in cancer, in which the spherical stem cell-derived colonies are termed tumorspheres. This denotes cancer stem cells (CSCs), which represent a small population of stem cells that drives tumorigenesis. Based on the CSC hypothesis, CSCs constitute the apex of the cellular hierarchy within tumours. CSCs were initially discovered in acute myeloid leukemia (AML) by Lapidot *et al.* in 1994. Here, the authors noted that a small fraction of human AML cells was phenotypically similar to normal hematopoietic stem cells, but the former were responsible for propagating the disease upon transplantation into immunodeficient mice. Cell surface markers, CD34+ CD38-, distinguished these AML CSCs from the remainder of the cell population (Bonnet & Dick, 1997; Lapidot et al., 1994). Similar CSC populations were later discovered in breast, brain, colon, and lung tumours, amongst other cancers (Al-Hajj, Wicha, Benito-Hernandez, Morrison, & Clarke, 2003; Eramo et al., 2008; O'Brien, Pollett, Gallinger, & Dick, 2007; Ricci-Vitiani et al., 2007; Singh et al., 2003; Singh et al., 2004). Irrespective of tumour type, CSCs can self-renew, differentiate, and recapitulate the immunophenotype of the primary tumour upon engraftment into immunocompromised mice (Kurpios et al., 2013). As a result, the gold standard for CSC functional experiments include both *in vitro* LDA and secondary sphere formation assays, and most importantly, *in vivo* tumour formation assays (Singh et al., 2004; Zhong, Astle, & Harrison, 1996). Specifically, *in vivo*

LDA can elucidate the frequency of tumour-forming CSCs, whereby various cell densities of an often-heterogeneous population of tumour cells are injected into mice.

1.2.2.3 Identification of medulloblastoma stem cells

Prior to these studies, a stem cell origin was postulated to drive MB tumorigenesis, given the marked resemblance between somatic and CSC mechanisms (Pardal, Clarke, & Morrison, 2003; Reya, Morrison, Clarke, & Weissman, 2001). Singh and colleagues identified CSCs specific to the brain, termed brain tumour-initiating cells (BTICs), which they determined were marked by CD133, a human neural stem cell marker (Singh et al., 2004; Uchida et al., 2000). Surrogate *in vitro* and *in vivo* stem cell assays elucidated that the CD133+ sub-population of human brain tumours (MB and GBM) propagate tumour initiation, recurrence, and metastasis. Moreover, Reya and colleagues demonstrated that determinants of stemness contribute to treatment failure and relapse, irrespective of whether such factors are present in the bulk tumour or rare clonal cells (Reya et al., 2001). This is in stark contrast to the remaining non-BTIC cell fraction that exhibit marked therapy-sensitivity, lack self-renewal capacity, and are unable to reform tumours at low clonal densities (Singh et al., 2003; Singh et al., 2004).

Individual cells within the bulk MB tumour may have variable proliferative, self-renewal, and differentiation ability, but BTICs still hold the greatest capacity to reform tumours. As a result, the overarching question in MB research concerns whether these BTICs emerge from de-differentiation of a normal brain cell, or a transformation event of a normal human

neural stem cell (hNSC) or progenitor cell (Reya et al., 2001). With significant brain tumour heterogeneity, a multi-potential cell of origin is highly plausible, particularly due to the presence of several neural lineage phenotypes with distinct gene expression profiles and cell surface markers (Pardal et al., 2003).

While normal and cancer stem cells undergo similar proliferation, differentiation and cell survival processes, self-renewal remains at the forefront of these shared stem cell properties. Upregulation of self-renewal in distinct clonal cells at diagnosis is thought to drive MB recurrence and metastasis (Reya et al., 2001; Wu et al., 2012). The presence of this rare sub-population of MB cells that retains the unique properties of somatic stem cells ensues MB tumour progression, resistance to conventional therapy, and disease dissemination (Dean, Fojo, & Bates, 2005).

1.3 Medulloblastoma recurrence

1.3.1 Genetic divergence between primary and recurrent specimens

Our current knowledge of MB is largely based on research investigating the bulk tumour population of treatment-naïve samples. Any therapeutic regimen identified to be effective on these specimens are poised to fail in treatment-refractory lesions, as recent studies provided insight on the complexity of recurrent MBs. Such literature indicated that local and metastatic recurrences of MB retain their subgroup affiliation from the tumour at diagnosis, but are highly genetically divergent from their matched primary tumour (Morrissy et al., 2016; Ramaswamy et al., 2013; Wu et al., 2012). Such differences arise

from the genetic changes that occur during tumour evolution, in which a minor clone present at diagnosis becomes the dominant clone driving recurrence (Morrissy et al., 2016). Unfortunately, this finding hinders data extrapolation of primary to recurrent tumour samples.

1.3.2 Local vs. metastatic tumour recurrence

Despite advances in molecular research and multimodal therapies, 25-40% of SHH, Group 3, and Group 4 MB patients experience tumour recurrence (Shih et al., 2014). Between 1991 and 2012, Ramaswamy and colleagues (2013) investigated whether particular subgroups favoured local (primary tumour bed) or metastatic (spinal cord) sites to establish a thriving recurrent nidus. In delineating these subgroup-specific recurrence patterns, they indicated that SHH MB recur locally, while metastatic recurrences were common in Group 3 and 4 MB tumours. Conversely, they noted that while WNT MBs are able to recur at both local and distal sites, this occurrence is rare (Ramaswamy et al., 2013; Shih et al., 2014). Even upon tumour recurrence, WNT MB patients can be more easily salvaged with conventional therapies, unlike relapsed MB patients with differential subgroup association (Ramaswamy et al., 2013). With improved diagnostic imaging, MRI detected that dissemination patterns of Group 3 MB are often diffused multifocal or laminar in comparison to the nodular pattern in SHH and Group 4 MB (Zapotocky et al., 2018). The latter were more frequently isolated focal metastases. In addition, Group 4 MB metastases were not exclusive to one location, arising in the supratentorial (cerebrum), infratentorial (cerebellum), suprasellar (above skull depression; contains pituitary gland), and spinal

regions of the CNS. Unlike SHH and Group 3 MB, Group 4 MB metastases were highly specific to the suprasellar region (Zapotocky et al., 2018).

In most cancer types, metastasis involves the epithelial-to-mesenchymal transition (EMT), wherein neoplastic cells relinquish their strong cell-cell adhesion for mesenchymal characteristics to be more migratory and invasive (Valastyan & Weinberg, 2011). This paradigm for hematogenous metastases consists of cell invasion into the extracellular matrix of the primary tumour site, intravasation into the bloodstream, extravasation out of the bloodstream to a distant organ, and colonization of a macroscopic metastasis (Fults et al., 2019). Conversely, MB dissemination undergoes an analogous invasion-metastasis cascade. The most frequent route of metastasis involves seeding of the leptomeningeal surfaces of the brain and spinal cord (hereafter, termed leptomeningeal metastases) (A. J. Gajjar, Robinson, G. W., 2014). The proposed mechanism at which MB spinal metastases develop was recently described: (i) tumour *initiation* where clonal expansion occurs, (ii) *dispersal* where metastatic clones move away from the primary site, (iii) after-which *colonization* of the surviving clones seed the leptomeningeal space to form the distal recurrence (Ramaswamy & Taylor, 2017).

In keeping with this mechanism, metastatic MB was initially posited to directly enter the CSF, given the close proximity of its origin (cerebellum) and the CSF-filled fourth ventricle (Fults et al., 2019). Characteristics of these metastases not only include enhanced migration and invasiveness, similar to other hematogenous metastases, but also weakened cell-cell

adhesion to promote leptomeningeal metastasis initiation. A recent study provided extensive data to support the hypothesis that MB can also metastasize via the bloodstream, by developing a MB parabiosis model (Garzia et al., 2018). Here, MB cells were grafted into the cerebellum of one immunodeficient mouse (donor), after-which the circulatory systems of the donor and another mouse (recipient) were surgically joined. The absence of interconnecting CSF channels and patency of the parabiosis system was then confirmed. As circulating MB tumour cells were found in the recipient mouse, the authors concluded that MB can metastasize through the vascular system, despite the CSF pathway offering a lower resistance route (Garzia et al., 2018). The relationship between leptomeningeal dissemination and the hematogenous system was previously supported with increased levels of vascular endothelial growth factor in patients with leptomeningeal metastasis (Herrlinger et al., 2004).

1.3.3 Clinical outcome of medulloblastoma recurrences

Clinical studies aim to integrate the molecular classification of MB into trial design for treating local and metastatic relapsed patients. However, current treatment protocols for these patients lack standardization, contributing to their unsuccessful clinical outcome. Patients with treatment-refractory MB carry an alarmingly high mortality rate, which account for nearly 10% of all pediatric cancer-related deaths (Pizer & Clifford, 2009). Disease management is focused on improving the quality of the patient's remaining life, as opposed to curative treatment. Therefore, relapsed MB patients are often limited to palliative care, as few therapeutic options exist beyond clinical trials, where salvage rates

are less than 10%, irrespective of treatment modality (Ramaswamy et al., 2013; Sabel et al., 2016).

The propensity of MB to metastasize almost exclusively to the spinal and intracranial leptomeninges through the CSF or blood poses additional challenges for treatment. In particular, MB leptomeningeal metastases strongly correlates with poor clinical prognosis amongst relapsed patients. Over 90% of relapsed MB patients present with leptomeningeal metastasis at autopsy, suggestive that current cytotoxic agents are particularly ineffective against treating MB metastatic recurrences (Allen & Epstein, 1982; Deutsch & Reigel, 1980; Heideman, 1979; Neville & Blaney, 2005). While only 3-5% of all cancer patients develop leptomeningeal metastases, disease dissemination occurs in nearly 40% of children with MB at diagnosis and nearly all patients at the time of tumour recurrence, where Group 3 MB metastatic recurrences constitute the majority (Chamberlain, 2010; J. Wang et al., 2018). Specifically, the incidence of Group 3 MB metastasis accounts for 40-45% of MB cases, as opposed to 10-15% and 35-40% in SHH and Group 4 MB, respectively (J. Wang et al., 2018). With the high incidence of recurrence and metastasis that are characteristic of Group 3 MB, relapsed patients of this subgroup have the worst clinical outcome with a ~50% chance of 5-year survivorship (Cavalli et al., 2017; M. D. Taylor et al., 2012). Given the failure rates of conventional therapies, the understanding of Group 3 MB metastatic recurrences is particularly encumbered by the rare clinical opportunities in which these often-inoperable specimens may be collected from relapsed patients. Therefore,

appropriate model systems to study this Group 3 MB metastatic recurrences are necessary to develop efficacious therapies to improve patient survival and quality of life.

1.3.4 Medulloblastoma leptomeningeal metastases

Our current understanding of MB leptomeningeal metastases is greatly limited to experimental studies from immortalized cell lines, genetically modified models, and one patient-derived brain and recurrent spinal metastasis matched pair, with particular focus on SHH MB dissemination (Callegari, Maegawa, Bravo-Alegria, & Gopalakrishnan, 2018; Gao, Lv, Zhang, Wang, & Chen, 2018; Garner et al., 2018; Garzia et al., 2018; Gholamin et al., 2017; Grausam et al., 2017; Grunder et al., 2011; Hatton et al., 2008; Jenkins et al., 2014; Mumert et al., 2012; Rodriguez-Blanco et al., 2019; Santhana Kumar et al., 2015; Wu et al., 2012). This research includes gene expression analysis that showed increased CD47 expression in the metastatic compartment by comparison to the primary tumour site (Gholamin et al., 2017). Macrophage-mediated phagocytosis showed potential in preclinical models of primary and metastatic Group 3 MBs and other malignant pediatric brain tumours, whereby a humanized CD47 antibody blocked anti-phagocytic interaction of CD47-SIRP α (Gholamin et al., 2017). Another targeted study reported efficacy of UAB30, a synthetic retinoid or vitamin A compound, in reducing CD133+ cell proliferation, migration, invasion, and tumour metastasis in Group 3 MB commercial cell lines, as previously shown in neuroblastoma (Garner et al., 2018). Additionally, genetic knockdown of tripartite motif containing 59 was resulted in a reduction of migration and invasion in immortalized SHH and Group 3 MB cell lines (Gao et al., 2018). Transforming

growth factor beta (TGF- β) contributes to MB metastasis by regulating pro-migratory basic fibroblast growth factor, which leads to MB cell invasion (Santhana Kumar et al., 2018). They provided better understanding of the interactions leading to tumour dissemination by identifying that adapter protein, FRS2 regulated tissue infiltration induced by these growth factors. Minigene ontology analyses showed enhanced TGF- β signalling pathway in Group 3 MB that is mediated by SMAD2/3, which in turn, is implicated in tumour metastasis (Ferrucci et al., 2018). Additionally, the Database for Annotation, Visualization and Integrated Discovery identified insulin signalling as a shared pathway amongst human MB metastases (Wu et al., 2012). NOTCH1 signalling pathway is also involved in Group 3 MB metastasis, whereby NOTCH1 activates BMI1 through the induced expression of TWIST1. Intrathecal injections of a NOTCH1-blocking antibody served to increase survival and reduce the frequency of spinal metastases in mice with MB (Kahn et al., 2018).

1.3.4.1 Current models of metastatic medulloblastoma

Wu et al. (2012) generated a Sleeping Beauty transposon model, wherein a specific transposase was expressed in the precursors of cerebellar granule neurons of transgenic mice. Addition of this Sleeping Beauty transposition led to disease metastasis, in a model system that would otherwise develop non-metastatic tumours (Wu et al., 2012). Transposon mutagenesis identified 584 candidate metastasis-driving genes of SHH MB. This includes the following encoded proteins: LIM homeobox protein (LHX1), Rab GDP dissociation inhibitor (GDI2), protein kinase B (AKT), cysteine-cysteine motif chemokine ligand (CCL2), cysteine-cysteine motif chemokine receptor (CCR2), cell cycle-related kinase

(CCRK), embryonic stem cell-expressed Ras (ERAS), and Aryl hydrocarbon nuclear translocator/hypoxia-inducible factor 1 β (ARNT). Of note, AKT and ERAS are activated in the phosphatidylinositol 3-kinase (PI3K) signalling pathway and mediate tumour cell invasion (Fults et al., 2019). In addition, chemoattractant cytokines recruit inflammatory monocytes and trigger their differentiation into phagocytic macrophages, which helps foster a tumorigenic microenvironment. These genes, all of which confer metastatic characteristics, coincide with the proposed 3-stage cascade of MB leptomeningeal dissemination. Specifically, Rab-GDI2, thrombospondin-1 (TSP1), LHX1, MYC, receptor tyrosine kinase (c-Met), hepatocyte growth factor (HGF), and Spint2 are thought to play a role in migration, invasion, and dissociation in the initiation stage. PI3K signalling, B-cell lymphoma 2 (Bcl-2), and p53 suppress apoptosis to allow for the survival of tumour cells through dispersal. Lastly, colonization is marked by proliferation and inflammation, which is the predominant function of the CCL2-CCR2 axis (Fults et al., 2019). Garzia *et al.* (2018) confirmed that metastatic MB samples highly express CCL2. They noted that it was required for leptomeningeal dissemination, and was thereby likely to drive clonal evolution of primary MB into metastatic recurrences (Garzia et al., 2018).

Consistent with previous findings, the function of MYC corroborates with the stem cell origin hypothesis for Group 3 MB. The *MYC* oncogene fosters an uncommitted and proliferative cell state in embryonic stem cells (Smith & Dalton, 2010). It was shown to promote cerebellar stem cell proliferation *in vitro* (Pei et al., 2012). This MYC-induced stem cell-like state also promotes cell motility and invasive properties through suppression

of TSP1 expression. TSP1 contributes to cell-cell adhesion and inhibits angiogenesis (Bornstein, 1995; Mirochnik, Kwiatek, & Volpert, 2008). In MB, *MYC*-amplification leads to loss of TSP1 and thereby increased migration and invasion of MB cell lines (Zhou et al., 2010). As a high affinity ligand for receptor CD47, low TSP1-CD47 axis in *MYC*-driven Group 3 MB might weaken cell adhesion, promoting leptomeningeal metastases (Gholamin et al., 2017; Rogers et al., 2017). Collectively, *MYC*-amplified Group 3 γ MB appear molecularly poised to metastasize. Given the positive correlation between *MYC* expression and poor patient prognosis, there is a dire need to develop effective therapeutic options for these patients.

Few animal models reliably generate *MYC*-driven human MB tumours. One PDX model with treatment-refractory *MYC*-amplified Group 3 MB cells displayed survival benefit of mice treated with palbociclib, a dual inhibitor of cyclin-dependent kinase 4 and 6 (Cook Sangar et al., 2017). However, this study did not specifically focus on disease recurrence or dissemination. Most notably, Pei *et al.* (2012) generated a mouse model, by which aggressive tumours developed from transplantation of cerebellar stem cells that were coinfecting with viruses expressing *Myc* and dominant-negative *p53*. From this model, it was reported that BET inhibitor, JQ1, reduced *MYC* expression and cell viability of *MYC*-driven Group 3 MB cells (Bandopadhyay et al., 2014). Modification to the model involved the addition of a dominant-negative form of cyclin dependent kinase inhibitor 2C that also conferred similarly aggressive *MYC*-driven Group 3 MB tumours, which were sensitive to folate pathway inhibitors (Morfouace et al., 2014). Assessment of human MB patient

biopsies at diagnosis and relapse confirmed *MYC* and *p53* as biomarkers of Group 3 MB recurrence (Hill et al., 2015). Shortly after, Pei *et al.* (2016) used their model system to show histone deacetylase (HDAC) inhibitors as a potent therapy for *MYC*-driven Group 3 MB patients. This group found that such agents work in part to enhance the expression of tumour suppressor, *FOXO1*, and synergize with *PI3K* inhibitors to inhibit tumour growth (Pei et al., 2016). Despite the molecular and pathological resemblance to human Group 3 MB, the caveat of these models is the fact that dominant-negative *TP53* SNVs are infrequent in Group 3 MB, while complete loss of one copy of *TP53* is most common (Ramaswamy et al., 2015).

1.3.4.2 Singh lab model of Group 3 γ medulloblastoma recurrence

The prominent focus on leptomeningeal dissemination in SHH MB models would be better positioned to study Group 3 MB metastases, specifically at the time of tumour recurrence. The Singh lab aimed to develop a more robust model system that mimics the aggressive and rapidly progressive clinical disease of Group 3 MB recurrence (unpublished data). Given the rarity of patient biopsy at disease recurrence and metastasis, this model enables the collection of human Group 3 MB cells from mouse brains and spinal cords to enable further investigation on the mechanisms driving MB metastatic recurrence. Development of our established PDX mouse-adapted therapy model provides a robust platform to recapitulate the treatment administered in the clinic. To model the human disease, intracranial xenografts of BTIC-enriched, *MYC*-amplified patient-derived Group 3 MB cells (HD-MB03: primary MB, SU_MB002: treatment-refractory MB) were performed in

non-obese diabetic severe combined immunodeficiency (NOD SCID) mice. Mice were divided into control and treatment cohorts, in which the latter received standard chemoradiotherapy regimens (Figure 1a). Following MRI to confirm engraftment and treatment administration, NOD SCID mice were sacrificed once the control group reached endpoint to assess tumour burden and survival advantage. RNA sequencing of HD-MB03 samples validated the genetic disparities between the tumour at engraftment and recurrence by identifying the subset of genes enriched at post-chemotherapy, post-irradiation and relapse timepoints. Functional studies confirmed increased aggressiveness of MB throughout therapy, as noted by experiments evaluating proliferation, self-renewal, and BTIC frequency following tumour formation. The study of tumorigenesis from the perspective of key stem cell properties, such as self-renewal, laid the foundation of this model system. Characterization of the genes regulating self-renewal identified the treatment-refractory population of MB cells that drive tumour relapse.

1.4 Summary of intent

Tumour recurrence and dissemination are common amongst Group 3 MB patients, by comparison to other subgroups. This is particularly frequent in *MYC*-amplified Group 3 MB, which constitutes the worst prognosis amongst all subtypes. These patients face mortality rates of virtually 100%. Current salvage therapies for these relapsed MB patients are cytotoxic and ineffective, especially for those with leptomeningeal metastases, which are often inoperable. This highlights a pivotal gap in current research.

With the rarity of tumour sample collection at patient relapse, the Singh lab developed a reliable and robust PDX model of recurrent MB. This model system recapitulated the therapies administered in the clinic and enabled the isolation of Group 3 γ MB metastatic recurrences. Given our limited understanding of treatment-refractory Group 3 γ MB metastases, we turned to published data on *MYC*-driven MB recurrence, MB leptomeningeal metastases, and other metastatic tumours, which emphasized the efficacy of kinase and HDAC inhibition. Therefore, we hypothesized that screening of kinase and HDAC inhibitors would identify effective therapeutic agents that selectively target treatment-refractory, Group 3 γ MB leptomeningeal metastases.

CHAPTER 2: Materials & Methods

5.1 Cell cultures

Treatment-refractory Group 3 MB (SU_MB002), which was kindly provided by Dr. Yoon-Jae Cho (Oregon Health and Science University, OR, United States of America), was derived from a patient sample, who received only cyclophosphamide and displayed expression markers of Group 3 MB (Facchino, Abdouh, Chato, & Bernier, 2010). SU_MB002 were cultured in NeuroCult Complete media (NCC), consisting of NeuroCult™ NS-A Basal Medium (STEMCELL™ technology #05750) supplemented with NeuroCult™ Supplement, 20ng/mL epidermal growth factor, 10ng/mL fibroblast growth factor, 0.1% heparin and 1% penicillin-streptomycin. To visualize spinal metastases in future *in vivo* experiments SU_MB002 were transduced with a lentiviral vector expressing enhanced Firefly luciferase (pCCL-effLuc-PuroR). Lentiviral production first

involved culturing Lenti-X HEK 293T cells in Dulbecco's Modified Eagle Medium (DMEM; Life Technologies #11965-118), supplemented with 10% fetal bovine serum (FBS), 1% sodium pyruvate, 1% non-essential amino acids and 1% L-glutamine. Replication-incompetent lentiviruses were produced by co-transfection of the Luciferase vector and packaging vectors pMD2G and psPAX2 in Lenti-X HEK29T using Lipofectamine 3000, as recommended by the manufacturer (Thermo Scientific). Viral supernatants were harvested 48 hours after transfection, filtered through a 0.45 μm cellulose acetate filter and concentrated by ultracentrifugation at 15,000 rpm for 2 hours at 4°C. The viral pellet was resuspended in 1 mL of media, aliquoted and stored at -80°C. For transductions, 5.0×10^5 SU_MB002 cells were plated in NCC in 6-well tissue-culture-treated plates. Cells were incubated in a humidified incubator at 37°C with 5% CO₂ for 8 hours, prior to adding 1 mL of NCC. Twenty-four hours post-transduction, an additional 2 mL of NCC was given to cells. Puromycin (1 $\mu\text{g}/\text{mL}$) in 1mL of NCC was added 72 hours after transduction and incubated for 48 hours, after which experiments were conducted.

Primary Group 3 MB (HD-MB03), which were provided by Dr. Robert Wechsler-Reya (Sanford Burnham Prebys Medical Discovery Institute, CA, United States of America), were cultured in NCC and supplemented with 10% of FBS. HD-MB03 cells were seeded in NCC 24 hours prior to *in vitro* experiments and preparation for intracranial injections. Following isolation of human MB cells from mouse spine samples at tumour recurrence (Figure 1a), culture conditions were consistent with original cell lines (i.e., HD-MB03-Re-

sp cultured in NCC supplemented with 10% FBS; NCC only conditions before experimentation).

Human fetal neural stem cells (hNSCs) were isolated using a previously described protocol (Venugopal et al., 2012) and were cultured in NCC. Unlike SU_MB002 and HD-MB03 that were directly plated on 10cm cell culture dishes (Thermo Fisher Scientific #150466), hNSCs first require coating prior to plating cells on 10cm cell culture dishes. This includes incubating 20% poly-L-ornithine (Sigma #P4957) in sterile DNase, RNase and protease free water for 1 hour in 37°C incubator, and subsequently 0.5% laminin (BD Biosciences #354232) in phosphate buffered saline (PBS; Thermo Fisher Scientific #10010049) for 2 hours. Prior to experimentation, hNSCs were enzymatically dissociated into single cells with 1X TrypLE™ Express Enzyme (Thermo Fisher Scientific #12605028).

All cell cultures are frozen stepwise into -80°C freezer and liquid nitrogen conditions, in media comprising of NeuroCult™ NS-A Basal Medium, NeuroCult™ Supplement, and 10% dimethyl sulfoxide (DMSO; Sigma D2650). Upon thawing low passages of each cell culture, we aimed to complete experiments within as short of a timeframe as possible. For culturing cells, all lines were placed in a humidified incubator at 37°C with 5% CO₂.

5.2 Patient-derived xenograft mouse-adapted therapy model

All *in vivo* experiments were conducted in strict accordance with McMaster University's Animal Research Ethics Board. Intracranial injections of HD-MB03 and SU_MB002, were

performed in NOD SCID mice, as previously described (Singh et al., 2004). Based on previous optimization studies (unpublished data), appropriate number of live cells (i.e., 1×10^6 cells of HD-MB03, 5×10^4 cells of SU_MB002), as determined by Trypan Blue exclusion (Thermo Fisher Scientific #15250061) via Countess™ II Automated Cell Counter (Thermo Fisher Scientific #A27977), were resuspended in 10-12 μL of PBS for injections. NOD SCID mice were anesthetized with isoflurane gas (5% induction, 2.5% maintenance) and cells were injected into the frontal lobe using a 10 μL Hamilton syringe. Mice were divided into five cohorts: control, engraftment, radiation, chemoradiotherapy, and relapse. Treatment consisted of 2 Gy of craniospinal irradiation (14 days post-engraftment), as well as single doses of cisplatin (2.5 mg/kg; 21 days post-engraftment), vincristine (0.4 mg/kg; 21 days post-engraftment) and cyclophosphamide (75 mg/kg), 22 days post-engraftment) (unpublished data).

Mice in the relapse cohort were administered a combination of these modalities. Mice were sacrificed when the control cohort reached endpoint (i.e., includes but is not limited to, head swelling, 25% reduction in weight loss, head tilt, and deviations from typical behaviour) to assess tumour volume. Relapsed mice survived longer than control mice and were sacrificed upon tumour recurrence (i.e., determined by mouse endpoint). Mouse brain and spines were isolated from each timepoint and processed for cell culturing, as previously described (Venugopal et al., 2012).

5.3 Inhibitors

Compounds in the high-throughput screen were used from frozen stocks from the David Braley Human Stem Cell Screening Facility, which were initially supplied by the Ontario Institute for Cancer Research (OICR). The annotated library of 640 kinase inhibitors are described in Figure 1b. Other compounds used were HDAC inhibitors, which were provided by the Gunning lab. They include belinostat, citarinstat, ricolinostat, and vorinostat, as well as novel HDAC6-selective inhibitors – compound N1, compound N2, compound N3, compound T1, compound T2, and compound T3. Top five screen hits (i.e., BI 2536, CHIR-124, Hesperadin, JNJ-10198409, and SB-218078) provided by the OICR, and HDAC inhibitors were dissolved in DMSO to 10 mM and further diluted to appropriate final concentrations in NCC upon time of experimentation.

5.4 Fluorescence-activated cell sorting

Tumorspheres were dissociated into single cells and resuspended in PBS, supplemented with 2mM EDTA (Thermo Fisher Scientific #15575020). The viability dye 7-Aminoactinomycin D is used to exclude dead cells by penetrating compromised membranes and directly bind to DNA (Arndt-Jovin & Jovin, 1989). Live cells were sorted using MoFlo XDP Cell Sorter (Beckman Coulter) directly into assay plates. Additionally, human TRA-1-85/CD147 APC-conjugated antibody (R&D Systems #FAB3195A) allowed for the isolation of human MB cells from extracted mouse brains and spinal cords.

5.5 Large scale high-throughput screening

5.5.1 Z prime (Z') assay and optimization

Single cells of HD-MB03-Re-sp were sorted into a 96-well tissue-culture-treated plate by Moflo XDP Cell Sorter at densities of 500, 1,000, 2,000, 2,500 cells/per well in 200 μ L of (i) NCC, (ii) NCC + 10% DMEM, or (iii) DMEM, in quadruplicates and were incubated for 48-72 hours in a humidified incubator at 37°C with 5% CO₂. DMSO (0.1%) was the negative control for cell death, as compounds from the OICR library were initially resuspended in it. Puromycin and belinostat (0.1%) were used as positive controls for cell death. Variations in media conditions were used to determine whether a specific culture medium yielded better separation in readout values between positive and negative controls, over others. Prior to readout of the Z' assay, we proposed that if results from all three conditions were comparable, NCC + 10% DMEM should be used for the high-throughput screen, as these cells typically grow in NCC, whilst DMEM was significantly less expensive than NCC. Furthermore, we reasoned this to be appropriate as additional validation experiments with screen hits would be completed in NCC. Based on these results, conformational Z' assays for hNSCs and SU_MB002-Re-sp were completed in NCC only conditions, which produced similar results. After 48-72 hours, PrestoBlue™ Cell Viability Reagent (Thermo Fisher Scientific #A13262), which measures cell viability *via* fluorescence of cell metabolism, was manually added to each treated and media control wells. Fluorescence intensity was measured 4 hours after the addition of PrestoBlue™, by FLUOstar Omega Fluorescence 556 Microplate reader (BMG LABTECH) at excitation and emission wavelengths of 540nm and 590nm, respectively. Results were analyzed by

Omega software. The following calculations were used to determine the respective Z' values for DMSO versus puromycin, and belinostat. Only the former comparison was shown below for simplicity (Dell, 2012).

- (1) Calculate low (DMSO) and high (Puromycin) readouts for each raw value from FLUOstar Omega Fluorescence 556 Microplate reader.

$$\text{Low: } \frac{\text{DMSO}_{\text{Raw Value}} - \text{DMSO}_{\text{Average}}}{\text{Puromycin}_{\text{Average}} - \text{DMSO}_{\text{Average}}}$$

$$\text{High: } \frac{\text{Puromycin}_{\text{Raw Value}} - \text{DMSO}_{\text{Average}}}{\text{Puromycin}_{\text{Average}} - \text{DMSO}_{\text{Average}}}$$

- (2) Average all low and high readouts, in each respective group.
- (3) Calculate standard deviation (STDEV) amongst both groups.
- (4) Calculate absolute value of averages.

$$|\text{DMSO}_{\text{Average}} - \text{Puromycin}_{\text{Average}}|$$

- (5) Taken together, calculate the following.

$$Z' = 1 - \left(\frac{3(\text{DMSO}_{\text{STDEV}} - \text{Puromycin}_{\text{STDEV}})}{|\text{DMSO}_{\text{Average}} - \text{Puromycin}_{\text{Average}}|} \right)$$

Cell density experiments in hNSCs and SU_MB002-Re-sp were completed in NCC only conditions and readout after 72-hour incubation.

5.5.2 High-throughput screen

HD-MB03-Re-sp cells were plated in NCC 24 hours prior to experimentation. Approximately 2,500 cells/well were seeded by Multidrop™ Combi Reagent Dispenser into 96-well tissue culture treated plates, following drug treatment. Microlab Nimbus

dispensed 1mM stock of kinase inhibitors into intermediate dilution plates with DMEM, resuspended solution, and subsequently transported 20 μ L/well to the corresponding 96-well plates. DMSO and Puromycin controls were plated at alternating terminals of each row on the plates (i.e., Puromycin plated in A1, B12, etc.; DMSO plated in A12, B1, etc.) to ensure proper comparison of cell viability with tested compounds. Screen experiments were conducted in duplicates with 1 μ M as the final concentration of drugs and controls (0.1% of total well volume). Following 72-hour incubation, PrestoBlue™ was added by the Multidrop™ Combi Reagent Dispenser and fluorescence intensity was measured by the FLUOstar Omega Fluorescence 556 Microplate reader. Cell viability percentage was calculated by dividing the intensity value in the presence of a particular compound by DMSO value in the respective row. Mean and standard deviation between duplicates were determined by Omega software. Drugs in which one or both replicates indicated 50% or more reduction in cell viability (i.e., 47 compounds) were marked as screen hits.

5.6 Madin-Darby canine kidney strain II (MDCKII) assay

5.6.1 MDCKII cell culture

MDCKII cells were derived from a heterogenous parental line (Dukes, Whitley, & Chalmers, 2011). MTOX1301 cell line (Sigma Aldrich) represent control MDCKII cells, wherein canine multidrug resistance protein 1 (cMDR1), otherwise known as canine p-glycoprotein (cP-gp), efflux transporter gene was knocked out in both alleles (MDCK11 cMDR1 KO). Similarly, MTOX1303 cells (Sigma Aldrich) contain no endogenous cMDR1 (cP-gp), but were transfected with human MDR1 (hMDR1, or hP-gp; MDCK11 hMDR1

KI). Low passages of both MDCKII cell lines were cultured in DMEM medium, supplemented with 10% FBS, 1% non-essential amino acids, 0.2% normocin, and 0.1% gentamicin. 3.2×10^5 cells/mL of each MDCKII cell lines were manually seeded on high density polyethylene terephthalate membrane inserts (1.0 μm pore size, 31 mm^2 surface area), with 15 mL of media plated on the basolateral side. Cell plates were placed in a humidified incubator at 37°C with 5% CO_2 for 72 hours. 400 μL of media was then added to the apical side of the membrane, while the basolateral side was replaced with fresh media. Cell cultures were left in incubators for an additional 24 hours prior to experimentation.

5.6.2 MDCKII permeability assay

Plates (described above) with MDCKII cell cultures on polyethylene terephthalate membrane inserts were used for this assay. The assay plates were washed with Hank's balanced salt solution (HBSS) twice, prior to measurements of transepithelial/transendothelial electrical resistance to confirm membrane integrity. Either dosing or receiving buffer was added to wells. The dosing buffer consisted of 25 mM HEPES-HBSS buffer (pH 7.4), supplemented with 1 μM atenolol, 1 μM metoprolol, and 50 μM Lucifer yellow, along with 5 μM of a drug candidate. 25mM HEPES-HBSS buffer alone comprised the receiving buffer.

The permeability from the apical to basolateral (AB) side of the membrane, and the reverse (BA) were used to determine the permeability of each drug. To test AB permeability,

dosing and receiving buffers were added to the apical (250 μ L) and basolateral (1 mL) chambers, respectively in duplicates, while the opposite was done for BA permeability (i.e., dosing buffer added to basolateral chamber, receiving buffer added to apical chamber). Plates were then incubated at 37°C on a 150 rpm shaker for 1 hour. At this time, aliquots were taken from each chamber. Acetonitrile (3x aliquot volume taken for measurements), which contains 20 nM verapamil, was then added to each sample aliquot (i.e., if 100 μ L sample was taken, 300 μ L solution with acetonitrile and verapamil was added). Verapamil was the internal standard, which helps to classify whether a drug candidate has low or high permeability (Volpe, 2010). Plates were then incubated on shaker for 2 minutes. Samples were then analyzed by liquid chromatography-mass spectrometry (LC/MS) *via* Waters Xevo quadrupole time-of-flight mass spectrometer, with a narrow-extraction mass window technique to ensure higher selectivity, as well as determine relative peak intensities (Glauser et al., 2016).

5.6.3 MDCKII assay data analysis

Permeability coefficient (P_{app}), post-assay recovery (PAR), efflux ratio (ER), and KI/KO ratio were determined based on the following formulas:

$$(1) P_{app} = \left(\frac{dC}{dt}\right) \left(\frac{1}{A \times C_0}\right),$$

where dC/dt represents the slope of the cumulative concentration in the receiving chamber versus time, A is the surface area of the MDCKII cell monolayer, and C_0 is the initial drug concentration in the dosing buffer.

(2) $PAR = \frac{((V_r \times C_r^{final}) + (V_d \times C_d^{final}))}{(V_d \times C_0)}$, where V_r and V_d are the volumes in the receiving and donor chambers, respectively, while C_r^{final} and C_d^{final} are the cumulative concentrations of drug in the corresponding receiver and donor chambers, and C_0 is the initial drug concentration in the dosing buffer.

$$(3) ER = \frac{P_{app}(BA)}{P_{app}(AB)}$$

$$(4) \frac{KI}{KO} \text{ ratio (or P-gp substrate)} = \frac{ER(KI)}{ER(KO)}$$

Of note, acceptance criteria for PAR was denoted as: good ($\geq 50\%$), moderate ($\geq 25\%$ to $< 50\%$), low ($< 25\%$), rejected ($< 15\%$). Dinacilib (compound 44 on Percepta list) was used as a positive control; $KI/KO=6.0$.

5.6.4 Liquid chromatography-mass spectrometry (LC/MS)

Drug concentrations were measured with an Acquity UPLC HSS T3 (2.1 x 100 mm, 1.7 μm) column, using ACQUITY UPLC II system. The mobile phase consisted of 0.1% formic acid in water (solvent A) and 0.1% formic acid in acetonitrile (solvent B). A gradient was established from 100% to 5% solvent A in 4.5 minutes, which was held for 30 seconds, and returned to 100% in 30 seconds, after which equilibrating the column took place for 1 minute. For mass spectrometric analysis, Waters Xevo QToF mass spectrometer with an electrospray ionization source and LockSpray ion source was employed. Source parameters included capillary voltage (0.8kV), cone voltage (25V), source temperature (150°C), desolvation temperature (500°C), and desolvation gas flow (600 L/hr). Accuracy in mass measurements was acquired by LockSpray automated exact mass measurement mode,

where leucine-enkephalin was used as a reference substance. Data was analyzed by MassLynx 4.1 software.

5.7 Cell viability

Single cells of HD-MB03, HD-MB03-Re-br, HD-MB03-Re-sp, SU_MB002, SU_MB002-Re-br, SU_MB002-Re-sp, and hNSCs were sorted into a 96-well tissue-culture-treated plates by Moflo XDP Cell Sorter at an appropriate cell density per well (i.e., 2,500 cells/well for dose response studies to determine IC₅₀ and 1,000 cells/well for assessing cell viability at IC₈₀ concentration in LDA assays, described below) in 200 µL of NCC in quadruplicates for each sample and incubated for three days. DMSO was the control for each experiment, as DMSO was the vehicle for all compounds tested. Given the potency of the kinase inhibitors to the metastatic MB cells to hNSCs, drug studies (refer to *Chapter 3*) involved treatment of cells with four-fold dilutions from 2 µM to 7.6 pM (0.1%). Only two-fold dilutions of HDAC inhibitors from 5 µM to 9.8 nM were required to capture the dose response curves of these inhibitors (refer to *Chapter 4*). After 72-hour incubation of inhibitor or DMSO treatment, 10% PrestoBlue™ was added to each well to estimate percent cell viability, as described in *Chapter 2: Section 2.5.1 Z prime (Z') assay and optimization*. Prism 6 software was used to construct dose response curves and IC₅₀ values were determined by plotting percent cell viability versus transformed dilutions of inhibitors on a logarithmic (log₁₀) scale. Henceforth, IC₅₀ values refer to the effective concentration of drug at which cell viability was reduced by 50%. IC₈₀ concentrations were determined

by the following formula: $IC_{(F)} = [(100-F)/F]^{1/HS} \times IC_{50}$, where F = desired percent response (i.e., 80 for 80% reduction in cell viability), HS = Hill Slope.

5.8 Sphere formation assays

A tumorsphere arises from a single self-renewing BTIC when cultured *in vitro* in serum-free conditions (Bellows & Aubin, 1989). Quantification of BTIC frequency involved identifying the number of cells capable of forming a single tumorsphere, through *in vitro* LDA. To determine this, single cells of all three cell lines were sorted into a 96-well tissue culture treated plate by Moflo XDP Cell Sorter at cell densities from 1,000 cells/well to 1cell/well, in quadruplicates for each treatment or control. Spheres were manually counted and defined as five or more cells in contact with each other. The percentage of wells without spheres for each respective cell density (*y-axis*; F_0) were scored 72 hours post-treatment and plotted against the number of cells per well (*x-axis*; x). Results were plotted using Prism 6 software. To form at least one tumorsphere in each well, the number of cells required were specified by the point where the line crosses the 0.37 level ($F_0 = e^{-x}$) (Bellows & Aubin, 1989; Tropepe et al., 1999). Concurrently, *in vitro* secondary sphere formation assays were performed. Tumorspheres in wells with a density of 200 cells/well in both treated and control wells were counted to assess the self-renewal capacity of cells.

CHAPTER 3: Identification of kinase inhibitors that effectively target recurrent

Group 3 γ medulloblastoma leptomeningeal metastases

3.1 Role of kinases in normal vs. cancer system

Nearly every signal transduction process almost unanimously occurs through a phosphorylation signalling cascade (Fabbro, Cowan-Jacob, & Moebitz, 2015; Manning, Whyte, Martinez, Hunter, & Sudarsanam, 2002). At the crux of these processes are kinases, which through coordinated action, add high-energy phosphate groups to specific serine, threonine or tyrosine residues. The human genome encodes 538 protein kinases (Manning et al., 2002). Functionally, these enzymes play an important role in cell proliferation, differentiation, migration, apoptosis, metabolism, and effector functions (Ardito, Giuliani, Perrone, Troiano, & Lo Muzio, 2017). Therefore, dysregulation of kinases has been implicated in various human cancers, amongst other diseases.

3.1.1 Implications of kinase inhibitors in medulloblastoma

Multiple studies have reported kinase inhibitors as effective therapeutic modalities to treat MB (MacDonald, Aguilera, & Castellino, 2014; Park et al., 2019). Recent data demonstrated the anti-neoplastic effects of combinatorial PI3K and mammalian target of rapamycin (mTOR) inhibition in SHH MB (Eckerdt et al., 2019). High-throughput screening of casein kinase 2 inhibitors in SHH MB exhibited marked sensitivity of one such compound (CX-4945) to temozolomide, a chemotherapeutic agent commonly used to treat GBM patients and in ongoing clinical trials for advanced MB patients (Nitta et al., 2019). Polo-like kinase (PLK) inhibitors were effective in treating high-risk pediatric patients with

MYC-amplified Group 3 MB, alone and in combination with bromodomain and extra-terminal motif (BET) inhibitor (MK-8628) (Han et al., 2019; Triscott et al., 2013). Previously, metastatic MB patient samples also showed enhanced kinase and growth factor receptor signalling (MacDonald et al., 2001). Moreover, effective multimodal approaches targeting metastatic melanoma, breast cancer, esophageal squamous cell carcinoma, renal cell carcinoma, and brain metastases involved the inhibition of PI3K and mitogen-activated protein kinase (MAPK) pathways (Aasen et al., 2019; Blazquez et al., 2018; Fatehi, Soltani, & Ghatrehsamani, 2018; B. Li et al., 2017; McKay et al., 2016; McRee et al., 2018). For the first time, we investigated the efficacy of kinase inhibitors against treatment-refractory Group 3 γ MB leptomeningeal metastases.

3.2 Results

To screen for compounds that target Group 3 γ MB metastatic recurrences, we isolated human *MYC*-driven Group 3 MB cells from the spinal compartment of relapsed mice (HD-MB03-Re-sp) from our established PDX model (Figure 1a). Preliminary optimization experiments involved the determination of *Z* prime (*Z'*) scores, which translates to the distribution between the positive and negative controls for cell death (i.e., *Z'* > 0.5 indicates a good score; minimal overlap between controls) (Dell, 2012). Positive controls for cell death included (i) puromycin, as HD-MB03-Re-sp cells were not resistant to antibiotic selection, and (ii) belinostat, a pan-HDAC inhibitor that was previously identified to kill HD-MB03-Re-sp cells. To optimize the screening assay, HD-MB03-Re-sp cells were plated at varying cell densities from 500-2,500 cells/well and treated with either 1 μ M

puromycin, belinostat or DMSO (0.1%) for 48 and 72 hours in each of the three different culture media (Supplementary Figure 1a, b). Cell density plot for 48 and 72 hours were similar (data not shown). DMSO-treated wells displayed comparable cell proliferation levels to live, untreated cells, whereas puromycin and belinostat effectively inhibited MB cells cell growth, irrespective of media conditions. While variation between each media condition was miniscule, maximal separation between Z' distribution curves were observed in puromycin-treated cells, as compared to the DMSO control after 72-hour incubation with a cell density of 2,500 cells/well ($Z' = 0.71, 0.72, \text{ and } 0.79$ for NCC, DMEM, and NCC + 10% DMEM, respectively). Based on these results, we chose 1 μM puromycin in NCC + 10% DMEM with 2,500 cells/well at the 72-hour timepoint for our screen.

We proceeded with screening a kinase library comprised of 640 compounds from the OICR (Figure 1b). This library includes a large selection of compounds in various kinase classes, of which some are currently in clinical trials and others have been previously validated in preclinical studies. The remaining are tool compounds that have not yet been rigorously studied. All compounds were tested in duplicates at 1 μM and defined as screen hits based on at least one replicate exhibiting a reduction in cell viability by 50% or more. Of the 640 compounds screened, 47 compounds met this criterion, as indicated by the blue dashed line (Figure 1c). As expected, the effect of the compounds that were screened showed a normal distribution with respect to cell viability (Supplementary Figure 1c).

As cells driving recurrent Group 3 MB leptomeningeal metastases originate in the brain, we sought to investigate whether our screen hits could penetrate the BBB. If compounds were BBB permeable and deemed effective by functional studies, they could be administered either alone or in combination with standard chemoradiotherapy, as to preclude or suspend disease dissemination. We completed BBB permeability analysis on the 47 hits using *in silico* software, Percepta (Supplementary Table 1) and SwissADME (Supplementary Figure 1d). Percepta calculates physiochemical, toxicity, along with absorption, distribution, metabolism, and excretion (ADME) properties of compounds. Its BBB permeability (termed CNS permeability) prediction analysis depends on the rate of passive diffusion to permeability, as well as equilibration rates and distribution ratio of compound in brain tissue and plasma. SwissADME is a web-based tool that uses the graphical Brain Or Intestinal Estimated permeation method (BOILED-Egg), which in turn uses lipophilicity, the established Wildman and Crippen (WlogP) partition coefficient, and topological polar surface area (tPSA) to predict the gastrointestinal absorption and brain penetration of compounds (Daina, Michielin, & Zoete, 2017; Daina & Zoete, 2016). Eight compounds were predicted to be BBB permeable in one or both software (Supplementary Figure 1e). Of these 8 compounds, 3 were eliminated based on previous reports of toxicity (Supplementary Figure 1e). The workflow described above is shown in Figure 1d. We identified five kinase compounds (BI 2536, CHIR-124, Hesperadin, JNJ-10198409, and SB-218078) that target HD-MB03-Re-sp with *in silico* predicted brain penetration and no current evidence of toxicity in literature (Figure 1e). The targets of these five compounds

include aurora kinase B (AURKB), PLK1, checkpoint kinase 1 (CHK1), and platelet-derived growth factor receptor beta (PDGFR β).

To validate that these compounds do not induce neurotoxicity of normal neural stem cells *in vitro*, dose response studies (four-fold dilutions ranging from 2 μ M to 7.6 pM) were conducted on hNSCs and an additional biological replicate of Group 3 MB metastatic recurrences (SU_MB002-Re-sp) (Figure 2). Similar cell density optimization assays were conducted using these cells (Supplementary Figure 2). As anticipated, 2,500 cells/well provided maximal readout values and was therefore used in subsequent experiments. With the exception of BI 2536, all compounds showed varied responses in HD-MB03-Re-sp and SU_MB002-Re-sp cells. Irrespective of this finding, compounds were effective at inhibiting cell viability in recurrent metastatic Group 3 MB cells, while sparing hNSCs.

We next aimed to confirm the results from the *in silico* predicted BBB permeability analysis. Percepta predicted that all compounds, except CHIR-124 was brain penetrable, while SwissADME noted that CHIR-124, JNJ-10198409, and SB-218078 were likely BBB permeable. To further characterize the hits, an established and widely used *in vitro* BBB permeability assay, termed MDCKII assay was performed to determine which, if any of the five compounds were BBB permeable. This assay is considered to be an *in vitro* industry standard for evaluating CNS permeability and drug efflux (Thiel-Demby et al., 2009). The efflux ratio of compounds would indicate whether or not it undergoes active efflux and would thereby help determine which compounds to pursue further. This experiment was

conducted by the OICR. They first plated monolayers of hMDR1 KI and cMDR1 KO cells on polyethylene terephthalate membrane inserts. These cells orient themselves by polarity into an apical (representative of blood) and basolateral (representative of the brain) chambers. Upon dosing, compounds that acted as substrates of the hMDR1 would be transported out of the brain, and thereby had poor brain penetration (Figure 3a). Higher KI/KO ratios are characteristic of these such compounds, as evident in BI 2536, Hesperadin, and SB-218078. Conversely, compounds with lower the KI/KO ratio, like CHIR-124 (KI/KO=1.0) and JNJ-10198409 (KI/KO=0.8) translate to effective BBB permeability (Figure 3b). Preliminary optimization experiments from OICR determined that the $P_{app}(BA)$ value of MDCKII hMDR1 KI cells correlated with brain concentration, where lower values relate to better brain penetration (data not yet validated). As the $P_{app}(BA)$ value of CHIR-124 is quite low, this compound is considered to be the best candidate of the tested inhibitors; however, JNJ-10198409 showed the best KI/KO ratio. Therefore, this data validated the *in silico* modelling and provide rationale to pursue CHIR-124 and JNJ-10198409.

Functional profiling of these two inhibitors involved the assessment of their role in BTIC properties upon IC_{80} treatment. CHIR-124 and JNJ-10198409 significantly reduced cell viability (Figure 3c), as well as ablate the self-renewal capacity of both recurrent Group 3 MB metastases through *in vitro* secondary sphere formation and LDA assays (Figure 3d, e). Dose response assays were performed in the parental (HD-MB03 and SU_MB002) and relapsed brain cells (HD-MB03-Re-br and SU_MB002-Re-br) (Supplementary Figure 3a-

d). We anticipated that IC_{50} concentrations of both compounds would reveal a stepwise and uniform decrease from the parental to relapsed brain or spine cells. However, this was only the case for CHIR-124 in SU_MB002, compared to SU_MB002-Re-br and SU_MB002-Re-sp, as well as JNJ-10198409 in HD-MB03, compared to HD-MB03-Re-sp (Supplementary Figure 3e, f). Irrespective of these findings, dose response studies of CHIR-124 and JNJ-10198409 showed selectivity for all *MYC*-driven parental, relapsed brain, and relapsed spine Group 3 MB cell lines compared to hNSCs.

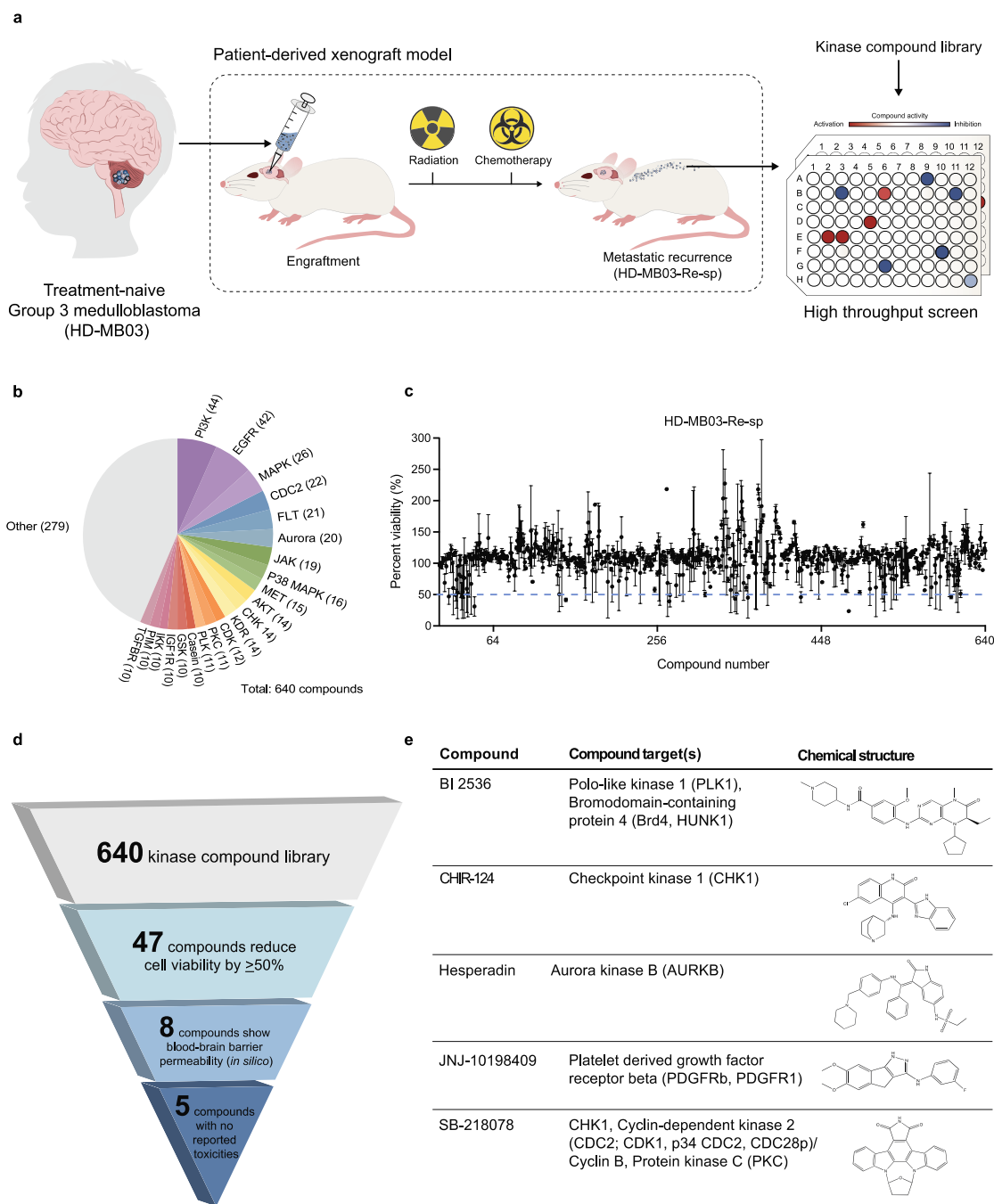


Figure 1. High-throughput screen identified kinase inhibitors that target Group 3y MB metastatic recurrences. (a) Schematic representation of patient-derived model of recurrent Group 3 MB spinal metastases and high-throughput screen. NOD SCID mice xenografted with treatment-naïve Group 3 MB cells (HD-MB03 and SU_MB002) were treated with 2 Gy of craniospinal irradiation (14 days post-engraftment), as well as cisplatin (2.5 mg/kg), vincristine (0.4 mg/kg) and cyclophosphamide (75 mg/kg; 21-22 days post-

engraftment for cisplatin/vincristine and cyclophosphamide, respectively). At endpoint, spinal metastatic cells at relapse (HD-MB03-Re-sp and SU_MB002-Re-sp, later not shown in figure) were harvested, isolated, and plated for chemical screen. **(b)** Major classes of 640 kinase compound library used in screen. Numbers in parentheses specify the number of compounds within each class. **(c)** Cell viability of recurrent Group 3 MB spinal metastatic cells (HD-MB03-Re-sp) following compound treatment. Cells (2,500 cells/well) were treated with 1 μ M of each compound or DMSO (0.1%) and incubated for 72 hours. Each point represents the mean of two technical replicates for a single compound, with percent viability calculated by dividing cell viability score of compound-treated by DMSO-treated wells for the respective row that was assayed. Error bars represent standard deviation. The dashed, blue line indicates reduction of cell viability by 50%; seen in at least one replicate of 47 compounds. **(d)** Stepwise workflow of filtering screen hits (47 of 640 compounds) include blood-brain barrier permeability via *in silico* software (Percepta and SwissADME; permeable in at least one software) and reported toxicity. Each tier of the flowchart shows the number of compounds that met each criterion; five compounds meet all criteria. **(e)** Table summarizes five hits from screen and subsequent filtering steps.

Abbreviations. PI3K, phosphoinositide 3-kinase; EGFR, epidermal growth factor receptor; MAPK, mitogen-activated protein kinase; CDC2, cyclin-dependent kinase; FLT, fms-like tyrosine kinase; JAK, janus kinase; AKT, protein kinase B; CHK, checkpoint kinase; KDR, kinase insert domain receptor; CDK, cyclin-dependent kinase; PKC, protein kinase C; PLK, polo-like kinase; GSK, glycogen synthase kinase; IGF1R, insulin-like growth factor 1 receptor; IKK, I kappa B kinase; PIM, proviral integration site for moloney murine leukemia virus; TGF β R, transforming growth factor beta receptor.

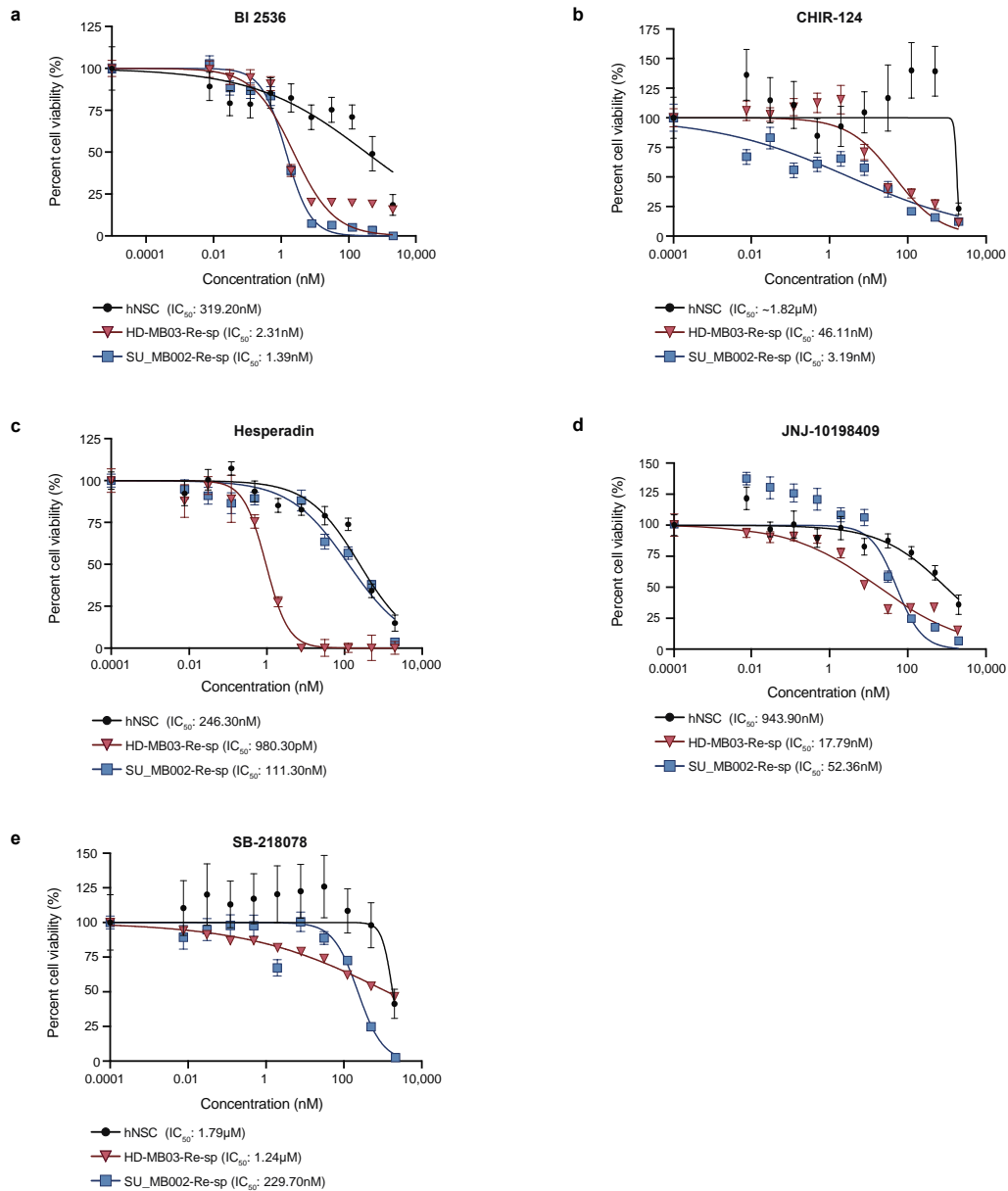


Figure 2. BI 2536, CHIR-124, Hesperadin, JNJ-10198409, and SB-218078 selectively targeted metastatic Group 3 γ MB cells at tumour recurrence and spared healthy neural cells. (a) B1 2536, (b) CHIR-124, (c) Hesperadin, (d) JNJ-10198409, and (e) SB-218078 kill metastatic recurrent Group 3 MB cells (n=2, HD-MB03-Re-sp and SU_MB002-Re-sp) at low nanomolar concentrations, but not neural stem cells (n=1, hNSC). Cells (2,500 cells/well) were treated with four-fold dilutions of inhibitors ranging from 2 μ M to 7.6 pM, or 0.1% DMSO for 72 hours. Points represent mean of at least three technical replicates, normalized to DMSO. Error bars represent standard error of the mean.

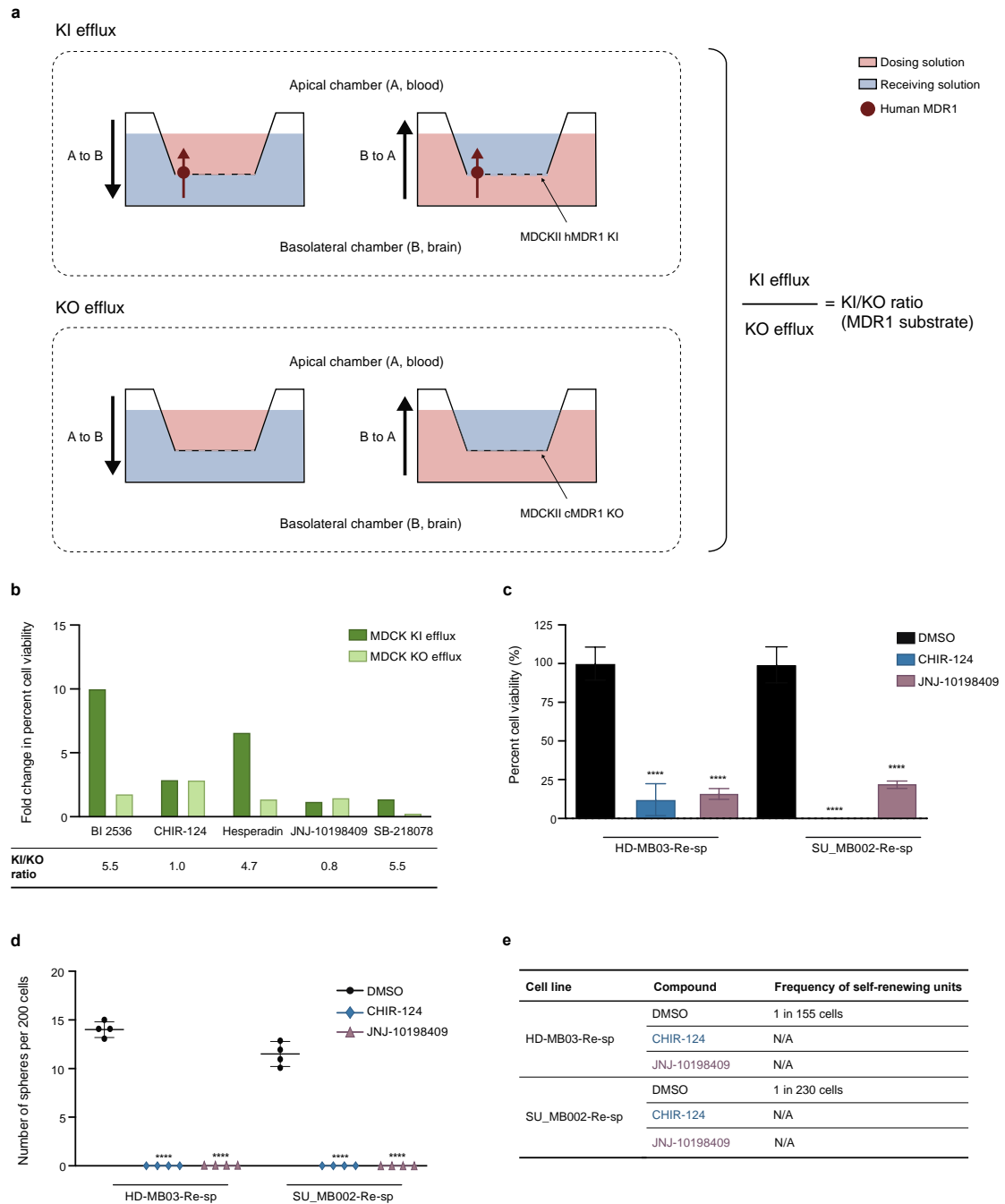
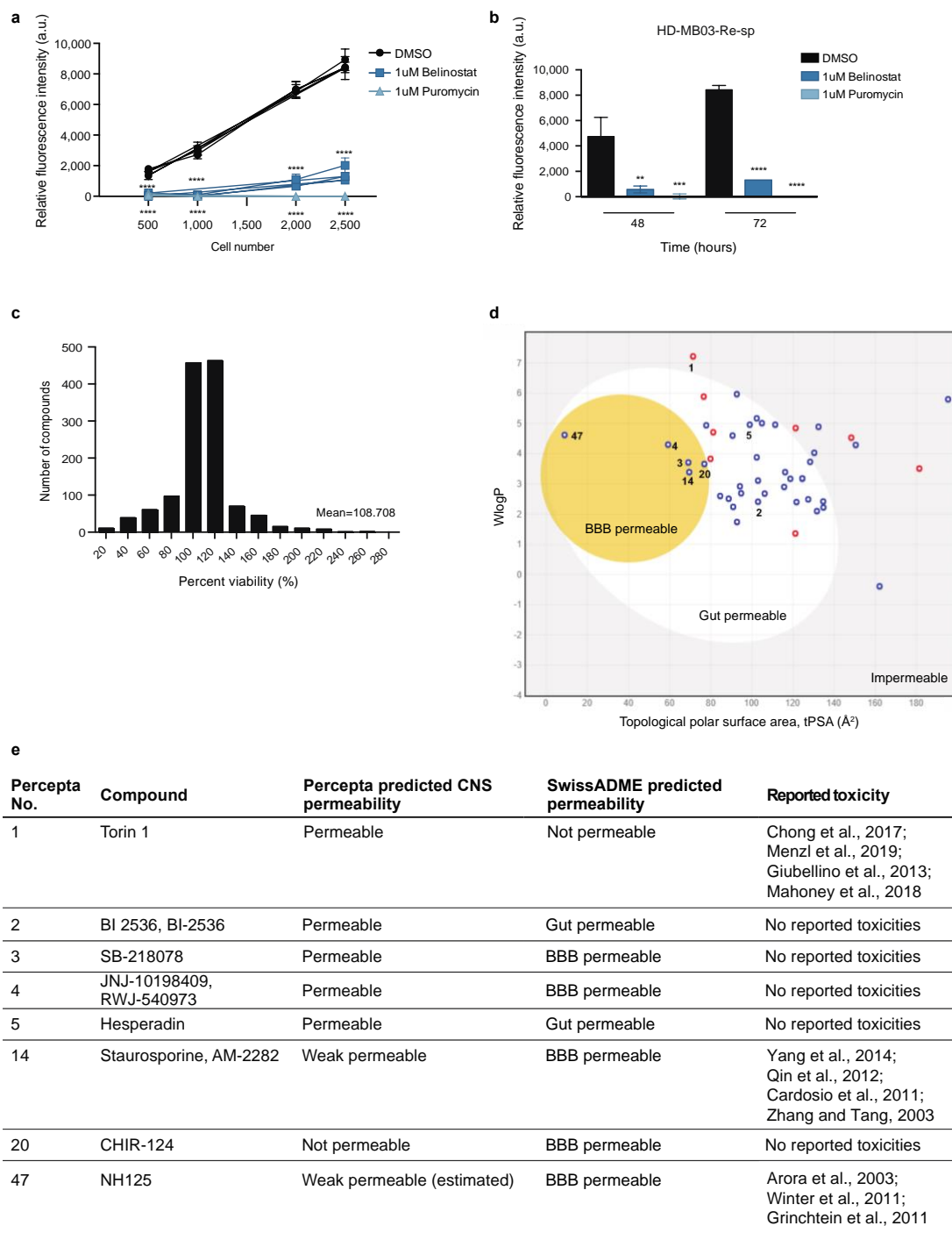


Figure 3. *In vitro* functional profile of CHK1 (CHIR-124) and PDGFR β (JNJ-10198409) inhibitors demonstrated reduced BBB permeability and stem cell properties. (a) Schematic of MDCKII BBB permeability assay. Monolayers of human MDCKII cells with multidrug resistant protein 1 knocked-in (MDCKII hMDR1 KI) and canine MDCKII cells with MDR1 endogenously knocked-out (MDCKII cMDR1 KO) were plated on cell membrane inserts. Inhibitors were dosed (pink) in either the apical (A; blood)

or basolateral (B; brain) chambers. The rate at which compounds cross the monolayer from their initial chamber to the other (blue) was measured by the amount of MDK1 substrate (red dot and arrow) and drug remaining in MDCKII hMDR1 KI and cMDR1 KO cells, respectively. **(b)** Results from this assay were used to calculate the KI or KO efflux, and thereafter the KI/KO ratio (listed below). The higher the KI/KO ratio, the more likely that the compound is a substrate of MDR1 and would be transported out of the brain. **(c)** Cell viability (1,000 cells/well), **(d)** self-renewal capacity (200 cells/well), **(e)** frequency of self-renewing units (1-1,000 cells/well) through LDA assays, were measured following drug treatment at 0.1% IC₈₀ concentration or DMSO for 72 hours. Points represent mean of at least three technical replicates. Error bars represent standard deviation. * $p \leq 0.05$, ** $p \leq 0.001$, *** $p \leq 0.0001$; **** $p \leq 0.00001$; unpaired t-test.

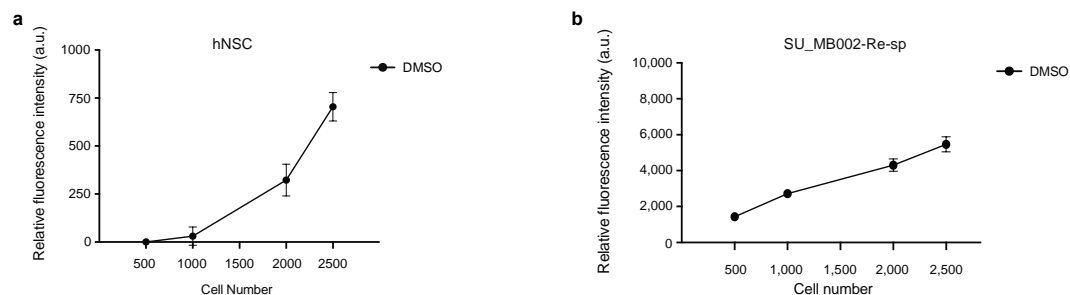


Supplementary Figure 1; Related to Figure 1. High-throughput screen optimization and filtering criteria. (a) Cell density measurement with various culture media conditions (n=3, NCC, NCC + 10% DMEM, DMEM) in HD-MB03-Re-sp cells after 72-hour incubation of 0.1% DMSO versus 1 μ M belinostat or puromycin (positive controls for cell

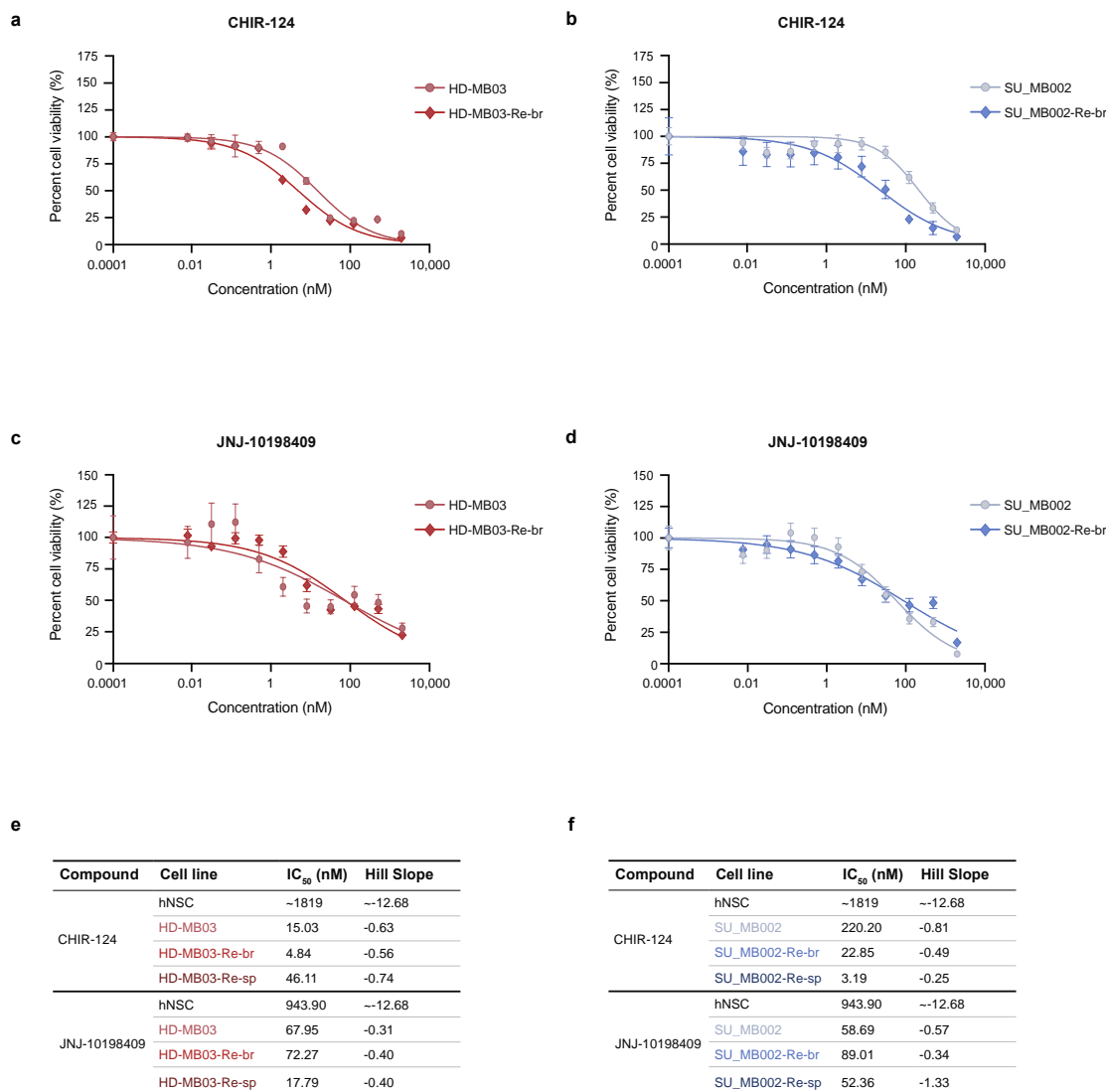
death). 48-hour incubation data not shown. **(b)** Cell viability measurement of HD-MB03-Re-sp to determine the most suitable positive control (1 μ M) and timepoint for readout (48 or 72 hours), in reference to live control (0.1% DMSO). Points (a) and bars (b) represent mean of at least three technical replicates. Error bars represent standard deviation. * $p \leq 0.05$, ** $p \leq 0.001$, *** $p \leq 0.0001$; **** $p \leq 0.00001$; unpaired t-test. **(c)** Histogram shows normal distribution of 640 screened compounds. **(d)** SwissADME BOILED-Egg plot displays distribution of compounds that are predicted to be BBB (yellow), gut (white) or no (grey) permeable. Numbers correlate to Percepta compound numbers (Table 1). Blue coloured points are predicted to be actively effluxed by MDR1; red coloured points are predicted as a non-substrate of MDR1. **(e)** Table summarizes additional filtering criteria of predicted BBB permeability (Percepta and SwissADME) and reported toxicity from preclinical studies.

Supplementary Table 1; Related to Figure 1. Predicted Percepta blood-brain barrier permeation properties of screen hits.

CNS permeability	No.	Compound	Compound target(s)	MW (Da)	CNS score
Permeable	1	Torin 1	Phosphatidylinositol 3-Kinase alpha (PI3Kalpha), Mammalian Target of Rapamycin (mTOR; FRAP1)	607.64	-2.66
	2	BI 2536, BI-2536	PLK1 (PLK, STPK13), Bromodomain-Containing Protein 4 (Brd4, HUNK1) Inhibitor	521.67	-2.76
	3	SB-218078	CHK1, CDC2 (CDK1, p34cdc2, CDC28p)/Cyclin B, PKC	393.40	-2.87
	4	JNJ-10198409, RWJ-540973	PDGFRb (PDGFR, PDGFR1)	325.34	-2.88
	5	Hesperadin	AURKB (AuroraB), Tyrosine Kinase inhibitor	516.66	-2.91
Weak permeable	6	K-252a, K-2151	TRKA (TRK), Na ⁺ /H ⁺ Exchanger (NHE) Inhibitor	467.48	-3.04
	7	PIK-75 hydrochloride	PI3K	488.74	-3.12
	8	BI-6727, volasertib	PLK1 (PLK, STPK13)	618.83	-3.14
	9	GDC-0032, RG-7604, Taselisib, L08J2O299M	Phosphatidylinositol 3-Kinase beta (PI3Kbeta), Phosphatidylinositol 3-Kinase alpha (PI3Kalpha), Phosphatidylinositol 3-Kinase gamma (PI3Kgamma), Phosphatidylinositol 3-Kinase delta (PI3Kdelta), Cytochrome P450 CYP3A4	460.54	-3.24
	10	AZD-2014, Vistusertib	mTOR Complex 1 (mTORC1) Inhibitor, mTOR Complex 2 (mTORC2) Inhibitor	462.55	-3.24
	11	ASC-069, APY 69	IRE1 (IRE1a, ERN1)	345.41	-3.25
	12	PI-103	PI3K	348.36	-3.27
	13	Gilteritinib, ASP2215, ASP-2215	AXL Kinase Inhibitor, Flt3 (FLK2/STK1) Inhibitor	552.72	-3.34
	14	Staurosporine, AM-2282	Pan kinase	466.54	-3.35
	15	Ro3280, RO-3280, Ro-5203280	Polo-like Kinase-1 (Plk-1) Inhibitors	543.62	-3.40
	16	Everolimus, RAD-001, Certican	FRAP (MTOR, FRAP1), FKBP12 (Rotamase), Angiogenesis inhibitor	958.24	-3.42
	17	AZD 7762, AZD-7762 hydrochloride	CHK1, CHK2	398.88	-3.50
Impermeable	18	BMS-754807	IGF1R (JTK13, IGFIR)	461.51	-3.59
	19	Alvocidib, HMR-1275, L-868275, MDL-107826A, NSC-649890, L-868276, Flavopiridol	CDC2 (CDK1, p34cdc2, CDC28p)/Cyclin B, CDK2/Cyclin A, CDK2/Cyclin E, CDK4/Cyclin D1, CDK6/Cyclin D3, CDK7, CDK9/Cyclin T1, Bcl-2, Mcl-1, Survivin, XIAP	401.84	-3.61
	20	CHIR-124	CHK1	419.91	-3.64
	21	VE-822, VX-970	ATR	463.56	-3.73
	22	TAE-684, NVP-TAE684	ALK	614.21	-3.74
	23	PKC-412, CGP41251, Midostaurin	FLT3 (STK1, FLK2)	570.65	-3.76
	24	SNS-314	AurA (AuroraA), AurB (AuroraB), AurC (AuroraC)	430.93	-3.78
	25	INK 128, INK-128, MLN0128, MLN-0128, MLN-128, TAK-228, JGH0DF1U03, Sapanisertib	mTOR Complex 1 (mTORC1), mTOR Complex 2 (mTORC2), Mammalian Target of Rapamycin (mTOR; FRAP1)	309.33	-3.83
	26	ASC-082, APY 82	IRE1 (IRE1a, ERN1)	395.47	-3.91
	27	VX-680, MK-0457, Tozasertib, VX6	AurA (AuroraA), AurB (AuroraB), AurC (AuroraC), ABL1 (ABL), FLT3 (STK1, FLK2), JAK2	464.59	-3.95
	28	NMS-1286937, NMS-P937	PLK1 (PLK, STPK13)	532.53	-3.96
	29	AZD 7762, AZD-7762 hydrochloride	CHK1, CHK2	398.88	-4.00
	30	PERK inhibitor, CP-22, CP-941222, PF-941222	PEK (PERK)	462.36	-4.10
	31	NVP-BEZ235, BEZ235, BEZ-235, Dactolisib	PI3K	469.55	-4.13
	32	WYE-125132, WYE-132	PI3K, FRAP (MTOR, FRAP1), mTORC1, mTORC2	519.61	-4.14
	33	Rapamycin, Sirolimus, Rapamune	FRAP (MTOR, FRAP1), CCR5 expression inhibitor	914.19	-4.17
	34	TCS JNK 5a	JNK1 (JNK), JNK2, JNK3, p38a	332.42	-4.22
	35	GDC-0980, G-038390, R-7422, RG-7422, Apatolisib	Phosphatidylinositol 3-Kinase (PI3K), Mammalian Target of Rapamycin (mTOR; FRAP1)	498.61	-4.32
	36	A-443654, A-654	AKT1 (PKBa)	470.40	-4.32
	37	Lestaurinib, CEP-701, KT-5555, SPM-924	FLT3 (STK1, FLK2), TRKA (TRK), JAK2	439.47	-4.34
	38	GSK-461364, GSK461364	PLK1 (PLK, STPK13)	543.61	-4.34
	39	LY-2606368	CHK1	365.40	-4.35
	40	AZD-1152-HQPA, Barasertib-HQPA	AurB (AuroraB)	507.57	-4.38
	41	Defactinib, PF-04554878, PF-4554878, VS-6063	Focal Adhesion Kinase 2 (FADK2; PTK2B; PYK2) Inhibitor, Focal Adhesion Kinase 1 (FADK1; PTK2) Inhibitor	510.50	-4.54
	42	ON-01910Na, Estybon, Rigosertib sodium, ON-1910Na, Onc-01910, SyB C-1101, SyB L-1101, Novonex	PLK1 (PLK, STPK13)	473.47	-4.65
	43	HDS 029	EGFR (ERBB1, HER1), ErbB2 (TKR1, HER2, NEU), ErbB4 (HER4)	355.76	-4.70
	44	Dinaciclib, MK-7965, NSC-727135, SCH-727965	CDK2/Cyclin A, CDK5/p25, CDC2 (CDK1, p34cdc2, CDC28p)/Cyclin B, CDK9/Cyclin T1	396.50	-4.79
45	Compound 71	DYRK1A (DYRK)	486.41	-5.14	
46	Cdk1/2 Inhibitor III	CDC2 (CDK1, p34cdc2, CDC28p)/Cyclin B, CDK2/Cyclin A	425.43	-5.92	
Weak permeable (estimate)	47	NH125	eEF2K activator	524.58	NA



Supplementary Figure 2; Related to Figure 2. Validation of optimal cell density plating in additional cell lines. Cell density measurements of 0.1% DMSO treated (a) hNSC and (b) SU_MB002-Re-sp cells were completed in NCC only conditions, after 72-hour incubation of 0.1% DMSO. Points represent mean of at least three technical replicates. Error bars represent standard deviation.



Supplementary Figure 3; Related to Figure 3. Dose response studies of CHIR-124 and JNJ-10198409 did not demonstrate selectivity to metastatic Group 3 γ MB cells at tumour recurrence. Four-fold dilutions of (a, b) CHIR-124 and (c, d) JNJ-10198409 from 2 μ M to 7.6 pM, or DMSO (0.1%) were plated with grafted Group 3 MB cells (HD-MB03, SU_MB002) and recurrent cells isolated from the brain (HD-MB03-Re-br, SU_MB002-Re-br) for 72 hours. Points represent mean of at least three technical replicates, normalized to DMSO. Error bars represent standard error of the mean. (e, f) Tables summarize data from dose response curves. Refer to *Chapter 2: Materials and Methods* for calculations in (e, f).

CHAPTER 4: Novel HDAC6 inhibitors target metastatic, treatment-refractory

Group 3 γ medulloblastoma

4.1 Role of histone deacetylases in normal vs. cancer system

Next-generation sequencing, methylation profiling and gene expression studies have determined that primary MB samples harbor mutations associated with epigenetic regulators, amongst other genetic alterations in oncogenes and tumour suppressors. One epigenetic modulator widely studied in the context of MB is histone deacetylase (HDAC) (Zwergel et al., 2018). This family consists of classes I (HDACs 1, 2, 3, 8), IIa (HDACs 4, 5, 7, 9), IIb (HDACs 6, 10) and IV (HDAC11) that catalyze removal of acetyl groups from lysine residues and promote gene silencing through chromatin condensation which block transcription (Kolbinger et al., 2018).

4.1.1 Implications of histone deacetylase inhibitors in medulloblastoma

HDAC inhibition has been shown to treat various hematological malignancies, along with MB (Zwergel et al., 2018) (mainly HDAC1, HDAC2, HDAC4, HDAC 6/8/10, class I HDACs and class IIa HDACs) (Canettieri et al., 2010; Ecker et al., 2015; Kolbinger et al., 2018; Lee et al., 2011; X. N. Li et al., 2005; Shu et al., 2006; J. Yuan, Llamas Luceno, Sander, & Golas, 2017). A recent study demonstrated that combining HDAC and MAPK/extracellular signal-regulated kinase (ERK) inhibitors may pose as an effective treatment for MB. Combining sodium butyrate, a class I and II HDAC inhibitor, with MAPK/ERK inhibition worked cooperatively to decrease MB proliferation (da Cunha Jaeger et al., 2020). Most interesting was the use of FDA approved pan-HDAC inhibitor,

panobinostat, which suppressed leptomeningeal seeding in commercialized Group 3 MB cell lines (Phi et al., 2017). Although promising, work on our patient-derived Group 3 MB lines would more accurately recapitulate metastatic recurrences of the human MB.

4.1.2 Migratory role of histone deacetylase 6 in cancer

Despite the use of HDAC inhibitors in MB, HDAC6 has yet to be studied. In comparison, HDAC6 is a widely characterized target in many other cancers due to its role in tumorigenesis, cell survival, motility, chemoresistance, and DNA damage response (Aldana-Masangkay & Sakamoto, 2011). HDAC6 inhibition resulted in cell cycle arrest and apoptosis in oral squamous cell carcinoma, while overexpression increased cell migration in multiple myeloma (Hideshima et al., 2005; Sakuma et al., 2006; Wickstrom, Masoumi, Khochbin, Fassler, & Massoumi, 2010). Dual HDAC6/8 inhibitor, BRD73954, effectively targets metastatic melanoma and hepatocellular carcinoma cells (J. Liu et al., 2016; Yin, Xu, Xu, Zheng, & Gu, 2018). Consistent with this study was the acceleration of metastatic traits in hepatocellular carcinoma cells upon HDAC6 overexpression (Kanno et al., 2012). In colorectal cancer metastases, SNAIL2, an important transcription factor involved in TWIST1-induced EMT, was shown to interact with HDAC6 (Hu et al., 2018). Subsequently, E-cadherin expression was inhibited, following recruitment of HDAC6 and polycomb repressive complex 2 to the promoter of E-cadherin, which promoted EMT, invasion and cell motility of colorectal cancer cells (Hu et al., 2018). HDAC6 expression mediated by ubiquitin-binding protein P62, promoted EMT in prostate adenocarcinomas (Jiang et al., 2018). Cooperation between HDAC6 and sirtuin 2 also promotes these

metastatic properties in bladder cancer (Zuo, Wu, Li, Zhao, & Chen, 2012). Virtual screening reported that HDAC6 inhibitors, particularly cefoperazone sodium, impede migration and invasion of human pancreatic cancer cells with an IC_{50} of $\sim 8.5 \mu\text{M}$ (Song et al., 2020). Even *in vitro* and *in vivo* models of triple negative breast cancer, which commonly metastasizes, demonstrated a significant reduction in metastasis upon HDAC6 inhibitor treatment (Hsieh, Tu, Pan, Liou, & Yang, 2019). In neuroblastoma, downregulation of HDAC6 decreased invasiveness of multiple human cell lines, while minimally affecting human normal glial cells (Zhang et al., 2014). Tubastatin A, a selective HDAC6 inhibitor, also reduced mesenchymal marker expression and migration properties, while enhancing temozolomide-induced cell death (Urdiciain et al., 2019). Similar results were found with another compound (J22352) in GBM, where the authors noted the inhibitor promoted anti-tumorigenic effects *via* autophagy modulation (J. R. Liu, Yu, Hung, Hsin, & Chern, 2019).

4.2 Results

Previous data demonstrated sensitivity of HD-MB03 to HDAC inhibitors (Milde et al., 2012). To validate that these compounds target our metastatic Group 3 γ MB recurrent samples, we tested a number of repurposed HDAC inhibitors. This included both pan-HDAC (belinostat and vorinostat) and HDAC6-selective (citarinostat and ricolinostat) inhibitors. Ricolinostat was the first HDAC6-selective inhibitor to be identified and is 10-15-fold selective for HDAC6. From ricolinostat, citarinostat was derived and demonstrates 13-18-fold selectivity for HDAC6, as opposed to HDAC1-3 (Cosenza & Pozzi, 2018;

Huang et al., 2017). Dose response studies of all compounds were completed in hNSCs and HD-MB03-Re-sp, using two-fold dilutions from 20 μ M to 39 nM (Figure 4). Cell density and timepoint readout were consistent with previous methods (refer to *Chapter 3: 3.2 Results*), but in NCC only culture conditions. All compounds show a mere two-fold difference between IC₅₀ concentrations, with the exception of belinostat with a nearly 25-fold difference.

Given our knowledge of HDAC6's role in migration, we tested the novel HDAC6-selective compounds from Dr. Patrick Gunning's lab (Aldana-Masangkay & Sakamoto, 2011). Compounds N2 and N3 were derived from N1. Similarly, compounds T2 and T3 were derived from T1. These compounds reported marked selectivity for HDAC6, more so than citarinostat and ricolinostat. Dose response studies completed on compounds T1, T2, and T3 displayed selectivity for HDAC6, compared to other HDACs (confidential; data not shown). In particular, compound N2 showed 125-fold selectivity for HDAC6 over other HDACs (confidential; data not shown). Additional selectivity profiles of the remaining compounds are currently underway.

Dose response curves were generated following two-fold dilutions from 20 μ M to 39 nM (data not shown). This data indicated that additional dilutions could better capture the IC₅₀ concentrations for both HD-MB03-Re-sp and SU_MB002-Re-sp. Consequently, we plated two-fold dilutions of each inhibitor from 5 μ M to 9.8 nM in hNSCs and both biological replicates of *MYC*-amplified Group 3 MB metastatic recurrences (Figure 5). Compared to

citarinostat, all compounds were highly potent in targeting metastatic MB cells at low nanomolar concentrations (Supplementary Figure 4a). Of note, the therapeutic window between hNSCs and MB cells was at least a 14-, 11-, and 5-fold difference in compounds N1, N3, and T3, respectively (Figure 5 a, c, e). Compound N2 showed similar IC_{50} concentrations amongst biological replicates but had at least a 3-fold therapeutic window between hNSCs and MB cells (Figure 5b). Similarly, a 2-6-fold difference in IC_{50} concentrations of hNSCs and MB cells was observed in compound T1 (Figure 5d). Compound T2 targeted hNSCs at lower nanomolar concentrations than HD-MB03-Re-sp (Supplementary Figure 4b). Based on this data, we discontinued studies of compound T1 and T2. To characterize the remaining compounds, we treated cells from both metastatic Group 3 γ MB recurrence samples with IC_{80} concentrations, comparing results to DMSO and citarinostat. Cell viability assays revealed compound N2 to be the most effective in both biological replicates (Figure 6a, b). All four novel HDAC6-selective inhibitors demonstrated similar self-renewal capacity to citarinostat in HD-MB03-Re-sp and SU_MB002-Re-sp (Figure 6c, d). The effect of these inhibitors on BTIC frequency was assessed (Figure 6e, f). DMSO wells were BTIC-enriched; however, variability was observed amongst all HDAC6 inhibitors. Due to the substantial therapeutic window of compounds N1 and N3, we anticipated that results would confer with functional profiling. However, compounds N1 and N3 were less effective than citarinostat. Compound T3 exhibited similar results to citarinostat in HD-MB03-Re-sp in each functional assay, but not in SU_MB002-Re-sp. Lastly, compound N2 was more effective at attenuating cell viability and self-renewal of both biological replicates when compared to citarinostat.

However, outsourced *in vitro* BBB permeability results reported high BBB permeability for compound T3, but not for compound N2.

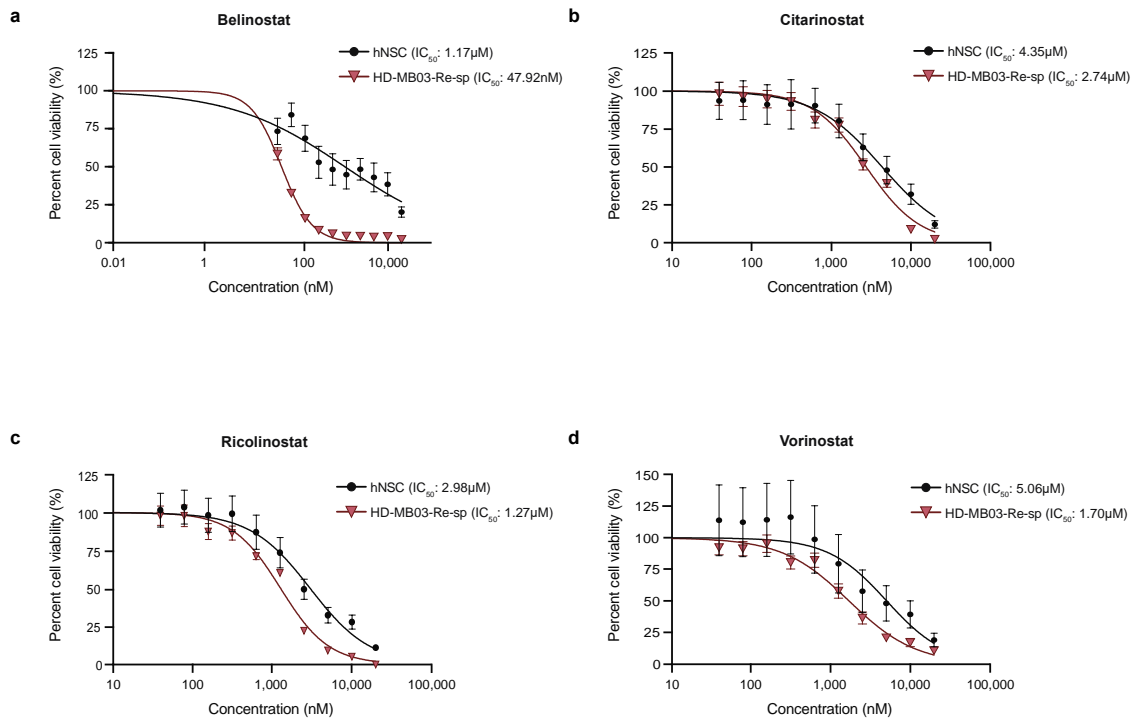


Figure 4. Belinostat showed a substantial therapeutic window between Group 3 γ MB leptomenigeal metastases at tumour recurrence and hNSCs. Two-fold dilutions of (a) belinostat, (b) citarinostat, (c) ricolinostat, and (d) vorinostat from 5 μ M to 9.8 nM, or DMSO (0.1%) were plated in HD-MB03-Re-sp and hNSCs for 72 hours. Points represent mean of at least three technical replicates, normalized to DMSO. Error bars represent standard error of the mean. Belinostat and vorinostat are non-selective HDAC inhibitors, while citarinostat and ricolinostat are selective for HDAC6.

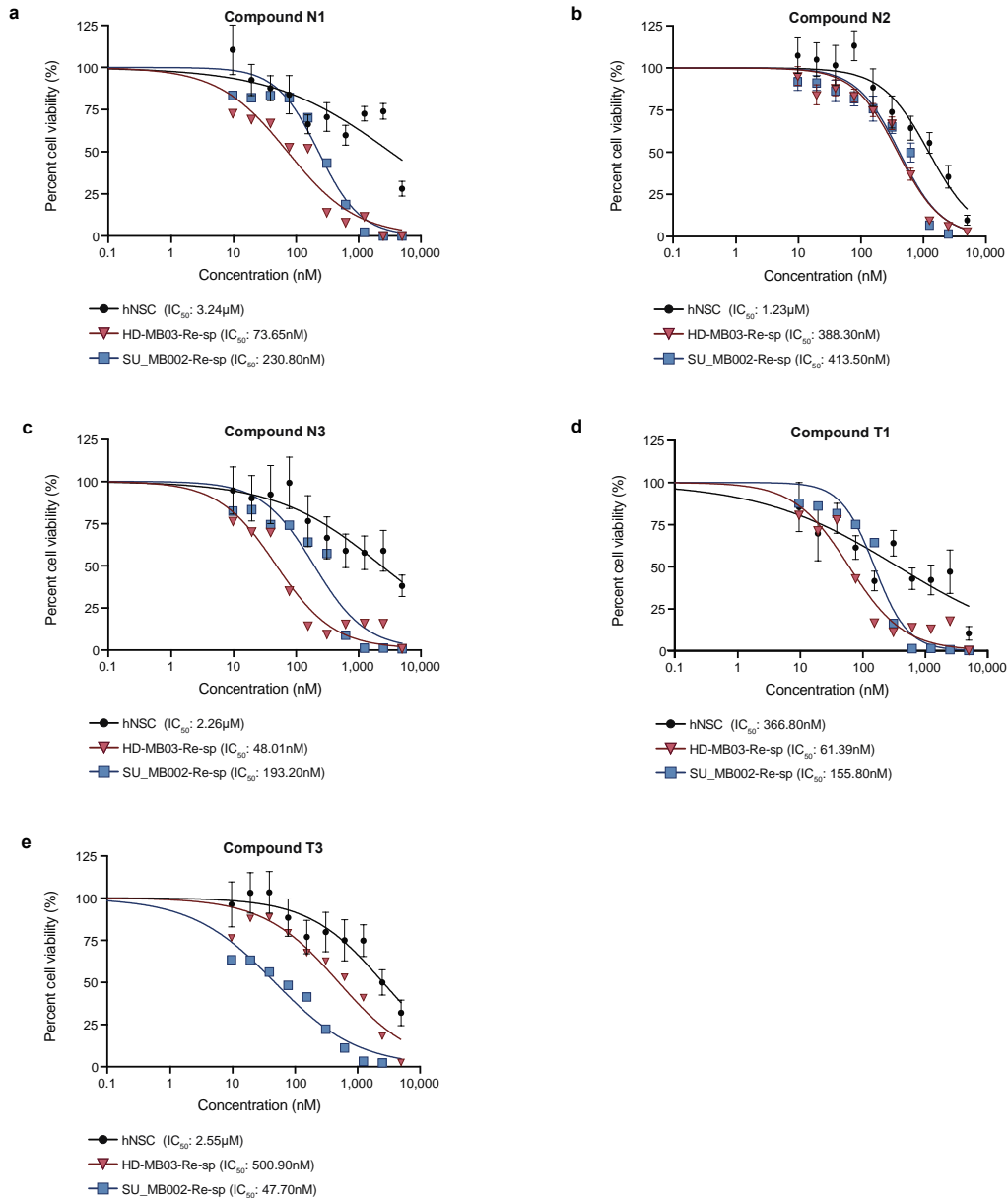


Figure 5. Dose response studies of novel HDAC6-selective inhibitors demonstrated variable therapeutic windows between Group 3 γ MB metastatic recurrences and hNSCs. Two-fold dilutions of compounds from 5 μ M to 9.8 nM, or DMSO (0.1%) were plated in HD-MB03-Re-sp, SU_MB002-Re-sp, and hNSCs for 72 hours. Points represent mean of at least three technical replicates, normalized to DMSO. Error bars represent standard error of the mean.

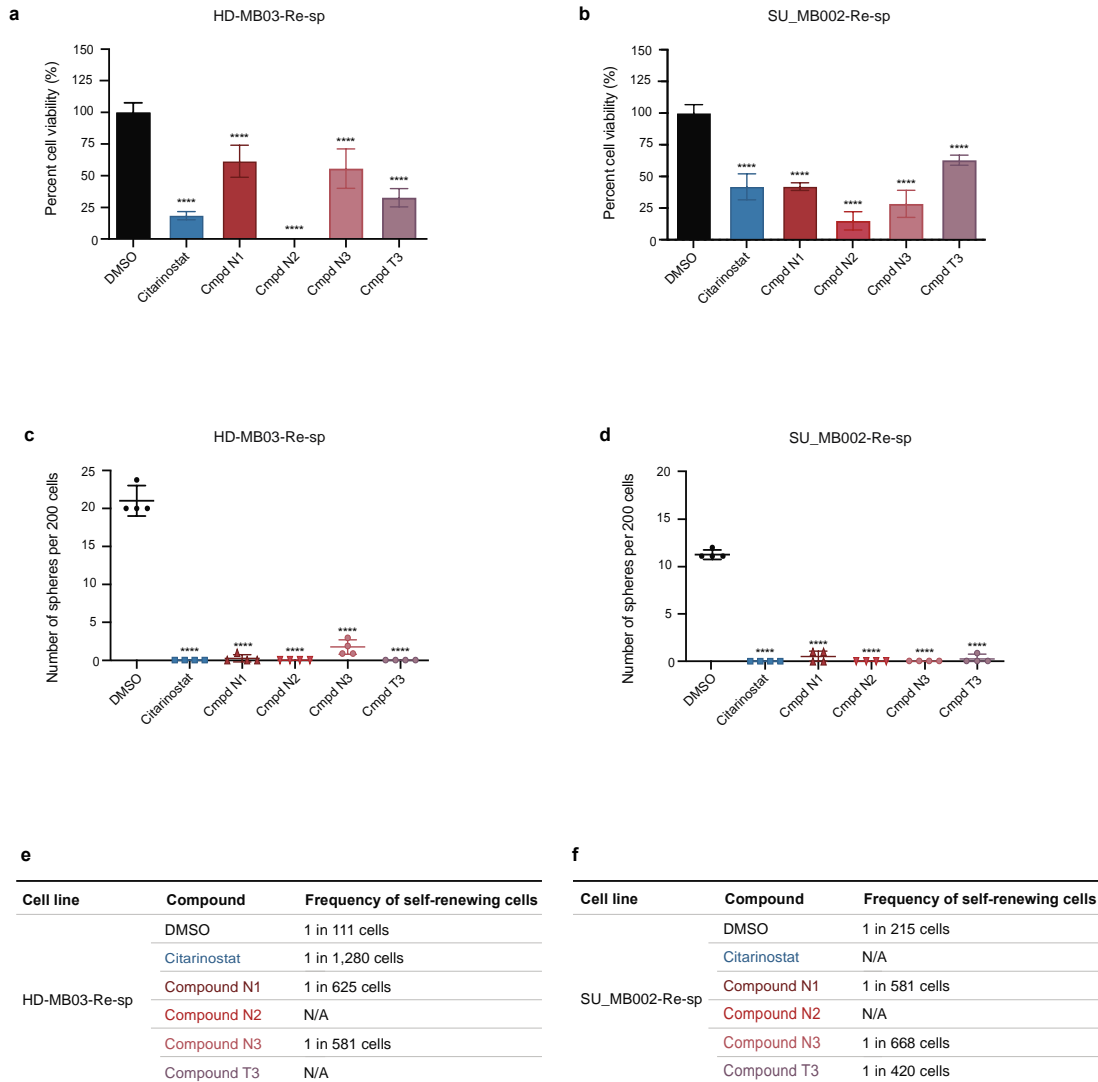
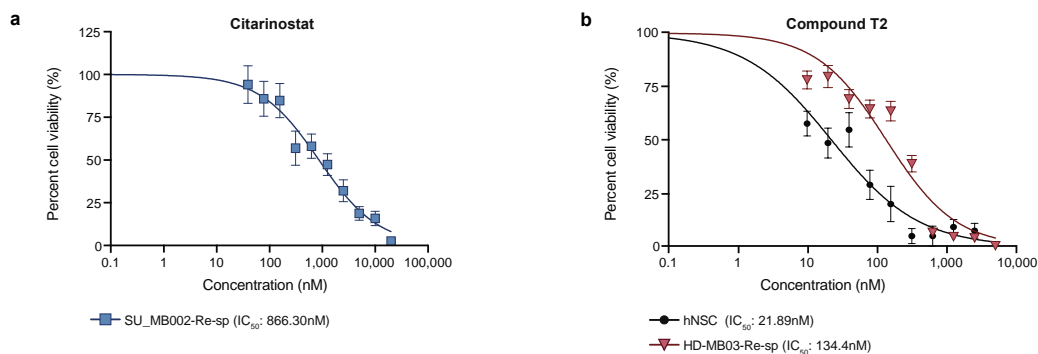


Figure 6. *In vitro* functional profile of top HDAC6-selective inhibitors revealed variable response in stem cell assays, compared to citarinosat. (a, b) Cell viability (1,000 cells/well), **(c, d)** self-renewal capacity (200 cells/well), **(e, f)** frequency of self-renewing units (1-1,000 cells/well) through LDA assays, were measured following compound (Cmpd) treatment at 0.1% IC₈₀ concentration, or DMSO for 72 hours. Points represent mean of at least three technical replicates. Error bars represent standard deviation. * $p \leq 0.05$, ** $p \leq 0.001$, *** $p \leq 0.0001$, **** $p \leq 0.00001$; unpaired t-test. Refer to *Chapter 2: Materials and Methods* for calculations in (e, f).



Supplementary Figure 4; Related to Figure 5. Additional dose response curves of selective HDAC6 compounds. Two-fold dilutions of (a) citarinosat from 5 μ M to 9.8 nM, or DMSO (0.1%) were plated with SU_MB002-Re-sp and incubated for 72 hours. Similar experimentation was conducted for (b) compound T2 in HD-MB03-Re-sp and hNSCs. Points represent average of quadruplicates, normalized to DMSO. Error bars represent standard error of the mean.

DISCUSSION

MYC-driven MB correlates with very high-risk stratification and extremely poor clinical outcome. Despite the best current therapeutic strategies comprising surgery and intensified chemoradiotherapy, *MYC*-amplified Group 3 γ MB often experience metastatic tumour recurrence in the spinal leptomeninges. These MB leptomeningeal metastases are poorly characterized, yet they remain the leading cause of death in MB patients that experience relapse. This highlights a pivotal gap in current research.

Despite our limited understanding of Group 3 γ MB metastatic recurrence, multiple studies highlighted the importance of kinases and HDACs in *MYC*-driven MB, leptomeningeal metastases, and metastatic cancers. This led to the conception of this thesis, where we hypothesized that kinase and HDAC inhibitors would serve as effective therapies against *MYC*-amplified Group 3 MB metastatic recurrences.

Previous studies have commonly used immortalized and genetically modified MB cell lines. Instead, we used MB cells isolated from the spines of tumour-bearing mice from our novel PDX model that recapitulates MB recurrence. As a control for toxicity, we used fetal hNSCs, which represent the population of healthy cells that must be unaffected by any prospective drug for the treatment of MB.

5.1 Biological relevance of high-throughput kinase screen hits

In Chapter 3, we identified the following five kinase inhibitors: BI 2536, CHIR-124, Hesperadin, JNJ-10198409, and SB-218078. We deduced that these inhibitors were biologically relevant for the treatment of recurrent Group 3 γ MB spinal metastases, as their targets were previously implicated in *MYC*-driven MB and metastasis literature. For instance, AURKB is involved in microtubule-kinetochore attachment, promoting cell cycle and survival of cancer cells (Tang et al., 2017). AURKB expression is regulated by *MYC* and MB cells expressing *MYC* are sensitive to these inhibitors (den Hollander et al., 2010; Diaz et al., 2015). Previous studies also revealed the sensitivity of *MYC*-expressing tumour cells to mitosis inhibition, which AURKB inhibitors ensue (D. Yang et al., 2010). Furthermore, AURKB inhibition decreased cell proliferation in metastatic melanoma (Porcelli et al., 2015). PLK1 is responsible for several parts of the cell cycle, ranging from mitotic entry regulation to facilitating DNA replication (van de Weerd & Medema, 2006). NanoString nCounter analysis of 72 MB patients indicated that PLK1 gene expression is very high in tumour samples, when compared to normal cerebellar tissue (Triscott et al., 2013). High expression of PLK1 also correlated with poor clinical outcome. Chemical screens of 129 compounds featured in clinical trials with primary MB samples determined that PLK1 inhibitors, particularly BI 2536, showed promise in SHH and Group 3 MB. BI 2536 attenuated cell proliferation, self-renewal, and cell cycle progression, while sparing hNSCs, which is consistent with the results of our screen (Triscott et al., 2013). Moreover, CHK1 plays a pivotal role in response to single strand DNA breaks and is responsible for later S and G2/M phase arrest (Matthews, Jones, & Collins, 2013). CHK1 is highly

expressed in MB and increased expression correlates with poor clinical prognosis of *MYC*-amplified Group 3 MB patients (Prince et al., 2016). Small molecule inhibitors and knockdown of *CHK1* showed efficacy against commercial primary and recurrent (brain) Group 3 and *SHH* MB cells (Prince et al., 2016). Transcription, proteomic and phosphoproteomic analysis on 41 flash-frozen primary MB samples revealed that kinases were involved in cell cycle regulation of Group 3 MB tumours (Forget et al., 2018). A study on B-cell lymphoma reported the correlative relationship between *MYC* and *CHK1*; strongly suggestive that these inhibitors constitute potential therapies for *MYC*-driven neoplasms (Tang et al., 2017). Lastly, *PDGFR β* is important in signal transduction. Gene expression profiling of 23 MB patient samples at diagnosis delineated the genes associated with metastatic and non-metastatic specimens (MacDonald et al., 2001). *PDGFR β* was shown to be overexpressed in metastatic MB patient samples (Gilbertson & Clifford, 2003; MacDonald et al., 2001). This receptor tyrosine kinase also contributed to the enhanced migration and invasion of commercially available Group 3 MB cell lines (Abouantoun & MacDonald, 2009). *PDGFR β* -mediated phosphorylation of *ERK*, concomitant activation of other serine/threonine kinases (*Rac1* and *Pak1*), and suppression of Ras-homologous (*Rho*) signalling collectively promoted migration (Abouantoun & MacDonald, 2009; L. Yuan, Santi, Rushing, Cornelison, & MacDonald, 2010).

Based on the BBB permeability data, we further investigated *CHIR-124* and *JNJ-10198409*. *CHIR-124* is a potent, quinolone-based inhibitor with over 2300-fold selectivity of *CHK1* over *CHK2* (Ronco, Martin, Demange, & Benhida, 2017). This compound is

orally bioavailable and previously exhibited anti-neoplastic activity in preclinical models of breast cancer (Tse et al., 2007). No studies with CHIR-124 monotherapy have been conducted. Instead, CHIR-124 is shown to act as a radiosensitizer in human colorectal cancer and synergize with gemcitabine (chemotherapy) in a pancreatic tumorsphere model, while cooperating with chemoradiotherapy in melanoma cell lines (Tao et al., 2009; Tse et al., 2007). This inhibitor promotes topoisomerase I damage in melanoma cell lines, but *in vivo* studies observed no evidence of toxicity or significant weight loss (Tao et al., 2009; Tse et al., 2007). While CHIR-124 has not been studied in the treatment of MB, another CHK1 inhibitor (prexasertib) showed promising BBB pharmacokinetics upon treatment to tumour-bearing mice and is currently in clinical trials for recurrent non-WNT MB patients in combination with cyclophosphamide or gemcitabine (Weiss et al., 2013).

In addition, studies showed the antiproliferative activity of JNJ-10198409 in colon cancer, melanoma, breast cancer, leukemia, and neuroblastoma (D'Andrea, Mei, Tuman, Galemmo, & Johnson, 2005; Fujitani, Grinshtein, Smith, & Kaplan, 2012; Ho et al., 2005). The compound is highly selective for PDGFR β , having showed significant and moderate activity against downstream proto-oncogene Abelson murine leukemia viral oncogene homolog 1 (c-Abl) and proto-oncogene tyrosine-protein kinase Src (c-Src), respectively (Plattner, Koleske, Kazlauskas, & Pendergast, 2004). Fujitani *et al.* (2012) demonstrated that the compound does not affect primary pediatric neural crest-like stem cells. Similarly, JNJ-10198409 induced mitotic arrest and cell death in GBM-derived neural tissue, but not hNSCs. This compound likely acts by an apoptotic mechanism, as cell death was caspase-

dependent, Annexin-V positive, and triggered PARP cleavage (Danovi et al., 2013). Preliminary work also demonstrated that JNJ-10198409 acts against angiogenesis – an important property in metastasis. Similar to CHIR-124, JNJ-10198409 has only been preclinically validated. A non-selective receptor tyrosine kinase inhibitor (sunitinib), dual Bcr-Abl and Src family tyrosine kinase inhibitor (dasatinib), and selective PDGFR α and β inhibitor (crenolanib) are currently in clinical trials for treatment of refractory GBMs, high-grade gliomas, diffuse intrinsic pontine gliomas, solid tumours, as well as non-small cell lung cancer patients with brain metastases (MD Anderson Cancer Center, 2020; National Cancer Institute, 2019; Pfizer, 2011; St. Jude Children's Research Hospital, 2017; University of Michigan Rogel Cancer Center, 2019).

5.2 HDAC6 inhibitor therapy for Group 3 γ medulloblastoma metastatic recurrences

For the first time, we demonstrated the efficacy of novel HDAC6-selective inhibitors against Group 3 MB, as described in Chapter 4. Most compounds effectively inhibited cell viability and self-renewal in treatment-refractory, metastatic Group 3 γ MB cells. However, only compound T3 was predicted to be BBB permeable and will thereby be the focus of future studies, as we aim to target the MB cells in the brain to prevent metastatic recurrence. Overall, our data revealed that HDAC6 inhibitors are a rationale therapeutic modality for leptomeningeal dissemination of recurrent, *MYC*-driven Group 3 MB.

HDAC6-selective inhibitor, ricolinostat, significantly inhibited cell proliferation and triggered G2/M arrest through PI3K/AKT/mTOR and ERK pathways in esophageal

squamous cell carcinoma (Cao et al., 2018). Similar effects were observed in colon cancer cells, with the addition of suppressing migration and invasion (Tan et al., 2019). Current clinical trials employ ricolinostat for relapse lymphoid malignancies, metastatic breast cancer, multiple myeloma, metastatic cholangiocarcinoma, and unresectable non-small cell lung cancer.

Analysis of MB leptomeningeal metastasis at diagnosis revealed that chemoattractant chemokines contribute to a tumorigenic microenvironment by infiltrating monocytes and triggering their differentiation (Wu et al., 2012). Conversely, HDAC6 deficiency attenuated this monocyte/macrophage recruitment and thereby may discourage this aberrant microenvironment (Yan et al., 2018). In addition, phosphatase and tensin homolog (PTEN) inhibition was recently implicated in driving metastatic *MYC*-driven Group 3 MB (Ferrucci et al., 2018). HDAC6 inhibition led to PTEN activation *via* K163 acetylation; both of which contributed to anti-tumour effects (Meng, Jia, & Gan, 2016). Taken together, HDAC6 inhibitors may activate PTEN in Group 3 γ MB to suppress disease dissemination. Rho-associated coiled-coil kinase (ROCK1 and 2) family are important in regulating EMT, cell cycle, migration, and invasion. High gene expression of ROCK2 was associated with metastatic, as compared to non-metastatic MB tumours (Dyberg et al., 2019). ROCK phosphorylation of tubulin polymerization promoting protein 1 (TPPP1) interfered with the interaction between TPPP1 and HDAC6, which elevated levels of HDAC6 (Schofield, Steel, & Bernard, 2012).

5.3 Future directions

While our data is promising, additional experiments are warranted to comprehensively understand the mechanism of action at which these compounds affect Group 3 γ MB metastatic recurrences. To first confirm the specificity of the compounds, analysis of protein expression of CHK1, PDGFR β , and HDAC6 in HD-MB03-Re-sp, SU_MB002-Re-sp, and hNSCs must be completed, both pre- and post- inhibitor treatment. Whole cell proteomics would elucidate the pathways inhibited by each compound. *In vitro* chemoradiotherapy, cell migration, cell cycle analysis, and apoptosis assays should also be conducted to gain a more comprehensive functional profile of these inhibitors. All studies should be replicated in additional hNSC and MB lines.

Results from *in vitro* chemoradiotherapy experiments will likely be useful in determining which compounds, if any, sensitize the aggressive MB cells to chemotherapy or radiation. This data may help dictate the timepoint (prior to radiation or chemotherapy) at which inhibitor treatment should be administered *in vivo*. Findings from previous studies suggest that CHK1 inhibition in *MYC*-amplified cells may complement radiotherapy (W. J. Wang et al., 2013). The fact that CHIR-124 sensitizes tumour cells to radiation and chemotherapy implies that it may induce a similar response in MB (Tao et al., 2009; Tse et al., 2007). In addition, CHK1 and HDAC6 depletion independently increased the sensitivity of MB and non-small cell lung cancer cells to cisplatin, respectively (Prince et al., 2016; L. Wang et al., 2012). This data suggest that CHIR-124 and compound T3 may also sensitize MB cells to this chemotherapeutic agent.

As CHIR-124, JNJ-10198409, and compound T3 are predicted to penetrate the brain, we aim to target the migratory MB cells in the brain to prevent metastatic tumour recurrence. Our findings that CHIR-124 and JNJ-10198409 are not selective to relapsed spine cells, by comparison to parental and relapsed brain cells, which further supports administering these inhibitors early in treatment (Supplementary Figure 3). Moreover, CHIR-124 and JNJ-10198409 are both orally bioavailable and were well tolerated in breast and colon cancer PDX models, respectively (D'Andrea et al., 2005; Tse et al., 2007). The vehicle and mode of delivery must be determined for compound T3. Following this, pharmacokinetic/pharmacodynamic and maximal tolerated dose studies in healthy mice must be performed for each inhibitor individually, and alongside standardized chemotherapy regimens and craniospinal irradiation. Similar experiments should be conducted with citarinostat to elucidate whether compound T3 demonstrates superior preclinical efficacy, as compared to citarinostat. Collectively, *in vivo* efficacy of each inhibitor will be defined by survival, tumour burden in local and metastatic sites, off-target effects, and toxicity both individually, and in combination with mouse-adapted chemoradiotherapy.

Notably, *in vitro* synergy between the three identified compounds should be evaluated, as combinatorial therapy is more effective than monotherapy. Moreover, development of rational combined therapies that concurrently inhibit multiple nodes of cell signalling pathways may be more efficacious than a single modality. As both HDAC6 and CHK1 are

involved in cell cycle regulation, compound T3 and CHIR-124 may cooperatively enhance their effect on Group 3 γ MB metastatic cells isolated at relapse. A recent study in non-small cell lung cancer revealed that HDAC6 directly interacts with CHK1 *via* ubiquitination *in vivo* (Moses et al., 2020). They noted that HDAC6 knockdown led to activation of CHK1 (Moses et al., 2020). In *MYC*-amplified Group 3 MB, high CHK1 expression correlated with poor clinical outcome (Prince et al., 2016). Therefore, we postulate that combined inhibition of HDAC6 and CHK1 *via* compound T3 and CHIR-124 may show improved therapeutic potential, as compared to monotherapy.

Overall, patients with Group 3 γ MB have the worst clinical outcome due to the high incidence of tumour recurrence and metastasis. Given their limited therapeutic options available beyond current, ineffective salvage therapies, our PDX model provided a robust platform to study this rapidly progressive, metastatic disease. Taken together, this thesis identified selective inhibitors that were effective at targeting aggressive, Group 3 γ MB leptomeningeal metastatic cells isolated at relapse. Characterization of these CHK1, PDGFR β , and HDAC6 inhibitors through additional preclinical investigation will be able to elucidate their clinical utility in treating relapsed MB patients with leptomeningeal dissemination, whom are often limited to palliation.

REFERENCES

- Aasen, S. N., Parajuli, H., Hoang, T., Feng, Z., Stokke, K., Wang, J., . . . Thorsen, F. (2019). Effective Treatment of Metastatic Melanoma by Combining MAPK and PI3K Signaling Pathway Inhibitors. *Int J Mol Sci*, *20*(17). doi:10.3390/ijms20174235
- Abouantoun, T. J., & MacDonald, T. J. (2009). Imatinib blocks migration and invasion of medulloblastoma cells by concurrently inhibiting activation of platelet-derived growth factor receptor and transactivation of epidermal growth factor receptor. *Mol Cancer Ther*, *8*(5), 1137-1147. doi:10.1158/1535-7163.MCT-08-0889
- Al-Hajj, M., Wicha, M. S., Benito-Hernandez, A., Morrison, S. J., & Clarke, M. F. (2003). Prospective identification of tumorigenic breast cancer cells. *Proc Natl Acad Sci U S A*, *100*(7), 3983-3988. doi:10.1073/pnas.0530291100
- Aldana-Masangkay, G. I., & Sakamoto, K. M. (2011). The role of HDAC6 in cancer. *J Biomed Biotechnol*, *2011*, 875824. doi:10.1155/2011/875824
- Allen, J. C., & Epstein, F. (1982). Medulloblastoma and other primary malignant neuroectodermal tumors of the CNS. The effect of patients' age and extent of disease on prognosis. *J Neurosurg*, *57*(4), 446-451. doi:10.3171/jns.1982.57.4.0446
- Ardito, F., Giuliani, M., Perrone, D., Troiano, G., & Lo Muzio, L. (2017). The crucial role of protein phosphorylation in cell signaling and its use as targeted therapy (Review). *Int J Mol Med*, *40*(2), 271-280. doi:10.3892/ijmm.2017.3036
- Arndt-Jovin, D. J., & Jovin, T. M. (1989). Fluorescence labeling and microscopy of DNA. *Methods Cell Biol*, *30*, 417-448. doi:10.1016/s0091-679x(08)60989-9
- Bailey, P., & Cushing, H. (1925). Medulloblastoma Cerebelli, a Common Type of Mid-Cerebellar Glioma of Childhood. *Archives of Neurologic Psychiatry*, *14*, 92-224.
- Bandopadhyay, P., Bergthold, G., Nguyen, B., Schubert, S., Gholamin, S., Tang, Y., . . . Cho, Y. J. (2014). BET bromodomain inhibition of MYC-amplified medulloblastoma. *Clin Cancer Res*, *20*(4), 912-925. doi:10.1158/1078-0432.CCR-13-2281
- Becker, A. J., McCulloch, E. A., & Till, J. E. (1963). Cytological demonstration of the clonal nature of spleen colonies derived from transplanted mouse marrow cells. *Nature*, *197*, 452-454. doi:10.1038/197452a0
- Bellows, C. G., & Aubin, J. E. (1989). Determination of numbers of osteoprogenitors present in isolated fetal rat calvaria cells in vitro. *Dev Biol*, *133*(1), 8-13.
- Blazquez, R., Wlochowitz, D., Wolff, A., Seitz, S., Wachter, A., Perera-Bel, J., . . . Pukrop, T. (2018). PI3K: A master regulator of brain metastasis-promoting macrophages/microglia. *Glia*, *66*(11), 2438-2455. doi:10.1002/glia.23485
- Bonnet, D., & Dick, J. E. (1997). Human acute myeloid leukemia is organized as a hierarchy that originates from a primitive hematopoietic cell. *Nat Med*, *3*(7), 730-737. doi:10.1038/nm0797-730
- Bornstein, P. (1995). Diversity of function is inherent in matricellular proteins: an appraisal of thrombospondin 1. *J Cell Biol*, *130*(3), 503-506. doi:10.1083/jcb.130.3.503

- Bouffet, E. (2010). Medulloblastoma in infants: the critical issues of the dilemma. *Curr Oncol*, 17(3), 2-3. doi:10.3747/co.v17i3.504
- Boyle, F. M., Eller, S. L., & Grossman, S. A. (2004). Penetration of intra-arterially administered vincristine in experimental brain tumor. *Neuro Oncol*, 6(4), 300-305. doi:10.1215/S1152851703000516
- Callegari, K., Maegawa, S., Bravo-Alegria, J., & Gopalakrishnan, V. (2018). Pharmacological inhibition of LSD1 activity blocks REST-dependent medulloblastoma cell migration. *Cell Commun Signal*, 16(1), 60. doi:10.1186/s12964-018-0275-5
- Canettieri, G., Di Marcotullio, L., Greco, A., Coni, S., Antonucci, L., Infante, P., . . . Gulino, A. (2010). Histone deacetylase and Cullin3-REN(KCTD11) ubiquitin ligase interplay regulates Hedgehog signalling through Gli acetylation. *Nat Cell Biol*, 12(2), 132-142. doi:10.1038/ncb2013
- Cao, J., Lv, W., Wang, L., Xu, J., Yuan, P., Huang, S., . . . Hu, J. (2018). Ricolinostat (ACY-1215) suppresses proliferation and promotes apoptosis in esophageal squamous cell carcinoma via miR-30d/PI3K/AKT/mTOR and ERK pathways. *Cell Death Dis*, 9(8), 817. doi:10.1038/s41419-018-0788-2
- Cavalli, F. M. G., Remke, M., Rampasek, L., Peacock, J., Shih, D. J. H., Luu, B., . . . Taylor, M. D. (2017). Intertumoral Heterogeneity within Medulloblastoma Subgroups. *Cancer Cell*, 31(6), 737-754 e736. doi:10.1016/j.ccell.2017.05.005
- Chamberlain, M. C. (2010). Leptomeningeal metastasis. *Curr Opin Oncol*, 22(6), 627-635. doi:10.1097/CCO.0b013e32833de986
- Chang, C. H., Housepian, E. M., & Herbert, C., Jr. (1969). An operative staging system and a megavoltage radiotherapeutic technic for cerebellar medulloblastomas. *Radiology*, 93(6), 1351-1359. doi:10.1148/93.6.1351
- Cho, Y. J., Tsherniak, A., Tamayo, P., Santagata, S., Ligon, A., Greulich, H., . . . Pomeroy, S. L. (2011). Integrative genomic analysis of medulloblastoma identifies a molecular subgroup that drives poor clinical outcome. *J Clin Oncol*, 29(11), 1424-1430. doi:10.1200/JCO.2010.28.5148
- Clifford, S. C., Lusher, M. E., Lindsey, J. C., Langdon, J. A., Gilbertson, R. J., Straughton, D., & Ellison, D. W. (2006). Wnt/Wingless pathway activation and chromosome 6 loss characterize a distinct molecular sub-group of medulloblastomas associated with a favorable prognosis. *Cell Cycle*, 5(22), 2666-2670. doi:10.4161/cc.5.22.3446
- Cook Sangar, M. L., Genovesi, L. A., Nakamoto, M. W., Davis, M. J., Knobluagh, S. E., Ji, P., . . . Olson, J. M. (2017). Inhibition of CDK4/6 by Palbociclib Significantly Extends Survival in Medulloblastoma Patient-Derived Xenograft Mouse Models. *Clin Cancer Res*, 23(19), 5802-5813. doi:10.1158/1078-0432.CCR-16-2943
- Cosenza, M., & Pozzi, S. (2018). The Therapeutic Strategy of HDAC6 Inhibitors in Lymphoproliferative Disease. *Int J Mol Sci*, 19(8). doi:10.3390/ijms19082337
- D'Andrea, M. R., Mei, J. M., Tuman, R. W., Galemno, R. A., & Johnson, D. L. (2005). Validation of in vivo pharmacodynamic activity of a novel PDGF receptor tyrosine kinase inhibitor using immunohistochemistry and quantitative image

- analysis. *Mol Cancer Ther*, 4(8), 1198-1204. doi:10.1158/1535-7163.MCT-05-0004
- da Cunha Jaeger, M., Ghisleni, E. C., Cardoso, P. S., Sinigaglia, M., Falcon, T., Brunetto, A. T., . . . Roesler, R. (2020). HDAC and MAPK/ERK Inhibitors Cooperate To Reduce Viability and Stemness in Medulloblastoma. *J Mol Neurosci*. doi:10.1007/s12031-020-01505-y
- Daina, A., Michielin, O., & Zoete, V. (2017). SwissADME: a free web tool to evaluate pharmacokinetics, drug-likeness and medicinal chemistry friendliness of small molecules. *Sci Rep*, 7, 42717. doi:10.1038/srep42717
- Daina, A., & Zoete, V. (2016). A BOILED-Egg To Predict Gastrointestinal Absorption and Brain Penetration of Small Molecules. *ChemMedChem*, 11(11), 1117-1121. doi:10.1002/cmdc.201600182
- Danovi, D., Folarin, A., Gogolok, S., Ender, C., Elbatsh, A. M., Engstrom, P. G., . . . Pollard, S. M. (2013). A high-content small molecule screen identifies sensitivity of glioblastoma stem cells to inhibition of polo-like kinase 1. *PLoS One*, 8(10), e77053. doi:10.1371/journal.pone.0077053
- Dasari, S., & Tchounwou, P. B. (2014). Cisplatin in cancer therapy: molecular mechanisms of action. *Eur J Pharmacol*, 740, 364-378. doi:10.1016/j.ejphar.2014.07.025
- Dean, M., Fojo, T., & Bates, S. (2005). Tumour stem cells and drug resistance. *Nat Rev Cancer*, 5(4), 275-284. doi:10.1038/nrc1590
- Dell, E.J. (2012). The Z prime value (Z'): BMG LABTECH.
- den Hollander, J., Rimpi, S., Doherty, J. R., Rudelius, M., Buck, A., Hoellein, A., . . . Keller, U. (2010). Aurora kinases A and B are up-regulated by Myc and are essential for maintenance of the malignant state. *Blood*, 116(9), 1498-1505. doi:10.1182/blood-2009-11-251074
- Deutsch, M., & Reigel, D. H. (1980). The value of myelography in the management of childhood medulloblastoma. *Cancer*, 45(8), 2194-2197.
- Diaz, R. J., Golbourn, B., Faria, C., Picard, D., Shih, D., Raynaud, D., . . . Rutka, J. T. (2015). Mechanism of action and therapeutic efficacy of Aurora kinase B inhibition in MYC overexpressing medulloblastoma. *Oncotarget*, 6(5), 3359-3374. doi:10.18632/oncotarget.3245
- Dukes, J. D., Whitley, P., & Chalmers, A. D. (2011). The MDCK variety pack: choosing the right strain. *BMC Cell Biol*, 12, 43. doi:10.1186/1471-2121-12-43
- Dyberg, C., Andonova, T., Olsen, T. K., Brodin, B., Kool, M., Kogner, P., . . . Wickstrom, M. (2019). Inhibition of Rho-Associated Kinase Suppresses Medulloblastoma Growth. *Cancers (Basel)*, 12(1). doi:10.3390/cancers12010073
- Ecker, J., Oehme, I., Mazitschek, R., Korshunov, A., Kool, M., Hielscher, T., . . . Milde, T. (2015). Targeting class I histone deacetylase 2 in MYC amplified group 3 medulloblastoma. *Acta Neuropathol Commun*, 3, 22. doi:10.1186/s40478-015-0201-7
- Eckerdt, F., Bell, J. B., Beauchamp, E. M., Clymer, J., Blyth, G. T., Kosciuzuk, E. M., . . . Plataniias, L. C. (2019). Potent Antineoplastic Effects of Combined PI3Kalpha-

- MNK Inhibition in Medulloblastoma. *Mol Cancer Res*, 17(6), 1305-1315.
doi:10.1158/1541-7786.MCR-18-1193
- Ellison, D. W. (2010). Childhood medulloblastoma: novel approaches to the classification of a heterogeneous disease. *Acta Neuropathol*, 120(3), 305-316.
doi:10.1007/s00401-010-0726-6
- Ellison, D. W., Kocak, M., Dalton, J., Megahed, H., Lusher, M. E., Ryan, S. L., . . . Clifford, S. C. (2011). Definition of disease-risk stratification groups in childhood medulloblastoma using combined clinical, pathologic, and molecular variables. *J Clin Oncol*, 29(11), 1400-1407. doi:10.1200/JCO.2010.30.2810
- Eramo, A., Lotti, F., Sette, G., Piloizzi, E., Biffoni, M., Di Virgilio, A., . . . De Maria, R. (2008). Identification and expansion of the tumorigenic lung cancer stem cell population. *Cell Death Differ*, 15(3), 504-514. doi:10.1038/sj.cdd.4402283
- Ezzat, S., Kamal, M., El-Khateeb, N., El-Beltagy, M., Taha, H., Refaat, A., . . . Zaghloul, M. S. (2016). Pediatric brain tumors in a low/middle income country: does it differ from that in developed world? *J Neurooncol*, 126(2), 371-376.
doi:10.1007/s11060-015-1979-7
- Fabbro, D., Cowan-Jacob, S. W., & Moebitz, H. (2015). Ten things you should know about protein kinases: IUPHAR Review 14. *Br J Pharmacol*, 172(11), 2675-2700.
doi:10.1111/bph.13096
- Facchino, S., Abdouh, M., Chatoo, W., & Bernier, G. (2010). BMI1 confers radioresistance to normal and cancerous neural stem cells through recruitment of the DNA damage response machinery. *J Neurosci*, 30(30), 10096-10111.
doi:10.1523/JNEUROSCI.1634-10.2010
- Fatehi, D., Soltani, A., & Ghatrehsamani, M. (2018). SRT1720, a potential sensitizer for radiotherapy and cytotoxicity effects of NVB-BEZ235 in metastatic breast cancer cells. *Pathol Res Pract*, 214(6), 889-895. doi:10.1016/j.prp.2018.04.001
- Ferrucci, V., de Antonellis, P., Pennino, F. P., Asadzadeh, F., Virgilio, A., Montanaro, D., . . . Zollo, M. (2018). Metastatic group 3 medulloblastoma is driven by PRUNE1 targeting NME1-TGF-beta-OTX2-SNAIL via PTEN inhibition. *Brain*, 141(5), 1300-1319. doi:10.1093/brain/awy039
- Forget, A., Martignetti, L., Puget, S., Calzone, L., Brabetz, S., Picard, D., . . . Ayrault, O. (2018). Aberrant ERBB4-SRC Signaling as a Hallmark of Group 4 Medulloblastoma Revealed by Integrative Phosphoproteomic Profiling. *Cancer Cell*, 34(3), 379-395 e377. doi:10.1016/j.ccell.2018.08.002
- Fouladi, M., Gajjar, A., Boyett, J. M., Walter, A. W., Thompson, S. J., Merchant, T. E., . . . Heideman, R. L. (1999). Comparison of CSF cytology and spinal magnetic resonance imaging in the detection of leptomeningeal disease in pediatric medulloblastoma or primitive neuroectodermal tumor. *J Clin Oncol*, 17(10), 3234-3237. doi:10.1200/JCO.1999.17.10.3234
- Fujitani, M., Grinshtein, N., Smith, K. M., & Kaplan, D. R. (2012). Potent and selective cytotoxic and cytostatic activity of JNJ-10198409 against neuroblastoma cells. *Chiba Medical J*, 88E, 27-34.

- Fults, D. W., Taylor, M. D., & Garzia, L. (2019). Leptomeningeal dissemination: a sinister pattern of medulloblastoma growth. *J Neurosurg Pediatr*, 1-9. doi:10.3171/2018.11.PEDS18506
- Gajjar, A., Chintagumpala, M., Ashley, D., Kellie, S., Kun, L. E., Merchant, T. E., . . . Gilbertson, R. J. (2006). Risk-adapted craniospinal radiotherapy followed by high-dose chemotherapy and stem-cell rescue in children with newly diagnosed medulloblastoma (St Jude Medulloblastoma-96): long-term results from a prospective, multicentre trial. *Lancet Oncol*, 7(10), 813-820. doi:10.1016/S1470-2045(06)70867-1
- Gajjar, A. J., Robinson, G. W. (2014). Medulloblastoma-translating discoveries from the bench to the bedside. *Nat Rev Clin Oncol*, 11(12), 714-722. doi:10.1038/nrclinonc.2014.181
- Gandola, L., Massimino, M., Cefalo, G., Solero, C., Spreafico, F., Pecori, E., . . . Fossati-Bellani, F. (2009). Hyperfractionated accelerated radiotherapy in the Milan strategy for metastatic medulloblastoma. *J Clin Oncol*, 27(4), 566-571. doi:10.1200/JCO.2008.18.4176
- Gao, R., Lv, G., Zhang, C., Wang, X., & Chen, L. (2018). TRIM59 induces epithelial-to-mesenchymal transition and promotes migration and invasion by PI3K/AKT signaling pathway in medulloblastoma. *Oncol Lett*, 15(6), 8253-8260. doi:10.3892/ol.2018.8432
- Garner, E. F., Stafman, L. L., Williams, A. P., Aye, J. M., Goolsby, C., Atigadda, V. R., . . . Beierle, E. A. (2018). UAB30, a novel RXR agonist, decreases tumorigenesis and leptomeningeal disease in group 3 medulloblastoma patient-derived xenografts. *J Neurooncol*, 140(2), 209-224. doi:10.1007/s11060-018-2950-1
- Garzia, L., Kijima, N., Morrissy, A. S., De Antonellis, P., Guerreiro-Stucklin, A., Holgado, B. L., . . . Taylor, M. D. (2018). A Hematogenous Route for Medulloblastoma Leptomeningeal Metastases. *Cell*, 172(5), 1050-1062 e1014. doi:10.1016/j.cell.2018.01.038
- Gholamin, S., Mitra, S. S., Feroze, A. H., Liu, J., Kahn, S. A., Zhang, M., . . . Cheshier, S. H. (2017). Disrupting the CD47-SIRPalpha anti-phagocytic axis by a humanized anti-CD47 antibody is an efficacious treatment for malignant pediatric brain tumors. *Sci Transl Med*, 9(381). doi:10.1126/scitranslmed.aaf2968
- Gibson, P., Tong, Y., Robinson, G., Thompson, M. C., Currie, D. S., Eden, C., . . . Gilbertson, R. J. (2010). Subtypes of medulloblastoma have distinct developmental origins. *Nature*, 468(7327), 1095-1099. doi:10.1038/nature09587
- Gilbertson, R. J., & Clifford, S. C. (2003). PDGFRB is overexpressed in metastatic medulloblastoma. *Nat Genet*, 35(3), 197-198. doi:10.1038/ng1103-197
- Glauser, G., Grund, B., Gassner, A. L., Menin, L., Henry, H., Bromirski, M., . . . Rochat, B. (2016). Validation of the Mass-Extraction-Window for Quantitative Methods Using Liquid Chromatography High Resolution Mass Spectrometry. *Anal Chem*, 88(6), 3264-3271. doi:10.1021/acs.analchem.5b04689
- Grausam, K. B., Dooyema, S. D. R., Bihannic, L., Premathilake, H., Morrissy, A. S., Forget, A., . . . Zhao, H. (2017). ATOH1 Promotes Leptomeningeal Dissemination

- and Metastasis of Sonic Hedgehog Subgroup Medulloblastomas. *Cancer Res*, 77(14), 3766-3777. doi:10.1158/0008-5472.CAN-16-1836
- Grunder, E., D'Ambrosio, R., Fiaschetti, G., Abela, L., Arcaro, A., Zuzak, T., . . . Grotzer, M. (2011). MicroRNA-21 suppression impedes medulloblastoma cell migration. *Eur J Cancer*, 47(16), 2479-2490. doi:10.1016/j.ejca.2011.06.041
- Han, Y., Lindner, S., Bei, Y., Garcia, H. D., Timme, N., Althoff, K., . . . Henssen, A. G. (2019). Synergistic activity of BET inhibitor MK-8628 and PLK inhibitor Volasertib in preclinical models of medulloblastoma. *Cancer Lett*, 445, 24-33. doi:10.1016/j.canlet.2018.12.012
- Hatten, M. E., & Roussel, M. F. (2011). Development and cancer of the cerebellum. *Trends Neurosci*, 34(3), 134-142. doi:10.1016/j.tins.2011.01.002
- Hatton, B. A., Villavicencio, E. H., Tsuchiya, K. D., Pritchard, J. I., Ditzler, S., Pullar, B., . . . Olson, J. M. (2008). The Smo/Smo model: hedgehog-induced medulloblastoma with 90% incidence and leptomeningeal spread. *Cancer Res*, 68(6), 1768-1776. doi:10.1158/0008-5472.CAN-07-5092
- Heideman, R. L. (1979). Tumors of the central nervous system in children. *Rocky Mt Med J*, 77(3), 27A-32A.
- Herrlinger, U., Wiendl, H., Renninger, M., Forschler, H., Dichgans, J., & Weller, M. (2004). Vascular endothelial growth factor (VEGF) in leptomeningeal metastasis: diagnostic and prognostic value. *Br J Cancer*, 91(2), 219-224. doi:10.1038/sj.bjc.6601953
- Hideshima, T., Bradner, J. E., Wong, J., Chauhan, D., Richardson, P., Schreiber, S. L., & Anderson, K. C. (2005). Small-molecule inhibition of proteasome and aggresome function induces synergistic antitumor activity in multiple myeloma. *Proc Natl Acad Sci U S A*, 102(24), 8567-8572. doi:10.1073/pnas.0503221102
- Hill, R. M., Kuijper, S., Lindsey, J. C., Petrie, K., Schwalbe, E. C., Barker, K., . . . Clifford, S. C. (2015). Combined MYC and P53 defects emerge at medulloblastoma relapse and define rapidly progressive, therapeutically targetable disease. *Cancer Cell*, 27(1), 72-84. doi:10.1016/j.ccell.2014.11.002
- Ho, C. Y., Ludovici, D. W., Maharroof, U. S., Mei, J., Sechler, J. L., Tuman, R. W., . . . Galemno, R. A., Jr. (2005). (6,7-Dimethoxy-2,4-dihydroindeno[1,2-c]pyrazol-3-yl)phenylamines: platelet-derived growth factor receptor tyrosine kinase inhibitors with broad antiproliferative activity against tumor cells. *J Med Chem*, 48(26), 8163-8173. doi:10.1021/jm050680m
- Hovestadt, V., Smith, K. S., Bihannic, L., Filbin, M. G., Shaw, M. L., Baumgartner, A., . . . Northcott, P. A. (2019). Resolving medulloblastoma cellular architecture by single-cell genomics. *Nature*, 572(7767), 74-79. doi:10.1038/s41586-019-1434-6
- Hsieh, Y. L., Tu, H. J., Pan, S. L., Liou, J. P., & Yang, C. R. (2019). Anti-metastatic activity of MPT0G211, a novel HDAC6 inhibitor, in human breast cancer cells in vitro and in vivo. *Biochim Biophys Acta Mol Cell Res*, 1866(6), 992-1003. doi:10.1016/j.bbamcr.2019.03.003
- Hu, Y., Dai, M., Zheng, Y., Wu, J., Yu, B., Zhang, H., . . . Yu, X. (2018). Epigenetic suppression of E-cadherin expression by Snail2 during the metastasis of colorectal cancer. *Clin Epigenetics*, 10(1), 154. doi:10.1186/s13148-018-0592-y

- Huang, P., Almeciga-Pinto, I., Jarpe, M., van Duzer, J. H., Mazitschek, R., Yang, M., . . . Quayle, S. N. (2017). Selective HDAC inhibition by ACY-241 enhances the activity of paclitaxel in solid tumor models. *Oncotarget*, *8*(2), 2694-2707. doi:10.18632/oncotarget.13738
- ISPN. (2020). Chemotherapy for Medulloblastomas in Children. *The ISPN Guide to Pediatric Neurosurgery*. Retrieved from <https://www.ispn.guide/tumors-of-the-nervous-system-in-children/chemotherapy-for-tumors-in-the-nervous-system-of-children-homepage/management-with-chemotherapy-of-tumors-in-the-nervous-system-of-children/chemotherapy-for-medulloblastomas-in-children/>
- Jakacki, R. I., Burger, P. C., Zhou, T., Holmes, E. J., Kocak, M., Onar, A., . . . Pollack, I. F. (2012). Outcome of children with metastatic medulloblastoma treated with carboplatin during craniospinal radiotherapy: a Children's Oncology Group Phase I/II study. *J Clin Oncol*, *30*(21), 2648-2653. doi:10.1200/JCO.2011.40.2792
- Jenkins, N. C., Kalra, R. R., Dubuc, A., Sivakumar, W., Pedone, C. A., Wu, X., . . . Fults, D. W. (2014). Genetic drivers of metastatic dissemination in sonic hedgehog medulloblastoma. *Acta Neuropathol Commun*, *2*, 85. doi:10.1186/s40478-014-0085-y
- Jiang, X., Huang, Y., Liang, X., Jiang, F., He, Y., Li, T., . . . Liu, L. (2018). Metastatic prostate cancer-associated P62 inhibits autophagy flux and promotes epithelial to mesenchymal transition by sustaining the level of HDAC6. *Prostate*, *78*(6), 426-434. doi:10.1002/pros.23487
- Johnston, D. L., Keene, D., Kostova, M., Strother, D., Lafay-Cousin, L., Fryer, C., . . . Bouffet, E. (2014). Incidence of medulloblastoma in Canadian children. *J Neurooncol*, *120*(3), 575-579. doi:10.1007/s11060-014-1588-x
- Kahn, S. A., Wang, X., Nitta, R. T., Gholamin, S., Theruvath, J., Hutter, G., . . . Cheshier, S. H. (2018). Notch1 regulates the initiation of metastasis and self-renewal of Group 3 medulloblastoma. *Nat Commun*, *9*(1), 4121. doi:10.1038/s41467-018-06564-9
- Kanno, K., Kanno, S., Nitta, H., Uesugi, N., Sugai, T., Masuda, T., . . . Maesawa, C. (2012). Overexpression of histone deacetylase 6 contributes to accelerated migration and invasion activity of hepatocellular carcinoma cells. *Oncol Rep*, *28*(3), 867-873. doi:10.3892/or.2012.1898
- Kawauchi, D., Robinson, G., Uziel, T., Gibson, P., Rehg, J., Gao, C., . . . Roussel, M. F. (2012). A mouse model of the most aggressive subgroup of human medulloblastoma. *Cancer Cell*, *21*(2), 168-180. doi:10.1016/j.ccr.2011.12.023
- Khanna, V., Achey, R. L., Ostrom, Q. T., Block-Beach, H., Kruchko, C., Barnholtz-Sloan, J. S., & de Blank, P. M. (2017). Incidence and survival trends for medulloblastomas in the United States from 2001 to 2013. *J Neurooncol*, *135*(3), 433-441. doi:10.1007/s11060-017-2594-6
- Kolbinger, F. R., Koeneke, E., Ridinger, J., Heimburg, T., Muller, M., Bayer, T., . . . Oehme, I. (2018). The HDAC6/8/10 inhibitor TH34 induces DNA damage-mediated cell death in human high-grade neuroblastoma cell lines. *Arch Toxicol*, *92*(8), 2649-2664. doi:10.1007/s00204-018-2234-8

- Kool, M., Korshunov, A., Remke, M., Jones, D. T., Schlanstein, M., Northcott, P. A., . . . Pfister, S. M. (2012). Molecular subgroups of medulloblastoma: an international meta-analysis of transcriptome, genetic aberrations, and clinical data of WNT, SHH, Group 3, and Group 4 medulloblastomas. *Acta Neuropathol*, *123*(4), 473-484. doi:10.1007/s00401-012-0958-8
- Kool, M., Koster, J., Bunt, J., Hasselt, N. E., Lakeman, A., van Sluis, P., . . . Versteeg, R. (2008). Integrated genomics identifies five medulloblastoma subtypes with distinct genetic profiles, pathway signatures and clinicopathological features. *PLoS One*, *3*(8), e3088. doi:10.1371/journal.pone.0003088
- Kortmann, R. D., Kuhl, J., Timmermann, B., Mittler, U., Urban, C., Budach, V., . . . Bamberg, M. (2000). Postoperative neoadjuvant chemotherapy before radiotherapy as compared to immediate radiotherapy followed by maintenance chemotherapy in the treatment of medulloblastoma in childhood: results of the German prospective randomized trial HIT '91. *Int J Radiat Oncol Biol Phys*, *46*(2), 269-279. doi:10.1016/s0360-3016(99)00369-7
- Kurpios, N. A., Girgis-Gabardo, A., Hallett, R. M., Rogers, S., Gludish, D. W., Kockeritz, L., . . . Hassell, J. A. (2013). Single unpurified breast tumor-initiating cells from multiple mouse models efficiently elicit tumors in immune-competent hosts. *PLoS One*, *8*(3), e58151. doi:10.1371/journal.pone.0058151
- Kuzan-Fischer, C. M., Guerreiro Stucklin, A. S., & Taylor, M. D. (2017). Advances in Genomics Explain Medulloblastoma Behavior at the Bedside. *Neurosurgery*, *64*(CN_suppl_1), 21-26. doi:10.1093/neuros/nyx248
- Lapidot, T., Sirard, C., Vormoor, J., Murdoch, B., Hoang, T., Caceres-Cortes, J., . . . Dick, J. E. (1994). A cell initiating human acute myeloid leukaemia after transplantation into SCID mice. *Nature*, *367*(6464), 645-648. doi:10.1038/367645a0
- Lassaletta, A., & Ramaswamy, V. (2016). Medulloblastoma in adults: they're not just big kids. *Neuro Oncol*, *18*(7), 895-897. doi:10.1093/neuonc/now110
- Laughton, S. J., Merchant, T. E., Sklar, C. A., Kun, L. E., Fouladi, M., Broniscer, A., . . . Gajjar, A. (2008). Endocrine outcomes for children with embryonal brain tumors after risk-adapted craniospinal and conformal primary-site irradiation and high-dose chemotherapy with stem-cell rescue on the SJMB-96 trial. *J Clin Oncol*, *26*(7), 1112-1118. doi:10.1200/JCO.2008.13.5293
- Lee, S. J., Krauthauser, C., Maduskuie, V., Fawcett, P. T., Olson, J. M., & Rajasekaran, S. A. (2011). Curcumin-induced HDAC inhibition and attenuation of medulloblastoma growth in vitro and in vivo. *BMC Cancer*, *11*, 144. doi:10.1186/1471-2407-11-144
- Li, B., Xu, W. W., Lam, A. K. Y., Wang, Y., Hu, H. F., Guan, X. Y., . . . Cheung, A. L. M. (2017). Significance of PI3K/AKT signaling pathway in metastasis of esophageal squamous cell carcinoma and its potential as a target for anti-metastasis therapy. *Oncotarget*, *8*(24), 38755-38766. doi:10.18632/oncotarget.16333

- Li, P., Du, F., Yuelling, L. W., Lin, T., Muradimova, R. E., Tricarico, R., . . . Yang, Z. J. (2013). A population of Nestin-expressing progenitors in the cerebellum exhibits increased tumorigenicity. *Nat Neurosci*, *16*(12), 1737-1744. doi:10.1038/nn.3553
- Li, X. N., Shu, Q., Su, J. M., Perlaky, L., Blaney, S. M., & Lau, C. C. (2005). Valproic acid induces growth arrest, apoptosis, and senescence in medulloblastomas by increasing histone hyperacetylation and regulating expression of p21Cip1, CDK4, and CMYC. *Mol Cancer Ther*, *4*(12), 1912-1922. doi:10.1158/1535-7163.MCT-05-0184
- Lindsey, J. C., Hill, R. M., Megahed, H., Lusher, M. E., Schwalbe, E. C., Cole, M., . . . Clifford, S. C. (2011). TP53 mutations in favorable-risk Wnt/Wingless-subtype medulloblastomas. *J Clin Oncol*, *29*(12), e344-346; author reply e347-348. doi:10.1200/JCO.2010.33.8590
- Liu, J., Gu, J., Feng, Z., Yang, Y., Zhu, N., Lu, W., & Qi, F. (2016). Both HDAC5 and HDAC6 are required for the proliferation and metastasis of melanoma cells. *J Transl Med*, *14*, 7. doi:10.1186/s12967-015-0753-0
- Liu, J. R., Yu, C. W., Hung, P. Y., Hsin, L. W., & Chern, J. W. (2019). High-selective HDAC6 inhibitor promotes HDAC6 degradation following autophagy modulation and enhanced antitumor immunity in glioblastoma. *Biochem Pharmacol*, *163*, 458-471. doi:10.1016/j.bcp.2019.03.023
- Louis, D. N., Ohgaki, H., Wiestler, O. D., Cavenee, W. K., Burger, P. C., Jouvett, A., . . . Kleihues, P. (2007). The 2007 WHO classification of tumours of the central nervous system. *Acta Neuropathol*, *114*(2), 97-109. doi:10.1007/s00401-007-0243-4
- Louis, D. N., Perry, A., Reifenberger, G., von Deimling, A., Figarella-Branger, D., Cavenee, W. K., . . . Ellison, D. W. (2016). The 2016 World Health Organization Classification of Tumors of the Central Nervous System: a summary. *Acta Neuropathol*, *131*(6), 803-820. doi:10.1007/s00401-016-1545-1
- Mabbott, D. J., Penkman, L., Witol, A., Strother, D., & Bouffet, E. (2008). Core neurocognitive functions in children treated for posterior fossa tumors. *Neuropsychology*, *22*(2), 159-168. doi:10.1037/0894-4105.22.2.159
- Mabbott, D. J., Spiegler, B. J., Greenberg, M. L., Rutka, J. T., Hyder, D. J., & Bouffet, E. (2005). Serial evaluation of academic and behavioral outcome after treatment with cranial radiation in childhood. *J Clin Oncol*, *23*(10), 2256-2263. doi:10.1200/JCO.2005.01.158
- MacDonald, T. J., Aguilera, D., & Castellino, R. C. (2014). The rationale for targeted therapies in medulloblastoma. *Neuro Oncol*, *16*(1), 9-20. doi:10.1093/neuonc/not147
- MacDonald, T. J., Brown, K. M., LaFleur, B., Peterson, K., Lawlor, C., Chen, Y., . . . Stephan, D. A. (2001). Expression profiling of medulloblastoma: PDGFRA and the RAS/MAPK pathway as therapeutic targets for metastatic disease. *Nat Genet*, *29*(2), 143-152. doi:10.1038/ng731
- Manning, G., Whyte, D. B., Martinez, R., Hunter, T., & Sudarsanam, S. (2002). The protein kinase complement of the human genome. *Science*, *298*(5600), 1912-1934. doi:10.1126/science.1075762

- Martin, A. M., Raabe, E., Eberhart, C., & Cohen, K. J. (2014). Management of pediatric and adult patients with medulloblastoma. *Curr Treat Options Oncol*, *15*(4), 581-594. doi:10.1007/s11864-014-0306-4
- Matthews, T. P., Jones, A. M., & Collins, I. (2013). Structure-based design, discovery and development of checkpoint kinase inhibitors as potential anticancer therapies. *Expert Opin Drug Discov*, *8*(6), 621-640. doi:10.1517/17460441.2013.788496
- McKay, R. R., De Velasco, G., Werner, L., Bellmunt, J., Harshman, L., Sweeney, C., . . . Choueiri, T. K. (2016). A phase 1 study of buparlisib and bevacizumab in patients with metastatic renal cell carcinoma progressing on vascular endothelial growth factor-targeted therapies. *Cancer*, *122*(15), 2389-2398. doi:10.1002/cncr.30056
- McRee, A. J., Marcom, P. K., Moore, D. T., Zamboni, W. C., Kornblum, Z. A., Hu, Z., . . . Dees, E. C. (2018). A Phase I Trial of the PI3K Inhibitor Buparlisib Combined With Capecitabine in Patients With Metastatic Breast Cancer. *Clin Breast Cancer*, *18*(4), 289-297. doi:10.1016/j.clbc.2017.10.014
- MD Anderson Cancer Center. (2020). Identifier: NCT02389309, Dasatinib, Temsirolimus, and Cyclophosphamide in Treating Patients With Advanced, Recurrent, or Refractory Solid Tumors. Retrieved from <https://clinicaltrials.gov/ct2/show/NCT02389309>
- Meng, Z., Jia, L. F., & Gan, Y. H. (2016). PTEN activation through K163 acetylation by inhibiting HDAC6 contributes to tumour inhibition. *Oncogene*, *35*(18), 2333-2344. doi:10.1038/onc.2015.293
- Milde, T., Lodrini, M., Savelyeva, L., Korshunov, A., Kool, M., Brueckner, L. M., . . . Deubzer, H. E. (2012). HD-MB03 is a novel Group 3 medulloblastoma model demonstrating sensitivity to histone deacetylase inhibitor treatment. *J Neurooncol*, *110*(3), 335-348. doi:10.1007/s11060-012-0978-1
- Mirochnik, Y., Kwiatek, A., & Volpert, O. V. (2008). Thrombospondin and apoptosis: molecular mechanisms and use for design of complementation treatments. *Curr Drug Targets*, *9*(10), 851-862. doi:10.2174/138945008785909347
- Montecucco, A., Zanetta, F., & Biamonti, G. (2015). Molecular mechanisms of etoposide. *EXCLI J*, *14*, 95-108. doi:10.17179/excli2015-561
- Morfouace, M., Shelat, A., Jacus, M., Freeman, B. B., 3rd, Turner, D., Robinson, S., . . . Roussel, M. F. (2014). Pemetrexed and gemcitabine as combination therapy for the treatment of Group3 medulloblastoma. *Cancer Cell*, *25*(4), 516-529. doi:10.1016/j.ccr.2014.02.009
- Morrissy, A. S., Garzia, L., Shih, D. J., Zuyderduyn, S., Huang, X., Skowron, P., . . . Taylor, M. D. (2016). Divergent clonal selection dominates medulloblastoma at recurrence. *Nature*, *529*(7586), 351-357. doi:10.1038/nature16478
- Moses, N., Zhangb, M., Wub, J-Y., Hub, C., Xiangc, S., Malysaa, A., . . . Mary Zhangb, X. (2020). HDAC6 Regulates Radiosensitivity of Non-Small Cell Lung Cancer by Promoting Degradation of Chk1. *bioRxiv* doi:10.1101/2020.02.10.942573
- Mumert, M., Dubuc, A., Wu, X., Northcott, P. A., Chin, S. S., Pedone, C. A., . . . Fults, D. W. (2012). Functional genomics identifies drivers of medulloblastoma

- dissemination. *Cancer Res*, 72(19), 4944-4953. doi:10.1158/0008-5472.CAN-12-1629
- Muoio, V. M., Shinjo, S. O., Matushita, H., Rosemberg, S., Teixeira, M. J., & Marie, S. K. (2011). Extraneural metastases in medulloblastoma. *Arq Neuropsiquiatr*, 69(2B), 328-331. doi:10.1590/s0004-282x2011000300012
- National Cancer Institute. (2019). Identifier NCT00423735, Dasatinib in Treating Patients With Recurrent Glioblastoma Multiforme or Gliosarcoma. Retrieved from <https://clinicaltrials.gov/ct2/show/NCT00423735>
- Neville, K. A., & Blaney, S. M. (2005). Leptomeningeal cancer in the pediatric patient. *Cancer Treat Res*, 125, 87-106. doi:10.1007/0-387-24199-x_6
- Nitta, R. T., Bolin, S., Luo, E., Solow-Codero, D. E., Samghabadi, P., Purzner, T., . . . Li, G. (2019). Casein kinase 2 inhibition sensitizes medulloblastoma to temozolomide. *Oncogene*, 38(42), 6867-6879. doi:10.1038/s41388-019-0927-y
- Northcott, P. A., Buchhalter, I., Morrissy, A. S., Hovestadt, V., Weischenfeldt, J., Ehrenberger, T., . . . Lichter, P. (2017). The whole-genome landscape of medulloblastoma subtypes. *Nature*, 547(7663), 311-317. doi:10.1038/nature22973
- Northcott, P. A., Jones, D. T., Kool, M., Robinson, G. W., Gilbertson, R. J., Cho, Y. J., . . . Pfister, S. M. (2012a). Medulloblastomics: the end of the beginning. *Nat Rev Cancer*, 12(12), 818-834. doi:10.1038/nrc3410
- Northcott, P. A., Korshunov, A., Witt, H., Hielscher, T., Eberhart, C. G., Mack, S., . . . Taylor, M. D. (2011). Medulloblastoma comprises four distinct molecular variants. *J Clin Oncol*, 29(11), 1408-1414. doi:10.1200/JCO.2009.27.4324
- Northcott, P. A., Shih, D. J., Peacock, J., Garzia, L., Morrissy, A. S., Zichner, T., . . . Taylor, M. D. (2012b). Subgroup-specific structural variation across 1,000 medulloblastoma genomes. *Nature*, 488(7409), 49-56. doi:10.1038/nature11327
- O'Brien, C. A., Pollett, A., Gallinger, S., & Dick, J. E. (2007). A human colon cancer cell capable of initiating tumour growth in immunodeficient mice. *Nature*, 445(7123), 106-110. doi:10.1038/nature05372
- Ostrom, Q. T., Cioffi, G., Gittleman, H., Patil, N., Waite, K., Kruchko, C., & Barnholtz-Sloan, J. S. (2019). CBTRUS Statistical Report: Primary Brain and Other Central Nervous System Tumors Diagnosed in the United States in 2012-2016. *Neuro Oncol*, 21(Suppl 5), v1-v100. doi:10.1093/neuonc/noz150
- Packer, R. J., Gajjar, A., Vezina, G., Rorke-Adams, L., Burger, P. C., Robertson, P. L., . . . Spoto, R. (2006). Phase III study of craniospinal radiation therapy followed by adjuvant chemotherapy for newly diagnosed average-risk medulloblastoma. *J Clin Oncol*, 24(25), 4202-4208. doi:10.1200/JCO.2006.06.4980
- Palmer, S. L., Armstrong, C., Onar-Thomas, A., Wu, S., Wallace, D., Bonner, M. J., . . . Gajjar, A. (2013). Processing speed, attention, and working memory after treatment for medulloblastoma: an international, prospective, and longitudinal study. *J Clin Oncol*, 31(28), 3494-3500. doi:10.1200/JCO.2012.47.4775
- Pardal, R., Clarke, M. F., & Morrison, S. J. (2003). Applying the principles of stem-cell biology to cancer. *Nat Rev Cancer*, 3(12), 895-902. doi:10.1038/nrc1232
- Park, A. K., Lee, J. Y., Cheong, H., Ramaswamy, V., Park, S. H., Kool, M., . . . Kim, S. K. (2019). Subgroup-specific prognostic signaling and metabolic pathways in

- pediatric medulloblastoma. *BMC Cancer*, 19(1), 571. doi:10.1186/s12885-019-5742-x
- Pei, Y., Liu, K. W., Wang, J., Garancher, A., Tao, R., Esparza, L. A., . . . Wechsler-Reya, R. J. (2016). HDAC and PI3K Antagonists Cooperate to Inhibit Growth of MYC-Driven Medulloblastoma. *Cancer Cell*, 29(3), 311-323. doi:10.1016/j.ccell.2016.02.011
- Pei, Y., Moore, C. E., Wang, J., Tewari, A. K., Eroshkin, A., Cho, Y. J., . . . Wechsler-Reya, R. J. (2012). An animal model of MYC-driven medulloblastoma. *Cancer Cell*, 21(2), 155-167. doi:10.1016/j.ccr.2011.12.021
- Pfizer. (2011). Identifier: NCT00372775, Study Tests The Safety And Effectiveness Of SU011248 In Patients With Non-Small Cell Lung Cancer Having Brain Metastases. Retrieved from <https://clinicaltrials.gov/ct2/show/NCT00372775>
- Phi, J. H., Choi, S. A., Kwak, P. A., Lee, J. Y., Wang, K. C., Hwang, D. W., & Kim, S. K. (2017). Panobinostat, a histone deacetylase inhibitor, suppresses leptomeningeal seeding in a medulloblastoma animal model. *Oncotarget*, 8(34), 56747-56757. doi:10.18632/oncotarget.18132
- Phoenix, T. N., Patmore, D. M., Boop, S., Boulos, N., Jacus, M. O., Patel, Y. T., . . . Gilbertson, R. J. (2016). Medulloblastoma Genotype Dictates Blood Brain Barrier Phenotype. *Cancer Cell*, 29(4), 508-522. doi:10.1016/j.ccell.2016.03.002
- Pizer, B. L., & Clifford, S. C. (2009). The potential impact of tumour biology on improved clinical practice for medulloblastoma: progress towards biologically driven clinical trials. *Br J Neurosurg*, 23(4), 364-375. doi:10.1080/02688690903121807
- Plattner, R., Koleske, A. J., Kazlauskas, A., & Pendergast, A. M. (2004). Bidirectional signaling links the Abelson kinases to the platelet-derived growth factor receptor. *Mol Cell Biol*, 24(6), 2573-2583. doi:10.1128/mcb.24.6.2573-2583.2004
- Polkinghorn, W. R., & Tarbell, N. J. (2007). Medulloblastoma: tumorigenesis, current clinical paradigm, and efforts to improve risk stratification. *Nat Clin Pract Oncol*, 4(5), 295-304. doi:10.1038/ncponc0794
- Porcelli, L., Guida, G., Quatrala, A. E., Cocco, T., Sidella, L., Maida, I., . . . Azzariti, A. (2015). Aurora kinase B inhibition reduces the proliferation of metastatic melanoma cells and enhances the response to chemotherapy. *J Transl Med*, 13, 26. doi:10.1186/s12967-015-0385-4
- Prince, E. W., Balakrishnan, I., Shah, M., Mulcahy Levy, J. M., Griesinger, A. M., Alimova, I., . . . Vibhakar, R. (2016). Checkpoint kinase 1 expression is an adverse prognostic marker and therapeutic target in MYC-driven medulloblastoma. *Oncotarget*, 7(33), 53881-53894. doi:10.18632/oncotarget.10692
- Pugh, T. J., Weeraratne, S. D., Archer, T. C., Pomeranz Krummel, D. A., Auclair, D., Bochicchio, J., . . . Cho, Y. J. (2012). Medulloblastoma exome sequencing uncovers subtype-specific somatic mutations. *Nature*, 488(7409), 106-110. doi:10.1038/nature11329

- Pui, C. H., Gajjar, A. J., Kane, J. R., Qaddoumi, I. A., & Pappo, A. S. (2011). Challenging issues in pediatric oncology. *Nat Rev Clin Oncol*, 8(9), 540-549. doi:10.1038/nrclinonc.2011.95
- Ramaswamy, V., Nor, C., & Taylor, M. D. (2015). p53 and Medulloblastoma. *Cold Spring Harb Perspect Med*, 6(2), a026278. doi:10.1101/cshperspect.a026278
- Ramaswamy, V., Remke, M., Bouffet, E., Bailey, S., Clifford, S. C., Doz, F., . . . Pomeroy, S. L. (2016). Risk stratification of childhood medulloblastoma in the molecular era: the current consensus. *Acta Neuropathol*, 131(6), 821-831. doi:10.1007/s00401-016-1569-6
- Ramaswamy, V., Remke, M., Bouffet, E., Faria, C. C., Perreault, S., Cho, Y. J., . . . Taylor, M. D. (2013). Recurrence patterns across medulloblastoma subgroups: an integrated clinical and molecular analysis. *Lancet Oncol*, 14(12), 1200-1207. doi:10.1016/S1470-2045(13)70449-2
- Ramaswamy, V., & Taylor, M. D. (2017). Medulloblastoma: From Myth to Molecular. *J Clin Oncol*, 35(21), 2355-2363. doi:10.1200/JCO.2017.72.7842
- Reya, T., Morrison, S. J., Clarke, M. F., & Weissman, I. L. (2001). Stem cells, cancer, and cancer stem cells. *Nature*, 414(6859), 105-111. doi:10.1038/35102167
- Reynolds, B. A., & Weiss, S. (1992). Generation of neurons and astrocytes from isolated cells of the adult mammalian central nervous system. *Science*, 255(5052), 1707-1710. doi:10.1126/science.1553558
- Reynolds, B. A., & Weiss, S. (1996). Clonal and population analyses demonstrate that an EGF-responsive mammalian embryonic CNS precursor is a stem cell. *Dev Biol*, 175(1), 1-13. doi:10.1006/dbio.1996.0090
- Ricci-Vitiani, L., Lombardi, D. G., Pilozzi, E., Biffoni, M., Todaro, M., Peschle, C., & De Maria, R. (2007). Identification and expansion of human colon-cancer-initiating cells. *Nature*, 445(7123), 111-115. doi:10.1038/nature05384
- Rodriguez-Blanco, J., Li, B., Long, J., Shen, C., Yang, F., Orton, D., . . . Robbins, D. J. (2019). A CK1alpha Activator Penetrates the Brain and Shows Efficacy Against Drug-resistant Metastatic Medulloblastoma. *Clin Cancer Res*, 25(4), 1379-1388. doi:10.1158/1078-0432.CCR-18-1319
- Rogers, N. M., Sharifi-Sanjani, M., Yao, M., Ghimire, K., Bienes-Martinez, R., Mutchler, S. M., . . . Isenberg, J. S. (2017). TSP1-CD47 signaling is upregulated in clinical pulmonary hypertension and contributes to pulmonary arterial vasculopathy and dysfunction. *Cardiovasc Res*, 113(1), 15-29. doi:10.1093/cvr/cvw218
- Ronco, C., Martin, A. R., Demange, L., & Benhida, R. (2017). ATM, ATR, CHK1, CHK2 and WEE1 inhibitors in cancer and cancer stem cells. *Medchemcomm*, 8(2), 295-319. doi:10.1039/c6md00439c
- Rossi, A., Caracciolo, V., Russo, G., Reiss, K., & Giordano, A. (2008). Medulloblastoma: from molecular pathology to therapy. *Clin Cancer Res*, 14(4), 971-976. doi:10.1158/1078-0432.CCR-07-2072
- Rowinsky, E. K., & Donehower, R. C. (1991). The clinical pharmacology and use of antimicrotubule agents in cancer chemotherapeutics. *Pharmacol Ther*, 52(1), 35-84. doi:10.1016/0163-7258(91)90086-2

- Rusert, J. M., Wu, X., Eberhart, C. G., Taylor, M. D., & Wechsler-Reya, R. J. (2014). SnapShot: Medulloblastoma. *Cancer Cell*, 26(6), 940-940 e941. doi:10.1016/j.ccell.2014.11.015
- Sabel, M., Fleischhack, G., Tippelt, S., Gustafsson, G., Doz, F., Kortmann, R., . . . Group, Siop- E. Brain Tumour. (2016). Relapse patterns and outcome after relapse in standard risk medulloblastoma: a report from the HIT-SIOP-PNET4 study. *J Neurooncol*, 129(3), 515-524. doi:10.1007/s11060-016-2202-1
- Sakuma, T., Uzawa, K., Onda, T., Shiiba, M., Yokoe, H., Shibahara, T., & Tanzawa, H. (2006). Aberrant expression of histone deacetylase 6 in oral squamous cell carcinoma. *Int J Oncol*, 29(1), 117-124.
- Santhana Kumar, K., Neve, A., Guerreiro Stucklin, A. S., Kuzan-Fischer, C. M., Rushing, E. J., Taylor, M. D., . . . Baumgartner, M. (2018). TGF-beta Determines the Pro-migratory Potential of bFGF Signaling in Medulloblastoma. *Cell Rep*, 23(13), 3798-3812 e3798. doi:10.1016/j.celrep.2018.05.083
- Santhana Kumar, K., Tripolitsioti, D., Ma, M., Grahlert, J., Egli, K. B., Fiaschetti, G., . . . Baumgartner, M. (2015). The Ser/Thr kinase MAP4K4 drives c-Met-induced motility and invasiveness in a cell-based model of SHH medulloblastoma. *Springerplus*, 4, 19. doi:10.1186/s40064-015-0784-2
- Schneider, C., Ramaswamy, V., Kulkarni, A. V., Rutka, J. T., Remke, M., Tabori, U., . . . Taylor, M. D. (2015). Clinical implications of medulloblastoma subgroups: incidence of CSF diversion surgery. *J Neurosurg Pediatr*, 15(3), 236-242. doi:10.3171/2014.9.PEDS14280
- Schofield, A. V., Steel, R., & Bernard, O. (2012). Rho-associated coiled-coil kinase (ROCK) protein controls microtubule dynamics in a novel signaling pathway that regulates cell migration. *J Biol Chem*, 287(52), 43620-43629. doi:10.1074/jbc.M112.394965
- Schuller, U., Heine, V. M., Mao, J., Kho, A. T., Dillon, A. K., Han, Y. G., . . . Ligon, K. L. (2008). Acquisition of granule neuron precursor identity is a critical determinant of progenitor cell competence to form Shh-induced medulloblastoma. *Cancer Cell*, 14(2), 123-134. doi:10.1016/j.ccr.2008.07.005
- Seyfrid, M., Bobrowski, D., Bakhshinyan, D., Tatari, N., Venugopal, C., & Singh, S. K. (2019). In Vitro Self-Renewal Assays for Brain Tumor Stem Cells. *Methods Mol Biol*, 1869, 79-84. doi:10.1007/978-1-4939-8805-1_7
- Shih, D. J., Northcott, P. A., Remke, M., Korshunov, A., Ramaswamy, V., Kool, M., . . . Taylor, M. D. (2014). Cytogenetic prognostication within medulloblastoma subgroups. *J Clin Oncol*, 32(9), 886-896. doi:10.1200/JCO.2013.50.9539
- Shu, Q., Antalffy, B., Su, J. M., Adesina, A., Ou, C. N., Pietsch, T., . . . Li, X. N. (2006). Valproic Acid prolongs survival time of severe combined immunodeficient mice bearing intracerebellar orthotopic medulloblastoma xenografts. *Clin Cancer Res*, 12(15), 4687-4694. doi:10.1158/1078-0432.CCR-05-2849
- Siegel, R., Naishadham, D., & Jemal, A. (2012). Cancer statistics, 2012. *CA Cancer J Clin*, 62(1), 10-29. doi:10.3322/caac.20138

- Siminovitch, L., McCulloch, E. A., & Till, J. E. (1963). The Distribution of Colony-Forming Cells among Spleen Colonies. *J Cell Comp Physiol*, *62*, 327-336. doi:10.1002/jcp.1030620313
- Singh, S. K., Clarke, I. D., Terasaki, M., Bonn, V. E., Hawkins, C., Squire, J., & Dirks, P. B. (2003). Identification of a cancer stem cell in human brain tumors. *Cancer Res*, *63*(18), 5821-5828.
- Singh, S. K., Hawkins, C., Clarke, I. D., Squire, J. A., Bayani, J., Hide, T., . . . Dirks, P. B. (2004). Identification of human brain tumour initiating cells. *Nature*, *432*(7015), 396-401. doi:10.1038/nature03128
- Smith, K., & Dalton, S. (2010). Myc transcription factors: key regulators behind establishment and maintenance of pluripotency. *Regen Med*, *5*(6), 947-959. doi:10.2217/rme.10.79
- Song, H., Niu, X., Quan, J., Li, Y., Yuan, L., Wang, J., . . . Ma, E. (2020). Discovery of specific HDAC6 inhibitor with anti-metastatic effects in pancreatic cancer cells through virtual screening and biological evaluation. *Bioorg Chem*, *97*, 103679. doi:10.1016/j.bioorg.2020.103679
- Spiegler, B. J., Bouffet, E., Greenberg, M. L., Rutka, J. T., & Mabbott, D. J. (2004). Change in neurocognitive functioning after treatment with cranial radiation in childhood. *J Clin Oncol*, *22*(4), 706-713. doi:10.1200/JCO.2004.05.186
- St. Jude Children's Research Hospital. (2017). Identifier: NCT01393912, PDGFR Inhibitor Crenolanib in Children/Young Adults With Diffuse Intrinsic Pontine Glioma or Recurrent High-Grade Glioma. Retrieved from <https://clinicaltrials.gov/ct2/show/NCT01393912>
- Suva, M. L., & Tirosch, I. (2019). Single-Cell RNA Sequencing in Cancer: Lessons Learned and Emerging Challenges. *Mol Cell*, *75*(1), 7-12. doi:10.1016/j.molcel.2019.05.003
- Tabori, U., Baskin, B., Shago, M., Alon, N., Taylor, M. D., Ray, P. N., . . . Hawkins, C. (2010). Universal poor survival in children with medulloblastoma harboring somatic TP53 mutations. *J Clin Oncol*, *28*(8), 1345-1350. doi:10.1200/JCO.2009.23.5952
- Tan, Y., Zhang, S., Zhu, H., Chu, Y., Zhou, H., Liu, D., & Huo, J. (2019). Histone deacetylase 6 selective inhibitor ACY1215 inhibits cell proliferation and enhances the chemotherapeutic effect of 5-fluorouracil in HCT116 cells. *Ann Transl Med*, *7*(1), 2. doi:10.21037/atm.2018.11.48
- Tang, A., Gao, K., Chu, L., Zhang, R., Yang, J., & Zheng, J. (2017). Aurora kinases: novel therapy targets in cancers. *Oncotarget*, *8*(14), 23937-23954. doi:10.18632/oncotarget.14893
- Tao, Y., Leteur, C., Yang, C., Zhang, P., Castedo, M., Pierre, A., . . . Deutsch, E. (2009). Radiosensitization by Chir-124, a selective CHK1 inhibitor: effects of p53 and cell cycle checkpoints. *Cell Cycle*, *8*(8), 1196-1205. doi:10.4161/cc.8.8.8203
- Taylor, M. D., Northcott, P. A., Korshunov, A., Remke, M., Cho, Y. J., Clifford, S. C., . . . Pfister, S. M. (2012). Molecular subgroups of medulloblastoma: the current consensus. *Acta Neuropathol*, *123*(4), 465-472. doi:10.1007/s00401-011-0922-z

- Taylor, R. E., Bailey, C. C., Robinson, K. J., Weston, C. L., Walker, D. A., Ellison, D., . . . Lashford, L. S. (2005). Outcome for patients with metastatic (M2-3) medulloblastoma treated with SIOP/UKCCSG PNET-3 chemotherapy. *Eur J Cancer*, *41*(5), 727-734. doi:10.1016/j.ejca.2004.12.017
- Taylor, R. E., Bailey, C. C., Robinson, K., Weston, C. L., Ellison, D., Ironside, J., . . . United Kingdom Children's Cancer Study, Group. (2003). Results of a randomized study of preradiation chemotherapy versus radiotherapy alone for nonmetastatic medulloblastoma: The International Society of Paediatric Oncology/United Kingdom Children's Cancer Study Group PNET-3 Study. *J Clin Oncol*, *21*(8), 1581-1591. doi:10.1200/JCO.2003.05.116
- Thiel-Demby, V. E., Humphreys, J. E., St John Williams, L. A., Ellens, H. M., Shah, N., Ayrton, A. D., & Polli, J. W. (2009). Biopharmaceutics classification system: validation and learnings of an in vitro permeability assay. *Mol Pharm*, *6*(1), 11-18. doi:10.1021/mp800122b
- Thompson, M. C., Fuller, C., Hogg, T. L., Dalton, J., Finkelstein, D., Lau, C. C., . . . Gilbertson, R. J. (2006). Genomics identifies medulloblastoma subgroups that are enriched for specific genetic alterations. *J Clin Oncol*, *24*(12), 1924-1931. doi:10.1200/JCO.2005.04.4974
- Triscott, J., Lee, C., Foster, C., Manoranjan, B., Pambid, M. R., Berns, R., . . . Dunn, S. E. (2013). Personalizing the treatment of pediatric medulloblastoma: Polo-like kinase 1 as a molecular target in high-risk children. *Cancer Res*, *73*(22), 6734-6744. doi:10.1158/0008-5472.CAN-12-4331
- Tropepe, V., Sibilina, M., Ciruna, B. G., Rossant, J., Wagner, E. F., & van der Kooy, D. (1999). Distinct neural stem cells proliferate in response to EGF and FGF in the developing mouse telencephalon. *Dev Biol*, *208*(1), 166-188. doi:10.1006/dbio.1998.9192
- Tse, A. N., Rendahl, K. G., Sheikh, T., Cheema, H., Aardalen, K., Embry, M., . . . Schwartz, G. K. (2007). CHIR-124, a novel potent inhibitor of Chk1, potentiates the cytotoxicity of topoisomerase I poisons in vitro and in vivo. *Clin Cancer Res*, *13*(2 Pt 1), 591-602. doi:10.1158/1078-0432.CCR-06-1424
- Uchida, N., Buck, D. W., He, D., Reitsma, M. J., Masek, M., Phan, T. V., . . . Weissman, I. L. (2000). Direct isolation of human central nervous system stem cells. *Proc Natl Acad Sci U S A*, *97*(26), 14720-14725. doi:10.1073/pnas.97.26.14720
- University of Michigan Rogel Cancer Center. (2019). Identifier: NCT03352427, Study of Dasatinib in Combination With Everolimus for Children and Young Adults With Gliomas Harboring PDGFR Alterations. Retrieved from <https://clinicaltrials.gov/ct2/show/NCT03352427>
- Urdiciain, A., Erasquin, E., Melendez, B., Rey, J. A., Idoate, M. A., & Castresana, J. S. (2019). Tubastatin A, an inhibitor of HDAC6, enhances temozolomide-induced apoptosis and reverses the malignant phenotype of glioblastoma cells. *Int J Oncol*, *54*(5), 1797-1808. doi:10.3892/ijo.2019.4739
- Valastyan, S., & Weinberg, R. A. (2011). Tumor metastasis: molecular insights and evolving paradigms. *Cell*, *147*(2), 275-292. doi:10.1016/j.cell.2011.09.024

- van de Weerd, B. C., & Medema, R. H. (2006). Polo-like kinases: a team in control of the division. *Cell Cycle*, 5(8), 853-864. doi:10.4161/cc.5.8.2692
- Venugopal, C., Wang, X. S., Manoranjan, B., McFarlane, N., Nolte, S., Li, M., . . . Singh, S. K. (2012). GBM secretome induces transient transformation of human neural precursor cells. *J Neurooncol*, 109(3), 457-466. doi:10.1007/s11060-012-0917-1
- Verstappen, C. C., Koeppen, S., Heimans, J. J., Huijgens, P. C., Scheulen, M. E., Strumberg, D., . . . Postma, T. J. (2005). Dose-related vincristine-induced peripheral neuropathy with unexpected off-therapy worsening. *Neurology*, 64(6), 1076-1077. doi:10.1212/01.WNL.0000154642.45474.28
- Vladoiu, M. C., El-Hamamy, I., Donovan, L. K., Farooq, H., Holgado, B. L., Sundaravadanam, Y., . . . Taylor, M. D. (2019). Childhood cerebellar tumours mirror conserved fetal transcriptional programs. *Nature*, 572(7767), 67-73. doi:10.1038/s41586-019-1158-7
- Volpe, D. A. (2010). Application of method suitability for drug permeability classification. *AAPS J*, 12(4), 670-678. doi:10.1208/s12248-010-9227-8
- Walker, E. V., Davis, F. G., & Affiliates, CBTR Founding. (2019). Malignant primary brain and other central nervous system tumors diagnosed in Canada from 2009 to 2013. *Neuro Oncol*, 21(3), 360-369. doi:10.1093/neuonc/noy195
- Wallace, V. A. (1999). Purkinje-cell-derived Sonic hedgehog regulates granule neuron precursor cell proliferation in the developing mouse cerebellum. *Curr Biol*, 9(8), 445-448. doi:10.1016/s0960-9822(99)80195-x
- Wang, J., Garancher, A., Ramaswamy, V., & Wechsler-Reya, R. J. (2018). Medulloblastoma: From Molecular Subgroups to Molecular Targeted Therapies. *Annu Rev Neurosci*, 41, 207-232. doi:10.1146/annurev-neuro-070815-013838
- Wang, L., Xiang, S., Williams, K. A., Dong, H., Bai, W., Nicosia, S. V., . . . Zhang, X. (2012). Depletion of HDAC6 enhances cisplatin-induced DNA damage and apoptosis in non-small cell lung cancer cells. *PLoS One*, 7(9), e44265. doi:10.1371/journal.pone.0044265
- Wang, W. J., Wu, S. P., Liu, J. B., Shi, Y. S., Huang, X., Zhang, Q. B., & Yao, K. T. (2013). MYC regulation of CHK1 and CHK2 promotes radioresistance in a stem cell-like population of nasopharyngeal carcinoma cells. *Cancer Res*, 73(3), 1219-1231. doi:10.1158/0008-5472.CAN-12-1408
- Wechsler-Reya, R. J., & Scott, M. P. (1999). Control of neuronal precursor proliferation in the cerebellum by Sonic Hedgehog. *Neuron*, 22(1), 103-114. doi:10.1016/s0896-6273(00)80682-0
- Weiss, G. J., Donehower, R. C., Iyengar, T., Ramanathan, R. K., Lewandowski, K., Westin, E., . . . McKane, S. (2013). Phase I dose-escalation study to examine the safety and tolerability of LY2603618, a checkpoint 1 kinase inhibitor, administered 1 day after pemetrexed 500 mg/m² every 21 days in patients with cancer. *Invest New Drugs*, 31(1), 136-144. doi:10.1007/s10637-012-9815-9
- Wickstrom, S. A., Masoumi, K. C., Khochbin, S., Fassler, R., & Massoumi, R. (2010). CYLD negatively regulates cell-cycle progression by inactivating HDAC6 and increasing the levels of acetylated tubulin. *EMBO J*, 29(1), 131-144. doi:10.1038/emboj.2009.317

- Wu, X., Northcott, P. A., Dubuc, A., Dupuy, A. J., Shih, D. J., Witt, H., . . . Taylor, M. D. (2012). Clonal selection drives genetic divergence of metastatic medulloblastoma. *Nature*, *482*(7386), 529-533. doi:10.1038/nature10825
- Yan, B., Xie, S., Liu, Y., Liu, W., Li, D., Liu, M., . . . Zhou, J. (2018). Histone deacetylase 6 modulates macrophage infiltration during inflammation. *Theranostics*, *8*(11), 2927-2938. doi:10.7150/thno.25317
- Yang, D., Liu, H., Goga, A., Kim, S., Yuneva, M., & Bishop, J. M. (2010). Therapeutic potential of a synthetic lethal interaction between the MYC proto-oncogene and inhibition of aurora-B kinase. *Proc Natl Acad Sci U S A*, *107*(31), 13836-13841. doi:10.1073/pnas.1008366107
- Yang, Z. J., Ellis, T., Markant, S. L., Read, T. A., Kessler, J. D., Bourbonlous, M., . . . Wechsler-Reya, R. J. (2008). Medulloblastoma can be initiated by deletion of Patched in lineage-restricted progenitors or stem cells. *Cancer Cell*, *14*(2), 135-145. doi:10.1016/j.ccr.2008.07.003
- Yin, Z., Xu, W., Xu, H., Zheng, J., & Gu, Y. (2018). Overexpression of HDAC6 suppresses tumor cell proliferation and metastasis by inhibition of the canonical Wnt/beta-catenin signaling pathway in hepatocellular carcinoma. *Oncol Lett*, *16*(6), 7082-7090. doi:10.3892/ol.2018.9504
- Yoo, Y. D., & Kwon, Y. T. (2015). Molecular mechanisms controlling asymmetric and symmetric self-renewal of cancer stem cells. *J Anal Sci Technol*, *6*(1), 28. doi:10.1186/s40543-015-0071-4
- Yuan, J., Llamas Luceno, N., Sander, B., & Golas, M. M. (2017). Synergistic anti-cancer effects of epigenetic drugs on medulloblastoma cells. *Cell Oncol (Dordr)*, *40*(3), 263-279. doi:10.1007/s13402-017-0319-7
- Yuan, L., Santi, M., Rushing, E. J., Cornelison, R., & MacDonald, T. J. (2010). ERK activation of p21 activated kinase-1 (Pak1) is critical for medulloblastoma cell migration. *Clin Exp Metastasis*, *27*(7), 481-491. doi:10.1007/s10585-010-9337-9
- Zapotocky, M., Mata-Mbemba, D., Sumerauer, D., Liby, P., Lassaletta, A., Zamecnik, J., . . . Ramaswamy, V. (2018). Differential patterns of metastatic dissemination across medulloblastoma subgroups. *J Neurosurg Pediatr*, *21*(2), 145-152. doi:10.3171/2017.8.PEDS17264
- Zeltzer, P. M., Boyett, J. M., Finlay, J. L., Albright, A. L., Rorke, L. B., Milstein, J. M., . . . Packer, R. J. (1999). Metastasis stage, adjuvant treatment, and residual tumor are prognostic factors for medulloblastoma in children: conclusions from the Children's Cancer Group 921 randomized phase III study. *J Clin Oncol*, *17*(3), 832-845. doi:10.1200/JCO.1999.17.3.832
- Zhang, L., Liu, N., Xie, S., He, X., Zhou, J., Liu, M., & Li, D. (2014). HDAC6 regulates neuroblastoma cell migration and may play a role in the invasion process. *Cancer Biol Ther*, *15*(11), 1561-1570. doi:10.4161/15384047.2014.956632
- Zhong, R. K., Astle, C. M., & Harrison, D. E. (1996). Distinct developmental patterns of short-term and long-term functioning lymphoid and myeloid precursors defined by competitive limiting dilution analysis in vivo. *J Immunol*, *157*(1), 138-145.
- Zhou, L., Picard, D., Ra, Y. S., Li, M., Northcott, P. A., Hu, Y., . . . Huang, A. (2010). Silencing of thrombospondin-1 is critical for myc-induced metastatic phenotypes

- in medulloblastoma. *Cancer Res*, 70(20), 8199-8210. doi:10.1158/0008-5472.CAN-09-4562
- Zhukova, N., Ramaswamy, V., Remke, M., Pfaff, E., Shih, D. J., Martin, D. C., . . . Tabori, U. (2013). Subgroup-specific prognostic implications of TP53 mutation in medulloblastoma. *J Clin Oncol*, 31(23), 2927-2935. doi:10.1200/JCO.2012.48.5052
- Zuo, Q., Wu, W., Li, X., Zhao, L., & Chen, W. (2012). HDAC6 and SIRT2 promote bladder cancer cell migration and invasion by targeting cortactin. *Oncol Rep*, 27(3), 819-824. doi:10.3892/or.2011.1553
- Zwergel, C., Romanelli, A., Stazi, G., Besharat, Z. M., Catanzaro, G., Tafani, M., . . . Mai, A. (2018). Application of Small Epigenetic Modulators in Pediatric Medulloblastoma. *Front Pediatr*, 6, 370. doi:10.3389/fped.2018.00370

APPENDIX: Academic Achievements

The following are highlights of academic achievements during my graduate studies.

A. Foundational Work for Thesis

1. Bakhshinyan D, **Adile AA**, Venugopal C, Liu J, Singh M, McFarlane N, Subapanditha MK, Qazi MA, Vora P, Kameda-Smith M, Gwynne WD, Custers S, Savage N, Desmond KL, Tatari N, Tran D, Seyfrid M, Hope K, Bock N, Bader GD, Singh SK. Stem cell longevity factor BPIFB4 is a driver of medulloblastoma recurrence. *Nature Cancer* (Near submission, 2020).

B. Additional Work

Published Refereed Papers

1. Vora P, Venugopal C, Salim SK, Tatari N, Bakhshinyan D, Singh M, Seyfrid M, Upreti D, Rentas S, Wong N, Williams R, Qazi MA, Chokshi C, Ding A, Subapanditha MK, Savage N, Mahendram S, Ford E, **Adile AA**, McKenna D, McFarlane N, Huynh V, Wylie RG, Pan J, Bramson J, Hope K, Moffat J, Singh SK. (2020). The rational development of CD133-targeting immunotherapies for glioblastoma. *Cell Stem Cell* S1934-5909, 30147-30148.
2. **Adile AA**, Kameda-Smith MM, Bakhshinyan D, Banfield L, Salim SK, Farrokhyar F, Fleming AJ. (2020). Salvage therapy for progressive, treatment-refractory or recurrent pediatric medulloblastoma: a systematic review protocol. *Systematic Reviews* 9, 47.
3. Kameda-Smith MM, Wang A, Abdulhadi N, Voth R, Sergeant A, Maharaj A, Bakhshinyan D, **Adile AA**, Pai AM, Ajani O, Yarascavitch B, Alyman MC, Duckworth J, Samaan MC, Farrokhyar F, Singh SK, Fleming A; Pediatric Brain Tumour Study Group. Salvage Therapy for Childhood Medulloblastoma: A Single Center Experience. (2019). *Canadian Journal of Neurological Science* 46, 403-414.
4. Bakhshinyan D, Venugopal C, **Adile AA**, Garg N, Manoranjan B, Hallett R, Wang X, Mahendram S, Vora P, Vijayakumar T, Subapanditha M, Singh M, Kameda-Smith MM, Qazi M, McFarlane N, Mann A, Ajani OA, Yarascavitch B, Ramaswamy V, Farooq H, Morrissy S, Cao L, Sydorenko N, Baiazitov R, Du W, Sheedy J, Weetall M, Moon YC, Lee CS, Kwiecien JM, Delaney KH, Doble B, Cho YJ, Mitra S, Kaplan D, Taylor M, Davis T, Singh SK. BMI1 is a therapeutic target in recurrent medulloblastoma. (2019). *Oncogene* 38, 1702-1716.
5. Shouksmith A, Shah F, Grimard ML, Gawel JM, Raouf Y, Geletu M, Berger-Becvar A, de Araujo ED, Luchman HA, Heaton WL, Bakhshinyan D, **Adile AA**, Venugopal C, O'Hare T, Deininger MW, Singh SK, Konieczny SF, Weiss S, Fishel ML, Gunning PT. (2019). Identification and Characterization of AES-135, a Potent HDAC Inhibitor that Prolongs Survival in an Orthotopic Mouse Model of Pancreatic Cancer. *Journal of Medicinal Chemistry* 62, 2651-2665.

Published Book Chapters

1. **Adile AA**, Bakhshinyan D, Venugopal C, Singh SK (2019). In Vitro Assays for Screening Small Molecules. In: Singh S., Venugopal C. (eds) Brain Tumor Stem Cells. Methods in Molecular Biology, Springer, vol 1869. Humana Press, New York, NY.
2. Subapanditha MK, **Adile AA**, Venugopal C, Singh SK (2019). Flow sorting and characterization of brain tumor stem cells. In: Singh S., Venugopal C. (eds) Brain Tumor Stem Cells. Methods in Molecular Biology, Springer vol, 1869. Humana Press, New York, NY.
3. Bakhshinyan D, **Adile AA**, Qazi MA, Singh M, Kameda-Smith MM, Yelle N, Chokshi C, Venugopal C, Singh SK. (2018). Introduction to Cancer Stem Cells: Past, Present and Future. In: Papaccio G., Desiderio V. (eds) Cancer Stem Cells. Methods in Molecular Biology, Springer, vol 1692. Humana Press, New York, NY.

Submitted Refereed Papers

1. Kameda-Smith MM, Zhu H, Luo EC, Venugopal C, Xella A, Yee B, Xing S, Tan F, Fox RG, Brown K, **Adile AA**, Bakhshinyan D, Chokshi C, Gwynne WD, Subapanditha MK, Burns I, Picard D, Moffat J, Fleming AJ, Hope K, Provias J, Remke M, Lu Y, Reya T, Reimand J, Wechsler-Reya R, Yeo G, Singh SK. (2020). Integrative multi-omic analyses reveal context-specific downstream targeting of MSI1-dependent childhood medulloblastoma. *Nature Neuroscience*.
2. Manoranjan B, Venugopal C, Bakhshinyan D, **Adile AA**, Richards L, Kameda-Smith MM, Whitley O, Dvorkin-Gheva A, Subapanditha MK, Savage N, Tatari N, Winegarden N, Hallet R, Provias JP, Yarascavitch B, Ajani O, Fleming A, Bader GD, Pugh TJ, Doble BW, Singh SK. (2020). Wnt activation as a therapeutic strategy in medulloblastoma. *Nature Communications* (Accepted, in pre-print).

Manuscripts in Preparation

1. Bakhshinyan D, Kuhlmann L, **Adile AA**, Ignatchenko V, Gwynne WD, Custers S, Mackling A, Venugopal C, Kislinger T, Singh SK. Characterization and therapeutic value of ITGA5 in recurrent medulloblastoma (Experiments underway).
2. Bakhshinyan, D, **Adile, AA**, Venugopal C, Qazi M, Subapanditha M, Amy Tong, Gwynne W, Custers S, Moffat J, Singh SK. Identifying therapeutic vulnerabilities of treatment refractory medulloblastoma using DNA barcoding and genome wide CRISPR-Cas9 screening technology (Experiments underway).

Scientific Meetings: Oral Presentations (*Presenter)

1. Kameda-Smith MM, Brown K, Zhu H, Luo EC, Yee B, Xing S, Venugopal C, van Nostrand E, Bakhshinyan D, Subapanditha MK, **Adile AA**, Provias J, Fleming AJ, Hope K, Reimand J, Lu Y, Yeo G, Wechsler-Reya R, Singh SK. Mushashi-1 is a master regulator of aberrant translation in Group 3 medulloblastoma. SNO Pediatric Neuro-

Oncology Basic and Translational Research Conference, Abstract MEDU-44, San Francisco, CA, USA.

2. Bakhshinyan D*, **Adile AA**, Venugopal C, Singh M, Subapanditha, M, McFarlane N, Singh SK. (2018). Genes preserving stem cell state in Group 3 MB BTICs contribute to therapy evasion and relapse. 18th Biennial Canadian Neuro-Oncology meeting, Banff, AB, Canada.
3. Bakhshinyan D, **Adile AA**, Venugopal C, Singh M, Subapanditha, M, McFarlane N, Singh SK*. (2017). Genes preserving stem cell state in Group 3 MB BTICs contribute to therapy evasion and relapse. Society for Neuro-Oncology, San Francisco, CA, USA

Scientific Meetings: Unpublished Poster Abstracts (*Presenter)

1. **Adile AA***, Bakhshinyan D, Venugopal C, Subapanditha MK, Weetall M, Davis TW, Singh SK. (2019). Small molecule inhibitor targeting self-renewal as a therapeutic option for medulloblastoma. SNO Pediatric Neuro-Oncology Basic and Translational Research Conference, Abstract THER-14, San Francisco, CA, USA.
2. Bakhshinyan D, **Adile AA***, Venugopal C, Singh M, Qazi MA, Kameda-Smith MM, Singh SK. (2019). Genes preserving stem cell state in Group 3 MB BTICs contribute to therapy evasion and relapse. Pediatric Neuro-Oncology Basic and Translational Research Conference, Abstract MEDU-25, New York City, NY, USA.
3. Kameda-Smith MM*, Venugopal C, Subapanditha M, Bakhshinyan D, **Adile AA**, Manoranjan B Hope K, Singh SK. (2018). Investigating the role of the RNA binding protein, Musashi, in pediatric medulloblastoma. Keystone DNA and RNA methylation conference, Vancouver, BC, Canada.
4. Kameda-Smith MM*, Venugopal C, Manoranjan B, Bakhshinyan D, **Adile AA**, Hope K, Singh SK. (2018). Investigating the role of the RNA binding protein, Musashi, in pediatric medulloblastoma. Cold Spring Harbour Laboratory Eukaryotic mRNA Processing Conference, Cold Spring Harbour, NY, USA.
5. **Adile AA***, Bakhshinyan D, Venugopal C, Subapanditha MK, Weetall M, Davis TW, Singh SK (2018). Small molecule inhibitor targeting self-renewal as a therapeutic option for medulloblastoma. 2018 Let's Talk Cancer, Hamilton, ON, Canada.

Scholarships & Awards

Lorne F. Lambier, Q.C., Scholarship (\$5,000)

McMaster University, February 2020

Awarded to a master's or doctoral student in the Faculties of Health Science and Science whose research aims to understand and/or cure cancer (one award granted annually).

Biochemistry Entrance Scholarship (\$1,000)

McMaster University, April 2018

Scholarly Activities: Invited Grant & Journal Reviewer

1. *Systematic Reviews* Meta-Analyses, 2020
2. *Systematic Reviews* Systematic Review Protocol, 2020
3. *Expert Opinion on Orphan Drugs* Review Article, 2019 (Secondary to Dr. Chitra Venugopal)
4. *Journal of Neuro-Oncology* Research Article, 2019 (Secondary to Dr. Sheila K. Singh)
5. *Knut & Alice Wallenberg Foundation* Grant, 2018 (Secondary to Dr. Sheila K. Singh)